CANADIAN JOURNAL OF RESEARCH

VOLUME 26 MAY, 1948 NUMBER 3

— SECTION A —

PHYSICAL SCIENCES

Contents

Page

The Initial Ionization Produced by Fission Fragments—*D. West* - - - - - - - - - - - - 115

Surface Area Measurements of Fine Powders Using Modified Permeability Equations—*P. C. Carman and J. C. Arnell* - - 128

Solar Eclipse Observations of the Ionosphere—*C. W. McLeish* - 137

A High Temperature Control Circuit—*Bruce C. Lutz and John H. Wood* - - - - - - - - - - - - 145

The Photoelectric Temperatures of the P Cygni Stars—*C. S. Beals and R. D. Hatcher* - - - - - - - - 149

A Radio Method of Studying the Yaw of Shells—*C. C. Gotlieb, P. E. Pashler, and M. Rubinoff* - - - - - - - 167

Gravity Anomalies in Northwestern Canada—*M. J. S. Innes* - 199

NATIONAL RESEARCH COUNCIL
OTTAWA, CANADA

CANADIAN JOURNAL OF RESEARCH

The *Canadian Journal of Research* is issued in six sections, as follows:

A. Physical Sciences	D. Zoological Sciences
B. Chemical Sciences	E. Medical Sciences
C. Botanical Sciences	F. Technology

For the present, Sections A, C, D, and E are to be issued six times annually, and Sections B and F, twelve times annually, each section under separate cover, with separate pagination.

The *Canadian Journal of Research* is published by the National Research Council of Canada under authority of the Chairman of the Committee of the Privy Council on Scientific and Industrial Research. The *Canadian Journal of Research* is edited by a joint Editorial Board consisting of members of the National Research Council of Canada, the Royal Society of Canada, and the Chemical Institute of Canada.

Sections B and F of the *Canadian Journal of Research* have been chosen by the Chemical Institute of Canada as its medium of publication for scientific papers.

EDITORIAL BOARD

Representing National Research Council	*Representing* Royal Society of Canada	
Dr. A. R. Gordon, (*Chairman*), Head, Department of Chemistry, University of Toronto, Toronto.	Dr. A. Norman Shaw, Chairman, Department of Physics, McGill University, Montreal.	Section III
Dr. C. H. Best, The Banting and Best Department of Medical Research, University of Toronto, Toronto.	Dr. J. W. T. Spinks, Department of Chemistry, University of Saskatchewan Saskatoon.	
Dr. Robert Newton, President, University of Alberta, Edmonton.	Dr. H. S. Jackson, Head, Department of Botany, University of Toronto, Toronto.	Section V
Dr. G. H. Henderson, Professor of Mathematical Physics, Dalhousie University, Halifax.	Dr. E. Horne Craigie, Department of Zoology, University of Toronto, Toronto.	

Ex officio	*Representing* The Chemical Institute of Canada
Dr. Léo Marion, Editor-in-Chief, Division of Chemistry, National Research Laboratories, Ottawa.	Dr. R. V. V. Nicholls, Associate Professor of Chemistry, McGill University, Montreal.
Dr. H. H. Saunderson, Director, Division of Information Services, National Research Laboratories, Ottawa.	

Editorial Committee

Editor-in-Chief,	Dr. Léo Marion	Editor, Section D,	Dr. E. Horne Craigie
Editor, Section A,	Dr. A. Norman Shaw	Editor, Section E,	Dr. J. B. Collip
Editor, Section B,	Dr. J. W. T. Spinks Dr. R. V. V. Nicholls	Editor, Section F,	Dr. J. A. Anderson Dr. R. V. V. Nicholls Dr. A. Norman Shaw
Editor, Section C,	Dr. H. S. Jackson		

Manuscripts should be addressed:

Editor-in-Chief,
Canadian Journal of Research,
National Research Council, Ottawa, Canada.

Canadian Journal of Research

Issued by THE NATIONAL RESEARCH COUNCIL OF CANADA

VOL. 26, SEC. A. MAY, 1948 NUMBER 3

THE INITIAL IONIZATION PRODUCED BY FISSION FRAGMENTS[1]

BY D. WEST

Abstract

The ionization produced by individual fission fragments over various lengths of track starting from the origin was measured in a pulse ionization chamber provided with a grid. The distribution of electron pulse sizes for the complete track showed the well known two peaks. As the length of track was diminished, the peaks corresponding to the high and low energy groups of fragments approached each other and merged together at a track length of about 6 mm. in nitrogen. In smaller distances measured from the beginning of the track the difference in ionization by the two groups of fragments was found to be small, and the two groups could not be resolved. From the progressive change in shape of the pulse spectrum it is tentatively concluded that the low energy group produces the greater initial ionization. The average energy spent in ionization by the fragments in the first 1.1, 2.3, and 5.3 mm. of their tracks was measured in nitrogen and found to be 7.6, 15.0, and 34.6 Mev. respectively. In the course of this work an effect due to the formation of negative ions by electron attachment was observed in the chamber filled with argon. Examination of this effect suggests that, at high collecting fields, formation of negative ions, perhaps in impurities such as oxygen and water vapor, is more pronounced in argon than in nitrogen.

Introduction

The general features of the loss of energy of fission fragments in passing through matter have been described by Bohr (2), who emphasized the essential differences in the mechanisms by which α-particles and fission fragments lose energy. In the first place, the effective charge of an α-particle is essentially equal to the nuclear charge during most of its range and decreases only towards the end of the range. On the contrary, the effective charge of a fission fragment is much less than the nuclear charge and decreases continuously from the beginning of the track. Consequently, the specific ionization of a fission fragment can be compared to that of an α-particle between the maximum in the Bragg curve and the end of its range. The energy region in which the specific ionization increases with decreasing velocity for particles as massive as fission fragments should occur at energies much higher than those actually attained in fission, while in the case of α-particles this region occurs at energies above one Mev. Thus, for α-particles the maximum value of the specific ionization occurs not far from the end of the range, while for fission fragments it actually occurs at the beginning of the tracks.

[1] *Manuscript received January 7, 1948.*

Contribution from the Nuclear Physics Branch, Chalk River Laboratory, Atomic Energy Division of the National Research Council of Canada. Issued as N.R.C. No. 1745. This paper was presented on September 4, 1946, at the Nuclear Physics Conference in Montreal, Que.

There is another mechanism by which charged particles lose energy in passing through matter: the 'indirect' ionization by nuclear collisions. This effect is of much greater importance for fission fragments than for α-particles. In fact, energy loss by nuclear collisions, which occurs with significant frequency only at the very end of the track of an α-particle, takes place all along the track of a fission fragment. However, even for a fission fragment, the amount of energy lost by this process is small in comparison to the energy lost by direct ionization, *except at the very end of the track.*

Calculations of the energy loss of fission fragments in passing through matter have been made by Lamb (11), Bohr (2), and Knipp and Teller (10). The detailed comparison of these calculations with experiment is, however, made difficult by the wide distribution in mass and energy of the fragments. The energy loss has been investigated in a cloud chamber by Bøggild, Brostrøm and Lauritsen (1). They used the recoil tracks that occur along the track of the fission fragment to deduce its velocity at various points. Their method is most accurate towards the end of the range where recoils are most frequent. Information about the initial part of the range was obtained by Lassen, who performed magnetic deflection experiments and deduced the initial effective charges of the light and heavy groups of fragments (12) and the effective charge and energy of the light group of fragments after they had traversed various thicknesses of mica (13). Lassen obtained results with which Bohr's theory does not agree in detail.

In view of this disagreement and the lack of more complete experimental data about the initial part of the range, a measurement of the initial ionization by fission fragments was undertaken.

Experimental Method

The principle of the method was as follows. A thin sample of fissile material, in this case uranium 233 (16), was placed at the center of a hemisphere. The sample holder and the hemisphere constituted two electrodes of a pulse ionization chamber. By varying the pressure of the gas in the chamber the ionization produced in various distances beginning at the origin of the track of a fission fragment could be investigated. The hemispherical arrangement ensures that the length of track in the gas is the same for all fragments. It was chosen in preference to a parallel-plate geometry and a well collimated beam of fission fragments to avoid loss of ionization in the channels of the collimator.

When the simple hemispherical chamber with two electrodes was filled with argon and tested, it was found to be unsatisfactory owing to the long collection time of positive ions in the electric fields that could be applied. Mr. D. H. Wilkinson suggested a form of grid chamber in which this difficulty is avoided. It was adopted for the experiment and is shown in Fig. 1. The hemispherical geometry is retained but the support for the source is made very small. The potential of the support is adjusted so that electrons produced by the ionizing fragments are not collected by it but move past to the collecting

electrode. A grid placed in front of the collecting electrode shields it from the effect of the motion of the positive ions. This grid consisted of a grating of parallel wires, 0.13 mm. in diameter, spaced at intervals of 1.4 mm., and it

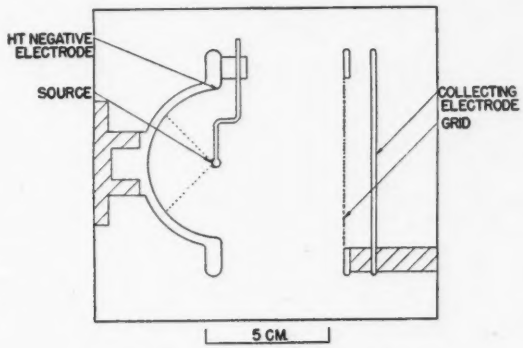

FIG. 1. *Sketch of pulse ionization chamber.*

was placed 1.1 cm. in front of the collecting electrode. According to the theory of grid chambers that has been given by Bunemann, Cranshaw, and Harvey (5), the residual effect of the positive ions produces a variation of less than 1% in the pulse size in this chamber.

The chamber was irradiated with neutrons in the low power, heavy water pile. The fission pulses were amplified by a linear amplifier, displayed on the screen of a cathode-ray oscilloscope, and photographed on 35 mm. film. The deflection on the screen varied linearly with the voltage applied to the input of the amplifier up to deflections corresponding to pulses of 200 v. A gain control that consisted of a bank of calibrated resistors constituting an anode load was used in the amplifier. It was placed in the first stage to ensure linearity at all gain settings. The bandwidth of the amplifier extended from 0.6 to 80 kc. per sec., at which frequencies the response fell to half of the maximum. This width was sufficient to ensure that the pulse height was independent of any variation of the collection time of the electrons that would be encountered in the experiment. The pulses on the oscilloscope screen were photographed on moving film. The horizontal sweep was not used. The direct spot of the stationary beam on the screen was covered with a narrow slit to eliminate fogging of the film along the base line. This arrangement gave a well defined base line on the photographic record from which precise measurements of the pulse heights could be made.

Preparation of the Fission Source

Since the initial ionization of the fission fragments is to be measured, the loss of energy in the layer of fissile material must be kept as small as possible. An idea of the amount of energy lost in the layer was obtained by calculating

the mean energy lost by an initially monokinetic group of fission fragments in a layer of thickness t. It was assumed that the relation between specific energy loss dE/dl and the residual range l is of the form

$$\frac{dE}{dl} = kl ,$$

where k is a constant. Over the initial part of the track this relation is a good approximation to the results of Bøggild, Brostrøm, and Lauritsen (1). The calculation was carried out for the case when the layer of fissile material was covered with a cylindrical collimator, since some collimation was found to be necessary. The behavior of the collimator was idealized by assuming that the number of particles emerging per unit solid angle is independent of the angle of emergence. Since in fact the number of particles per unit solid angle emerging from the collimator decreases almost linearly with the tangent of the angle of emergence, falling to zero at the maximum angle, the expression to be written for the mean energy loss will be an upper limit. The expression derived on the above assumptions is

$$\triangle E = \frac{E_0 t}{R}\left\{\frac{1}{1 - \cos\alpha}\log\sec\alpha - \frac{t}{3R}\sec\alpha\right\}$$

for $t \sec\alpha < R$,

where $\triangle E$ = mean energy spent in the layer by fragments that emerge from the collimator,

E_0 = initial energy of the fragment,

t = thickness of the layer,

R = range of the fragment in the fissile material,

and α = maximum angle of emergence of fragments from the cylindrical collimator, measured from the normal to the layer.

The layer of fissile material was uranium oxide weighing about 0.04 mgm. per cm.^{2} The collimator consisted of holes, 0.75 mm. in diameter, drilled in a metal sheet 0.5 mm. thick. Considering the light group of fission fragments, which have an initial energy of about 90 Mev. and a range $R \sim 6$ mgm. per cm.^{2} in uranium oxide, the mean energy loss in the layer is about 1 Mev.

The error on the measured ionization in the gas of the chamber, caused by the loss of energy in the solid layer, depends upon the pressure of the gas. It is more important at low pressure and sets a lower limit to the pressure at which significant results can be obtained. However, the effect of the layer even at low pressures is not as important as it may appear at first sight.

Consider a solid layer of equivalent depth t of gas and a depth r of gas in the chamber. Fission fragments that originate in the bottom of the layer lose an amount of energy equal to that spent in the first t cm. of the range before they enter the gas. Thus in traversing the chamber they lose an amount of energy equal to that spent between t and $t + r$ (instead of between 0 and r). Hence the energy lost in the layer is replaced by an amount equal to the energy spent between r and $r + t$. The net effect is only a small reduction

in the energy spent in the gas, this reduction being a small fraction of the energy spent in the layer. The amount by which the energy spent in the gas is reduced can be estimated using the approximate energy-range relation given above. The maximum reduction in energy spent in the gas due to the thickness of the layer of fissile material chosen was estimated to be about 1% for a chamber depth equivalent to 1 mm. of air. The layer chosen (0.04 mgm. per cm.^{2}) was therefore sufficiently thin for the measurements.

The layer of fissile material was prepared by evaporating a solution of uranium nitrate in pyridine on a platinum foil. About 40 μgm. of U_3O_8 was converted to nitrate and dissolved in pyridine. This material was evaporated on 1 sq. cm. of foil in many stages. At the end of each stage of evaporation the deposit was ignited. The final deposit appeared to have a uniform yellow color. The gain in weight of the foil showed that no appreciable impurity had accumulated from the evaporation of the pyridine. A small portion of this layer was selected and used as the source.

Chamber Characteristics

In view of the unusual design of the chamber, a detailed study was made of the variation of pulse size with the voltages applied to the electrodes.

A sample of polonium was placed on the source electrode and the chamber filled with argon (99.8% pure) at a pressure just sufficient to prevent the α-particles from reaching the hemisphere. The potentials of the electrodes were adjusted to give the maximum pulse size, and the distribution of sizes was investigated. A well defined peak was obtained, but in addition about one-third of the pulses were of smaller sizes. These small pulses were shown not to be due to the thickness of the source. It was thought that electrons released near the rim of the hemisphere might be collected on the case of the chamber and hence not contribute to the pulse on the collecting electrode. This explanation was shown to be right, since the small pulses were, in fact, eliminated by placing a shallow collimator over the source. This collimator, described in the previous section, reduced the number of small pulses to less than 5% of the total. It limited the emission of ionizing particles to an angle that is indicated by dotted lines in Fig. 1.

The variation of pulse size with the potentials of the grid and source electrode was studied, the potential of the hemisphere being kept constant. (The electron-collecting electrode is connected to ground through a resistance.) Two of the characteristics obtained are shown in Fig. 2.

The grid characteristic (*A* in Fig. 2) has a well defined plateau when its potential is made sufficiently negative to prevent its collecting any electrons. At the upper end of the plateau there is a falling-off in mean pulse size, which is associated with a broadening of the spectrum of pulses. This is due to the increased ratio of leakage field (between hemisphere and case) to collecting field (between hemisphere and grid) as the potential of the grid is made more negative. The effect is similar to that produced by reducing the degree of

collimation of the source. In fact, the length of the plateau on the grid characteristic was found to depend on the degree of collimation used. As one would expect, the plateau was shorter when a wider collimator was used.

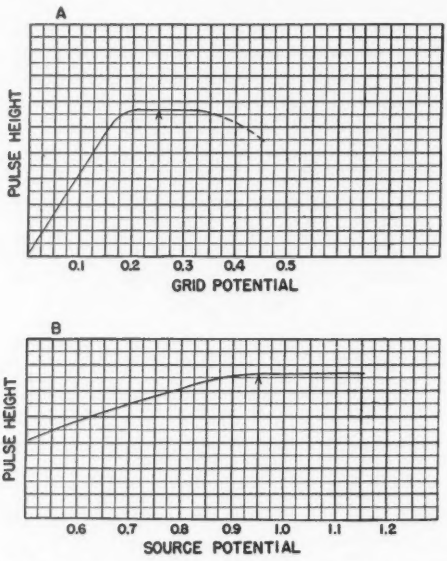

FIG. 2. *A. Graph of pulse height against the grid potential when the source potential was 0.95.*

B. Graph of pulse height against the source potential when the grid potential was 0.25.

Potentials are expressed in units of that of the hemisphere. The electron-collecting electrode is grounded through a resistance.

A characteristic (*B*) for the source electrode is also shown in Fig. 2. As the potential of the source is made more negative, fewer electrons are collected on it and the pulse height increases to a steady value. The potentials of source and grid that were chosen as optimum values are indicated by arrows in Fig. 2.

After the preliminary investigation of the characteristics of the chamber with polonium α-particles was completed, the saturation voltage needed to collect the ions produced by fission fragments was investigated at various pressures of argon. The voltages were applied to the electrodes by means of a potentiometer that varied the total voltage without changing the fractional voltages on the different electrodes. The pulse heights were measured directly on a graduated oscilloscope screen. The mean pulse size was determined at a series of applied voltages, and from the curve of mean pulse size versus applied voltage the saturation voltage was determined.

At a pressure (70 cm. of mercury) sufficient to stop the fragments in the gas of the chamber, saturation was obtained with -1400 v. applied to the

hemisphere. It is of interest to compare this voltage with that required to collect the ions from polonium α-particles at the same pressure of gas. In that case -300 v. on the hemisphere was required to produce saturation.

Investigation of the saturation characteristics for fission fragments at lower pressures of argon revealed a phenomenon that proved to be of importance and led to the use of nitrogen instead of argon.

In argon at a pressure of 10 cm. of mercury, the mean pulse size reached a maximum with -100 v. applied to the hemisphere. On increasing the voltage above 100 v. the mean pulse size decreased, and with -1000 v. the pulse size was only one-tenth of its maximum size. A similar behavior was observed at higher pressures. A check of the reproducibility of the phenomenon was made by refilling the chamber at 10 cm. pressure: the effect was observed again but the variation of the pulse size with voltage could not be reproduced exactly.

Observation of the pulse shape showed that the decrease of pulse height was associated with the appearance of a second pulse that occurred about one millisecond later. This delayed pulse rose much more slowly than the first and was consequently not amplified as much.

It was apparent from these observations that some electrons were becoming attached to gas molecules during their passage across the chamber. The negative ions so formed move much more slowly than the electrons, and, since a pulse is produced on the collecting electrode only after the ions have reached the grid of the chamber, the slow pulse from the negative ions is delayed with respect to that due to the electrons.

The lack of reproducibility of the phenomenon on refilling suggests that the negative ions are formed with impurities in the argon. The argon used was 99.8% pure; the effect, however, was also observed with argon 99.96% pure. The impurities were not identified, but for the purpose of the present argument they are assumed to be oxygen and water vapor. For both these molecules the probability of negative ion formation by electron attachment rises rapidly with electron energy above a certain region of energy (3, 4, 8). Direct measurements of electron attachment by oxygen or water vapor present in small amount in argon are not available. Nevertheless, it is believed that the range of electron energies attained in the present chamber extended into the region where the probability of electron attachment is rising rapidly. This would explain the dependence of the pulse size on the applied electric field. The collecting field in the region traversed by fission fragments is sufficient to collect electrons, but it would be inadequate to prevent recombination of positive and negative ions. Consequently, the fact that the negative ions produced a pulse rather than recombining with the positive ions is an indication that they were formed away from the positive ions, i.e., away from the region traversed by fission fragments (see Fig. 1).

One can thus visualize the effect as follows: the velocities of the electrons in the region beyond the sample, where positive ions are not produced, increase

with increasing field, so that the higher the field, the greater the amount of negative ion formation from impurities. These negative ions can now reach the collecting electrode notwithstanding their low mobility, because in the region considered there are no positive ions produced.

The effect described above introduces a serious difficulty for the measurement of the initial specific ionization of fission fragments when argon is used. The following considerations suggest that other gases may be more desirable in connection with this difficulty.

The motion of electrons in gases has recently been summarized by Healey and Reed (8). The motion under the action of an electric field is a diffusion process that is characterized by two velocities, the agitational velocity and the drift velocity. The drift velocity will determine the collection time of the electrons. It is the mean, in the direction of the field, of the generally much larger agitational velocities. It will be the agitational velocity that determines the formation of negative ions, however. Now the agitational velocity in argon is much higher than in most other gases for a given applied field. Consequently the degree of negative ion formation in impurities of oxygen and water vapor will be considerable even for very small quantities of impurity, as, for example, is indicated by the occurrence of negative ion formation in argon of 99.96% purity mentioned above.

In nitrogen the agitational velocity of electrons is much less than in argon for the same drift velocity. This is essentially due to the larger loss of energy that occurs in a collision of an electron with a nitrogen molecule. On this account one may expect nitrogen to be considerably less sensitive to impurity than argon and in particular that negative ion formation will be much less probable than in argon for a given drift velocity.

The nitrogen used was the commercial grade, which was purified by passing it over heated copper to remove oxygen. No indication of negative ion formation was obtained with this gas even with a field strength five times as great as that at which it became important in the case of argon. The voltage required to produce saturation of the pulses was, however, about twice as great as with argon under similar conditions. Consequently, it was decided to use nitrogen in order to avoid the extreme purity of gas that would have been required had argon been selected.*

Results

In order to verify that the operation of the apparatus as a whole (chamber and associated electronic equipment) was satisfactory, the distribution of the total energy of fission fragments from uranium 233 was measured at a pressure (72.5 cm. of mercury) sufficient to stop all the fragments in the chamber. Unfortunately it was not possible to use nitrogen for this measurement as the necessary saturation voltage could not be applied to the chamber owing

** Margenau et al. (15) have shown that electron attachment in argon takes place to a measurable degree even after extreme precautions to remove impurities have been taken.*

to electrical breakdown. With argon the plateau on the characteristic of mean pulse size versus total voltage, however, extended from -1600 to -2000 v. (above which the decrease due to negative ion formation set in). Consequently, it was thought that even with argon this experiment on the total energy of fission fragments would give significant results for control purposes. The pulse heights were measured on the photographic record of the oscilloscope screen. The spectrum of pulses obtained for the total energy of fission fragments from uranium 233 is shown in Fig. 3, *A*. A calibration of the apparatus

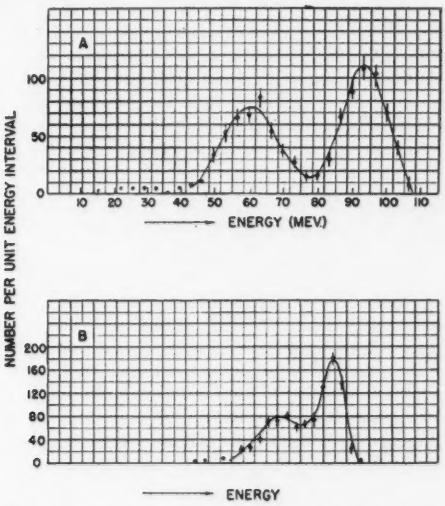

FIG. 3. *A. Energy distribution of 1038 fission fragments from uranium 233 in argon. The depth of the chamber exceeded the range.*

B. Energy distribution of 2040 fission fragments from uranium 233 in nitrogen, made with an electronic pulse analyzer. The depth of the chamber was equivalent to 8.8 mm. path in standard nitrogen. The analyzer was not calibrated in Mev., hence the abscissae are in arbitrary units proportional to the energy spent in ionization.

was obtained by photographing the pulses from polonium α-particles with a pressure of argon sufficient to absorb the whole track within the gas of the chamber. The calibration was performed at a different setting of the gain of the amplifier. Knowing the relative values of the gain in the two cases the energy of the fission pulses could be determined. The energy spectrum of the fission fragments is in close agreement with the energy spectra obtained by Jentschke (9) for the fission fragments from uranium 235 and uranium 238. It was concluded that the operation of the chamber was satisfactory.

The actual experiment on the initial ionization of fission fragments was carried out using nitrogen for the reasons already explained. A separate calibration was performed with polonium α-particles in nitrogen. In order to be able to apply this calibration to all subsequent measurements the gain

of the amplifier was measured in each case so that changes of gain could be allowed for. At each pressure the relation between the mean pulse height and high voltage was investigated, and a suitable collecting voltage chosen. The distributions obtained for the energy spent in ionization in the first 5.3, 2.3, and 1.1 mm. of the tracks in nitrogen reduced to normal temperature and pressure are reproduced in Figs. 4, *A*, 4, *B*, and 4, *C*, respectively. In these

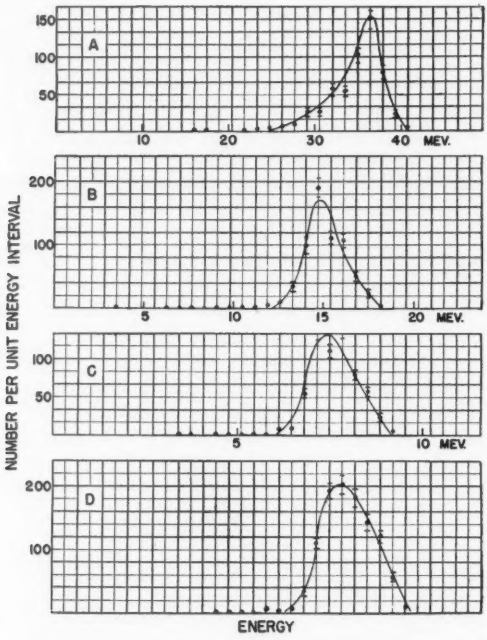

FIG. 4. *A. Energy distribution of 566 fission fragments from uranium 233 in nitrogen. The depth of the chamber was equivalent to 5.3 mm. path in standard nitrogen.*

B. 662 fragments. 2.3 mm. path in nitrogen.

*C. 680 fragments. 1.1 mm. path in nitrogen.**

D. 1274 fragments. 1.1 mm. path in nitrogen.

While the spectra in A, B, and C were obtained by the photographic method, that in D was obtained with an electronic pulse analyzer. As the analyzer was not calibrated in Mev. the abscissae are in arbitrary units.

spectra the energy lost by the two groups of fragments cannot be resolved. A definite separation into two groups can be made only at greater equivalent depths of the chamber. For instance, Fig. 3, *B*, shows the spectrum of pulse heights in the first 8.8 mm. of track. Here the two groups give energy losses that are sufficiently different for resolution.

* *Two experimental points have unfortunately been omitted. These lie just outside the upper border of the graph.*

The spectrum of pulses obtained with a depth of chamber equivalent to 1.1 mm. of nitrogen shows an interesting asymmetry (Fig. 4, *C*). A similar asymmetry is also evident for a depth equivalent to 2.3 mm. of nitrogen (Fig. 4, *B*). The spectrum rises more steeply on the low energy side in contrast to the behavior at depths of 5.3 mm. (Fig. 4, *A*) and 8.8 mm. (Fig. 3, *B*). This point was confirmed by repeating the measurement of the spectrum for a depth equivalent to 1.1 mm. using an electronic pulse analyzer (7), which was capable of giving better resolution than the photographic method. The spectrum of pulses is shown in Fig. 4, *D*, and its shape confirms the existence of the features observed using the photographic method. It is not possible to account for this behavior in terms of source thickness as energy losses in it would result in a more gradual rise on the low energy side of the peak. Consequently the observed spectra indicate the following.

1. The low energy group of fragments, represented by the left hand peak in the spectrum of total energies shown in Fig. 3, *A*, gives rise to a broader spectrum than does the high energy group. The ratio of the most probable energy of the low energy group to that of the high energy group is about 0.65, in agreement with earlier work (9).

2. In Fig. 3, *B* (equivalent depth of chamber = 8.8 mm. of nitrogen), the two peaks are closer together. If the left hand peak is again identified as the low energy group, the spectrum representing the low energy group is still broader than that representing the high energy group. The ratio of the energies spent by the two groups is now greater and equal to about 0.8.

3. In Fig. 4, *A* (equivalent depth of chamber = 5.3 mm. of nitrogen), the two peaks are no longer resolved, but the more gradual rise on the left hand side of the spectrum indicates that the ratio of the energies spent by the two groups is still less than unity.

4. In Figs. 4, *B*, and 4, *C*, (equivalent depths of chamber = respectively 2.3 mm. and 1.1 mm. of nitrogen), the two peaks are still unresolved, but the more gradual fall on the right hand side of the spectrum indicates that the ratio of the energies spent by the two groups of fragments has become greater than unity. In other words, the 'unresolved peaks' representing the two groups, which have gradually become closer together with decreasing pressure, have crossed over. In physical terms this means that the initial ionization of the low energy group is greater than that of the high energy group.

Finally, in Fig. 5 is plotted the mean energy spent in ionization by fission fragments in various distances from the beginning of the track obtained from these distributions. The mean energy spent in the first millimeter of the track in nitrogen at N.T.P. is 6.5 Mev.

Discussion

The conclusion that the initial ionization is greater for the low energy group of fission fragments than for the high energy group is in accord with the results

of measurements of the specific ionization of fission fragments made by Lassen (14), which were published after the completion of the present work.

There is a disagreement on this point among the various theoretical estimates of the initial ionization that have been made. The ratio of the energy spent in the first millimeter of track by the low energy group of fragments to that

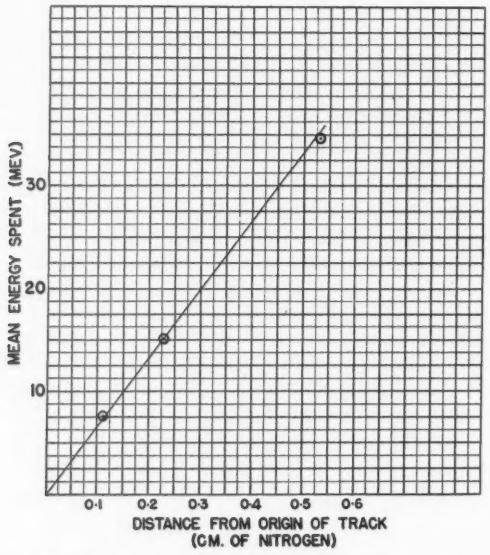

FIG. 5. *Graph of mean energy spent by the fission fragments (both groups) as a function of the distance from the source in nitrogen at N.T.P.*

spent by the high energy group is according to Bohr (2) less than unity. Lamb (11) and Knipp and Teller (10), on the other hand, obtain values for the ratio that are greater than unity. The results of the present work as well as those of Lassen mentioned above are thus in qualitative agreement with the predictions of Lamb and Knipp and Teller as far as the ratio of initial ionization by the two groups is concerned. It should be mentioned that evidence conflicting with the results of Lassen and the present work has recently been published by Demers (6) and Sherr and Peterson (17), who obtain a higher initial ionization by the high energy group of fragments.

Acknowledgments

The author wishes to express his gratitude to Dr. B. W. Sargent and Dr. B. Pontecorvo for helpful advice and encouragement in this work, and to Miss F. M. Gauthier and Miss E. J. Mooney for assistance with the measurements of the pulse heights.

References

1. BØGGILD, J. K., BROSTRØM, K. J., and LAURITSEN, T. Kgl. Danske Videnskab. Selskab. Math.-fys. Medd. 18 : No. 4. 1940.
2. BOHR, N. Phys. Rev. 59 : 270. 1941.
3. BRADBURY, N. E. Phys. Rev. 44 : 883. 1933.
4. BRADBURY, N. E. and TATEL, H. E. J. Chem. Phys. 2 : 835. 1934.
5. BUNEMANN, O., CRANSHAW, T. E., and HARVEY, J. A. Unpublished report, CRP-247. The use of grid chambers for α-ray analysis. National Research Council of Canada. 1946. (Report to be published.)
6. DEMERS, P. Phys. Rev. 70 : 974. 1946.
7. FREUNDLICH, H. F., HINCKS, E. P., and OZEROFF, W. J. Rev. Sci. Instruments, 18 : 90. 1947.
8. HEALEY, R. H. and REED, J. W. The behaviour of slow electrons in gases. Amalgamated Wireless (Australasia) Ltd., Sydney, Australia. 1941.
9. JENTSCHKE, W. Z. Physik, 120 : 165. 1943.
10. KNIPP, J. and TELLER, E. Phys. Rev. 59 : 659. 1941.
11. LAMB, W. E., Jr. Phys. Rev. 58 : 696. 1940.
12. LASSEN, N. O. Phys. Rev. 68 : 142. 1945.
13. LASSEN, N. O. Phys. Rev. 69 : 137. 1946.
14. LASSEN, N. O. Phys. Rev. 70 : 577. 1946.
15. MARGENAU, H., MCMILLAN, F. L., Jr., DEARNLEY, I. H., PEARSALL, C. S., and MONTGOMERY, C. G. Phys. Rev. 70 : 349. 1946.
16. SEABORG, G. T., GOFMAN, J. W., and STOUGHTON, R. W. Phys. Rev. 71 : 378. 1947.
17. SHERR, R. and PETERSON, R. Rev. Sci. Instruments, 18 : 567. 1947.

SURFACE AREA MEASUREMENTS OF FINE POWDERS USING MODIFIED PERMEABILITY EQUATIONS[1]

By P. C. Carman and J. C. Arnell

Abstract

The several modified Kozeny equations for the measurement of the specific surface of fine powders by gas-permeability methods have been compared. The equations all give very similar surface area values for a set of experimental data. The physical significance of the empirical constants used is discussed and preference is indicated.

Introduction

Within the past two years, two very similar equations have been proposed as modifications of the Kozeny equation for the measurement of the surface area of very fine powders by gas-permeability methods. The use of the Kozeny equation for the determination of the specific surface of powders by the permeability method was first proposed by Carman (5) and was found to give values for the specific surface of a powder for particles having specific surfaces of less than about 5,000 sq. cm. per cc. that were in satisfactory agreement with other methods, such as sedimentation and microscope counting. It was found, however, that, as the particle size decreased and the specific surface increased, divergences were observed between the gas-permeability value of specific surface and that obtained by other methods. These divergences have been accounted for by modifying the Kozeny equation to account for the 'slip' that occurs when a gas flows through capillaries of the same order of magnitude as the mean free path of the flowing gas.

A comparison of two similar modifications of the Kozeny equation is presented in this paper.

Theoretical

The Poiseuille type of equation for capillaries of any shape takes the form (4),

$$u_e = \frac{m^2}{k_0 \eta} \cdot \frac{\triangle p}{L_e}, \qquad (1)$$

where u_e = actual velocity of the fluid through the bed in centimeters per second,

m = mean hydraulic radius in centimeters,

$\triangle p$ = pressure drop across the bed in dynes per square centimeter,

k_0 = shape factor, whose value generally lies between 2 and 3 (4),

η = viscosity of the fluid in poises, and

L_e = actual length of path traversed by the fluid through the bed in centimeters.

[1] *Manuscript received November 26, 1947.*

Joint contribution from the National Chemical Research Laboratory, Pretoria, South Africa, and the Defence Research Chemical Laboratories, Ottawa, Canada.

For circular capillaries, $m = r/2$, where r = radius of the capillary, and $k_0 = 2$ and Equation (1) takes the form of the usual Poiseuille equation. Application of this equation to granular beds (4) by putting

$$u = u_e \cdot \epsilon \cdot \frac{L}{L_e} = \frac{Q}{A},$$

$$m = \frac{\epsilon}{S_v(1 - \epsilon)}, \quad \text{and}$$

$$k = k_0 \cdot \left(\frac{L_e}{L}\right)^2,$$

leads to a form of the original Kozeny equation (7),

$$Q = \frac{A \triangle p}{k \eta L} \cdot \frac{\epsilon^3}{S_v^2(1 - \epsilon)^2}, \tag{2}$$

where u = approach (apparent) velocity of the fluid in centimeters per second,

ϵ = volume of pore space per unit volume (porosity),

L = length of bed in centimeters,

Q = rate of flow of the fluid in cubic centimeters per second,

A = cross-sectional area of the bed in square centimeters,

S_v = specific surface of the granules in square centimeters per cubic centimeter, and

k = Kozeny's constant, which is approximately equal to 5.

Rigden (9) applied the same considerations as used above to the classical Poiseuille equation corrected for 'slip', and arrived at an equation having the form:

$$Q = \frac{A \epsilon \triangle p}{k \eta L} \left[\left\{\frac{\epsilon}{S_v(1 - \epsilon)}\right\}^2 + \frac{2 \epsilon x \lambda}{S_v(1 - \epsilon)}\right], \tag{3}$$

where x = a constant, having the value of 0.874, and

λ = mean free path of the gas molecules.

Carman (6) has since pointed out that the slip correction factor used by Rigden was in the form used for circular capillaries, whereas, for granular beds, the correction should be larger than that used by Rigden. He recommends the use of a slightly modified equation used by Lea and Nurse (8, pp. 27-33), which may be written:

$$Q = \frac{A \epsilon \triangle p}{k \eta L} \left[\left\{\frac{\epsilon}{S_v(1 - \epsilon)}\right\}^2 + \left(\frac{2}{f} - 1\right) \sqrt{\frac{\pi}{2} \frac{R_0 T}{M}} \frac{k_0 \eta \epsilon}{S_v(1 - \epsilon) p}\right]. \tag{4}$$

where f = fraction of molecules evaporated from the surface, or $(1 - f)$ = the fraction of molecules undergoing elastic collisions with the surface, and

$p = (p_1 + p_2)/2$ = mean pressure of the gas in dynes per square centimeter.

Arnell (1), by analogy with the Knudsen semiempirical equation for the flow of gas through capillary tubes at all pressures, arrived at the following equation:

$$Q = \frac{A\epsilon\triangle p}{k\eta L}\left[\left\{\frac{\epsilon}{S_v(1-\epsilon)}\right\}^2 + \frac{8}{3}\sqrt{\frac{2R_0T}{\pi M}}\,\frac{k\eta\delta\alpha}{S_v(1-\epsilon)p}\right], \qquad (5)$$

where R_0 = gas constant in absolute units,
T = absolute temperature,
M = molecular weight of the gas,
δ = variable factor, having a value of approximately 0.9.
α = fraction effective void area and is given by the equation, $\log_{10}\alpha = 1.41\epsilon - 1.40$.

From a comparison of Equations (4) and (5), it is seen that the first terms on the right-hand sides are equal and identical to the simple Kozeny equation (Equation (2)). The second terms on the right-hand sides should also be equal, hence:

$$\left(\frac{2}{f} - 1\right)\sqrt{\frac{\pi}{2}}\,\frac{R_0T}{M}\,\frac{k_0\eta\epsilon}{S_0(1-\epsilon)p} = \frac{8}{3}\sqrt{\frac{2R_0T}{\pi M}}\,\frac{k\eta\delta\alpha}{S_v(1-\epsilon)p},$$

which reduces to:

$$\left(\frac{2}{f} - 1\right)\sqrt{\frac{\pi}{2}}\,k_0\epsilon = \frac{8}{3}\sqrt{\frac{2}{\pi}}\,k\delta\alpha.$$

If f is taken equal to 0.84 (6) and δ as 0.9 (1),

$$\left(\frac{2}{f} - 1\right)\sqrt{\frac{\pi}{2}} \simeq \frac{8}{3}\sqrt{\frac{2}{\pi}}\,\delta,$$

and actual equality is obtained, if $f = 0.79$, which is quite a reasonable value. Thus, if Equations (4) and (5) are identical,

$$\frac{\alpha}{\epsilon} \simeq \frac{k_0}{k}. \qquad (6)$$

Arnell (1) has defined α as a function of ϵ, which could be expressed by the equation $\log_{10}\alpha = 1.41\epsilon - 1.40$, and α/ϵ was therefore a variable, which increased with increasing porosity and approached 1 in the limit. Carman (4) defined k_0/k as equal to $(L/L_e)^2$, that is, he attributed this factor to the tortuous path that must be followed by a fluid in traversing a granular bed. Within the normal working range of porosities, k_0/k has been found to have a value that lies between 0.4 and 0.6, and k_0/k should be constant for any bed where the ratio of the actual length of path traversed, L_e, to the length of the bed, L, is a constant. It now is necessary to re-examine available data to determine whether α/ϵ (or its equivalent) increases with increasing porosity or remains approximately constant.

Calculations

It is possible to study this aspect of the permeability equation by recalculating the data quoted by Arnell (2) for the flow of air through beds of finely powdered quartz and inorganic pigment powders. Arnell originally evaluated

α, using his empirical relation between α and ϵ, and calculated the specific surface using only the second term on the right-hand side of Equation (5). The specific surface can also be calculated using the Kozeny part (first term) of either Equation (4) and (5) and then applying the result to give a value of α/ϵ. This has been done here and the results are given in Table I, together with the original specific surface values.

TABLE I

VALUES OF THE SPECIFIC SURFACE CALCULATED BY DIFFERENT METHODS FROM THE EXPERIMENTAL DATA OBTAINED BY ARNELL (2) ON BEDS OF FINE POWDERS

Porosity, ϵ	Specific surface (original), S_v, sq.m./cc.	Specific surface (recalculated), S_v, sq.m./cc.	$\frac{\alpha}{\epsilon}$
Powdered quartz			
0.425	9	9.4	0.40
0.428	8	9.3	0.43
0.439	7	8.5	0.48
0.475	7	8.0	0.50
0.475	9	9.3	0.40
0.498	10	10.3	0.38
0.510	10	10.1	0.39
0.514	9	9.4	0.40
0.517	9	9.7	0.40
0.528	10	10.0	0.40
0.537	9	8.7	0.46
0.545	9	9.0	0.44
0.563	8	7.8	0.52
0.584	10	8.9	0.42
0.585	11	9.4	0.39
0.604	10	8.8	0.41
0.610	11	9.1	0.45
0.619	10	9.3	0.43
0.621	9	7.6	0.51
	9.1	9.1	0.43
Mapico Red No. 297			
0.636	32	46.3	0.61
0.677	34	39.9	0.63
0.692	40	43.2	0.54
0.718	40	37.3	0.56
0.721	41	40.2	0.55
0.752	44	33.5	0.55
0.766	40	39.8	0.61
	38.7	39.1	0.58
Mapico Yellow Lemon			
0.676	25	29.6	0.48
0.700	29	28.4	0.51
0.704	24	25.8	0.60

TABLE I—*Concluded*

VALUES OF THE SPECIFIC SURFACE CALCULATED BY DIFFERENT METHODS FROM THE EXPERIMENTAL DATA OBTAINED BY ARNELL (2) ON BEDS OF FINE POWDERS—*Concluded*

Porosity, ϵ	Specific surface (original), S_v, sq.m./cc.	Specific surface (recalculated), S_v, sq.m./cc.	$\frac{\alpha}{\epsilon}$
Mapico Yellow Lemon—Concluded			
0.754	26	24.1	0.63
0.767	29	27.3	0.56
0.780	28	27.2	0.62
0.807	24	21.4	0.74
	26.4	26.3	0.59
Hydrated yellow iron oxide			
0.702	31	33.9	0.56
0.721	36	33.9	0.52
0.747	32	29.3	0.60
0.771	33	31.6	0.54
0.778	38	28.5	0.53
0.781	32	27.9	0.64
	33.5	30.9	0.57
Hydrated chromic oxide			
0.656	71	37	—
0.664	49	29	—
0.682	58	33	—
0.691	39	23	—
0.706	33	17	—
0.711	27	16	—
	46	26	
Pure red iron oxide			
0.479	10	12.4	0.48
0.491	13	15.1	0.39
0.543	12	12.6	0.42
0.552	12	12.2	0.44
0.568	10	10.5	0.51
0.583	12	11.0	0.48
	11.4	12.3	0.45
Pure chromic oxide			
0.464	13	14.9	0.34
0.487	13	11.7	0.35
0.493	11	13.8	0.39
0.521	11	7.7	0.43
0.526	11	7.7	0.40
	11.8	11.2	0.38

Discussion

Lea and Nurse (8, pp. 27-33), in discussing the modified equations, expressed no physical picture, but used a slip factor, Z, which on comparison with the equations previously discussed, gives the following equivalents:

$$\text{Equation (4)} \qquad Z = k_0 \left(\frac{2}{f} - 1\right)$$

$$\text{Equation (5)} \qquad Z = \frac{16}{3\pi} \frac{\delta k \alpha}{\epsilon} = 7.65 \frac{\alpha}{\epsilon}, \tag{7}$$

if $\delta = 0.9$ and $k = 5.0$.

Lea and Nurse have calculated the values of the slip factor, Z, for several powders. It is of interest to consider these Z values and to convert them to values of α/ϵ by means of Equation (7). These valuations are reproduced in Table II.

TABLE II

SLIP FACTORS AND VALUES OF α/ϵ FOR VARIOUS SUBSTANCES

(From Lea and Nurse (8, pp. 27-33))

Substance	Porosity	Slip factor, Z	α/ϵ
Cement 240	0.450	3.29	0.43
	0.475	3.25	0.43
	0.500	3.53	0.46
	0.525	3.27	0.43
Cement 299	0.475	3.32	0.43
Zinc dust	0.425	3.63	0.47
Lithopone	0.500	4.07	0.53
	0.540	3.53	0.46
	0.600	2.94	0.38
	0.650	3.77	0.49
Kaolin	0.500	2.73	0.36
	0.600	2.78	0.36
	0.625	3.21	0.42
	0.650	2.91	0.38

Rigden (9) found that his equation (Equation (2)) did not give a constant value for the specific surface of a powder over a range of mean pressures, but showed a fall-off in the value for the surface at low pressures. This effect is due to the use of a constant, X, having too small a value. By reading from his curves in Figs. 3 and 4 and using Table II of his paper, it is possible to recalculate Rigden's data using either the Lea and Nurse type equation or Equation (5) and thus obtain constant values for the specific surfaces. The resulting values are given in Table III.

From the calculations in Tables I, II, and III, it appears that the values of α/ϵ lie, in general, within the range of 0.4 and 0.6 and show no real trend with increasing porosity. This is the same range as was found for k_0/k

TABLE III

SLIP FACTORS AND VALUES OF α/ϵ FOR VARIOUS SUBSTANCES

(After Rigden (9))

Substance	Specific surface (original) S_v, sq.m./cc.	Slip factor, Z	$\frac{\alpha}{\epsilon}$	Specific surface (recalculated) S_v, sq.m./cc.
Portland cement	1.28	4.3	0.56	1.41
Rapid-hardening cement	1.55	3.4	0.44	1.58
Fine slate powder	2.80	3.9	0.51	3.05
'Air-blown' slate	8.43	3.5	0.46	9.44

and it therefore seems reasonable to assume that Equation (6) is a true equality. The term k_0/k is expressed in terms of the increased length of the tortuous path, followed by a fluid in traversing a bed of granules, over the actual length of the bed, and, as it appeared in the derivation of the original Kozeny equation, it should appear in the modifying term. Also the ratio α/ϵ does not show a definite increase with increasing porosity, as it should by definition, and it therefore appears advisable to substitute k_0/k for α/ϵ in Equation (5) and to use it in the following form:

$$Q = \frac{A\epsilon\triangle p}{k\eta L}\left[\left\{\frac{\epsilon}{S_v(1-\epsilon)}\right\}^2 + \frac{8}{3}\sqrt{\frac{2R_0T}{M}}\,\frac{\delta k_0\eta\epsilon}{S_v(1-\epsilon)p}\right], \qquad (8)$$

where k_0 has a probable value of about 2.5.

It is now of interest to re-examine the permeability data on carbon blacks reported by Arnell (3) and compare the specific surface values of these blacks given by Equation (8) with those quoted in his paper. The carbon blacks are of particular interest in that the majority of the beds examined showed a constant mass flow over a fairly wide mean pressure range, so that only the second term on the right-hand side of Equation (8) enters into the calculation of specific surface.

In Table IV are presented the recalculated values of the specific surfaces of the carbon blacks using $k_0 = 2.5$ and $\delta = 0.96$ (3) in Equation (8), together with the original values obtained from the permeability data and electron microscope counting. Where the first term on the right-hand side of Equation (8) (Kozeny equation) could be applied, the data are included.

In general, the specific surfaces of the carbon blacks calculated by means of Equation (8) agree very closely with the original calculations. This fact lends support to the view that α/ϵ is probably equivalent to k_0/k and may be replaced by it. Further experimentation should be carried out to settle this point, but for the present either Equation (4) or Equation (8) may be used for the calculation of the specific surface of very fine powders where 'slip' occurs in the gas flow measurements.

TABLE IV

SURFACE AREAS OF CARBON BLACKS

(From Arnell (3))

Black	Porosity	Specific surface, sq.m./cc.			
		Permeability			Electron microscope
		Original	Equation (8)	Kozeny	
Kosmos 20	0.554	43	50		
	0.568	43 } 42	48 } 48	—	47
	0.579	41	45		
Kosmos 40	0.584	67	74		
	0.634	59 } 65	60 } 68	—	72
	0.638	69	70		
Shawinigan 100% Comp.	0.729	67	57	38	
	0.762	82 } 74	66 } 59	42 } 41	78
	9.791	72	55	44	
Statex B	0.601	97	104	—	
	0.610	99	105	—	
	0.619	103 } 99	107 } 103	—	72
	0.636	98	97	—	
	0.645	96	102	73	
Statex A	0.603	98	104	—	
	0.639	100 } 100	101 } 102	—	86
	0.656	103	101	89	
Kosmobile 77	0.638	155	156		
	0.670	150	143		
	0.672	155 } 146	148 } 141	—	161
	0.673	131	125		
	0.674	131	125		
	0.675	155	147		
	0.715	93	80		
	0.721	70	61		
Dixiedensed HM	0.696	164	150	118	
	0.704	144 } 150	129 } 134	91	165
	0.716	141	124	66	
Kosmobile S	0.653	178	175	—	
	0.666	197 } 182	189 } 176	—	162
	0.673	171	163	—	
	0.692	126	116	—	
	0.707	71	64	43	
	0.718	45	39	—	
Spheron 9	0.676	189	179		
	0.696	180 } 184	164 } 170	—	144
	0.696	182	166		
Voltex	0.707	344	307		
	0.717	328 } 326	288 } 280	—	220
	0.765	306	245		
Neo Spectra Mk. II	0.823	435	309		
	0.825	418 } 428	296 } 303	—	259
	0.828	430	303		

References

1. ARNELL, J. C. Can. J. Research, A, 24 : 103. 1946.
2. ARNELL, J. C. Can. J. Research, A, 25 : 191. 1947.
3. ARNELL, J. C. and HENNEBERRY, G. O. Can. J. Research, A, 26 : 29. 1948.
4. CARMAN, P. C. Trans. Inst. Chem. Engrs. London, 15 : 150. 1937.
5. CARMAN, P. C. J. Soc. Chem. Ind. Trans. 57 : 225. 1938.
6. CARMAN, P. C. Nature, 160 : 301. 1947.
7. KOZENY, J. Akad. Wiss. Wien. Math.-naturw. Klasse Sitzber 136 (Abt. IIa) : 271. 1927.
8. LEA, F. M. and NURSE, R. W. Trans. Inst. Chem. Engrs. London, and Soc. Chem. Ind. Symposium on "Particle Size Analysis". Advance copy, Feb. 4, 1947.
9. RIGDEN, P. J. J. Soc. Chem. Ind. 66 : 130. 1947.

SOLAR ECLIPSE OBSERVATIONS OF THE IONOSPHERE[1]

By C. W. McLeish

Abstract

The results are presented of ionosphere measurements made in the region of totality during the eclipse of July 9, 1945. An analysis of the results shows effective recombination coefficients of 1.6×10^{-8} for E region, 1.4×10^{-8} for F_1 region, and 1.0×10^{-9} for F_2 region. Evidence of a variable coefficient for E region agrees with the suggestion of Massey and others of a high negative ion density at this level.

Introduction

Because the presence of the ionized regions of the atmosphere, commonly known as the ionosphere, is due mainly to absorbed ultraviolet energy from the sun, a solar eclipse affords an unusual opportunity to study the effect of a known change in radiation over a short period.

For the 1945 total eclipse in Canada, a site was chosen at Victoria Beach, Manitoba, on the shores of Lake Winnipeg. Fig. 1 is a general view showing the lorry, which housed the equipment, the antenna mast, darkroom hut, and supplies tent. This point (lat. 50°48′N, long. 96°32′W) was directly beneath the totality belt at the 200 km. level. Obscuration of the sun here was about 95% on the ground, 98% at 100 km., and 100% at 200 km. The eclipse occurred in the early morning, the sun's elevation being less than 7° on first contact and about 25° on fourth contact.

Observations

An automatic ionosphere recorder was constructed at the National Research Laboratories especially for the eclipse observations, and the equipment was set up on the site and in operation by July 5. Details of this equipment are to be found in the N.R.C. Radio Branch Report PRA No. 132 (3). Fig. 2 is a front view showing the transmitter–receiver rack on the left, the scanner and visual monitor center, and the camera recording unit on the right. The equipment produced virtual height versus frequency curves on 35 mm. film, covering the range 1 Mc. per sec. to 16 Mc. per sec. logarithmically in just over two minutes. Following an observational program laid down by the Canadian Radio Wave Propagation Committee for the ionosphere stations in Canada, records were obtained at 15 min. intervals throughout the month from July 5 to Aug. 5 except on the eclipse day when records were made at five minute intervals over an eight hour period (Fig. 3).

Conditions were quite disturbed for a few days preceding the eclipse when strong auroral displays were seen. Data for the eclipse day are compared with control data for three days before and three days after the event. Owing

1 *Manuscript received October 7, 1947.*

Contribution from the Radio and Electrical Engineering Division, National Research Laboratories, Ottawa, Canada. Issued as N.R.C. No. 1718.

to slight disturbances in the E region on July 6 and 12, data for these two days were eliminated in E region calculations.

The photographic records for the days July 6 to 12 inclusive have been carefully analyzed. Virtual heights of the ionized regions were read to an accuracy of 10 km. and critical penetration frequencies to ± 0.05 Mc. per sec. The actual time of observation of any particular critical frequency was tabulated to the nearest half-minute.

Analysis of Results

The object of the following analysis is to investigate the general behavior of maximum electron density in each of the regions E, F_1, and F_2. The correlation between the observed values of maximum density during the eclipse and the values predicted by the simple recombination law, $\frac{dN}{dt} = q - \alpha N^2$, is studied for the three regions. Maximum electron density, N, is derived from the equation relating it to the critical penetrating frequency of the ordinary ray, $N = 1.24 \times 10^{-8} f^2$, where N is maximum electron density in the region in terms of electrons per cubic centimeter, q is ionizing rate at the level of maximum density N, in terms of electrons per cubic centimeter per second, α is recombination coefficient, and f is frequency in cycles per sec.

The following is the method of analysis used in interpreting the eclipse effects in the ionosphere. From the control data a normal day electron density curve for July 9 was drawn by interpolation for each of the three regions, F_1, E, and F_2 (Curve 1 in Figs. 4, 5, and 6). By assuming values of recombination coefficient, α, for each of the three regions the curve of ionizing rate, q, was drawn as Curve 2 in Figs. 4, 5, and 6. Making a further assumption that the ionizing rate at a given time during the eclipse was proportional to the visible area of the sun's disc, Curve 3 was constructed for each region. Finally by using values of q from Curve 3, the initial value of N and $\frac{dN}{dt}$ from Curve 1 at first contact, and the assumed value of α, curves were constructed graphically to satisfy the equation $\frac{dN}{dt} = q - \alpha N^2$. For each region several values of α were assumed and curves constructed although only those lying close to the observed points are shown.

Let us first consider the correlation shown for F_1 region results in Fig. 4. Because F_1 does not regularly appear until around 6 a.m. in July, Curve 1 is extrapolated beyond the mean of the observed values, back to the time of the beginning of the eclipse. Curves 4 and 5 are electron density curves calculated from assumed values of α of 0.7×10^{-8} and 1.4×10^{-8}. Observed points for F_1 maximum electron density are in fairly close agreement with the curve for $\alpha = 1.4 \times 10^{-8}$ except near the beginning of the eclipse. The deviation here is most probably due partly to error in extrapolation of the mean data and partly to the normal day to day spread in F_1 density. It can be seen that the minimum value of N for F_1 and the time after totality at which it occurs correspond quite closely to the curve for $\alpha = 1.4 \times 10^{-8}$.

FIG. 1. *Site at Victoria Beach, Man.*

PLATE II

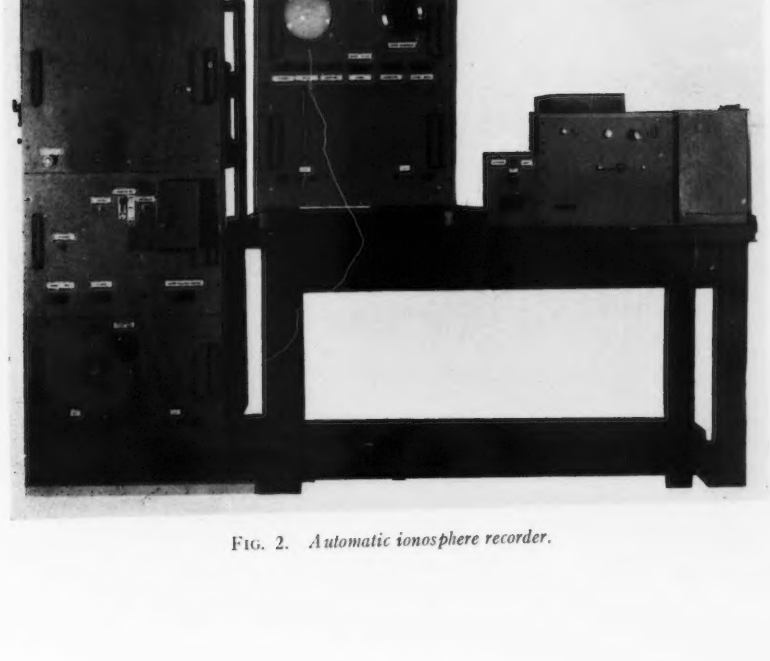

FIG. 2. *Automatic ionosphere recorder.*

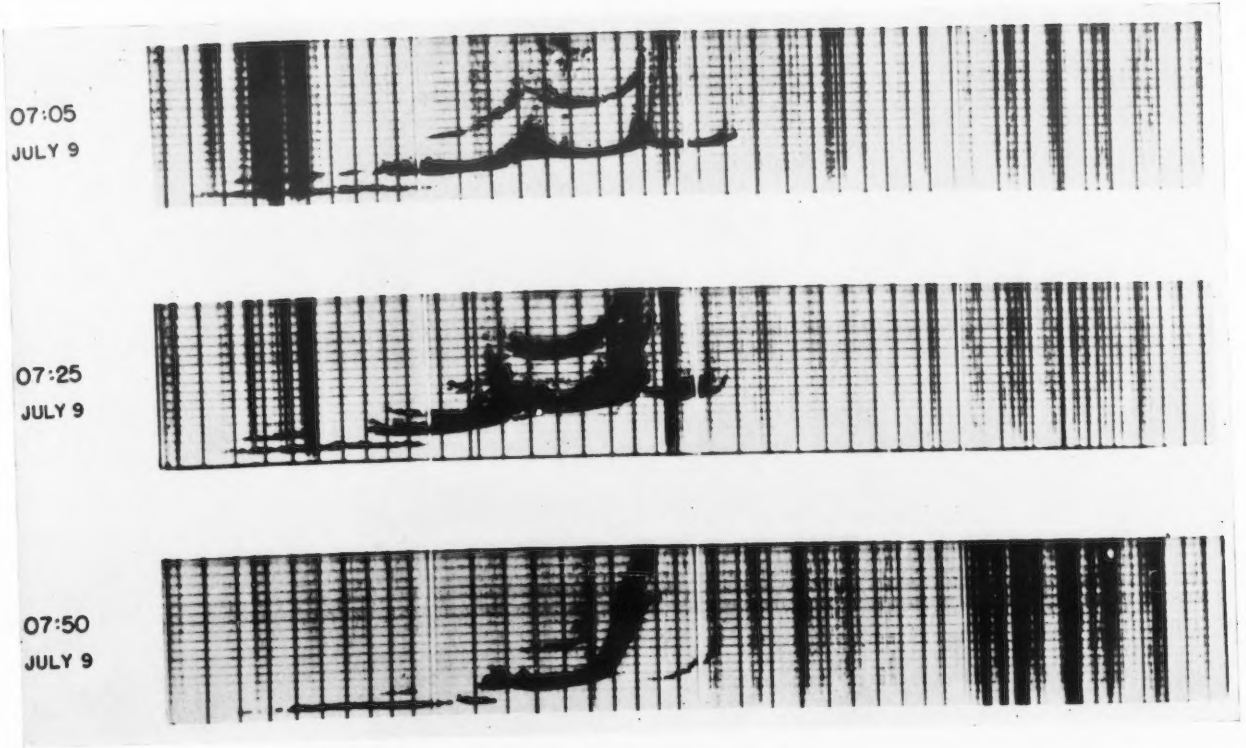

FIG. 3. *Eclipse day ionosphere records.*

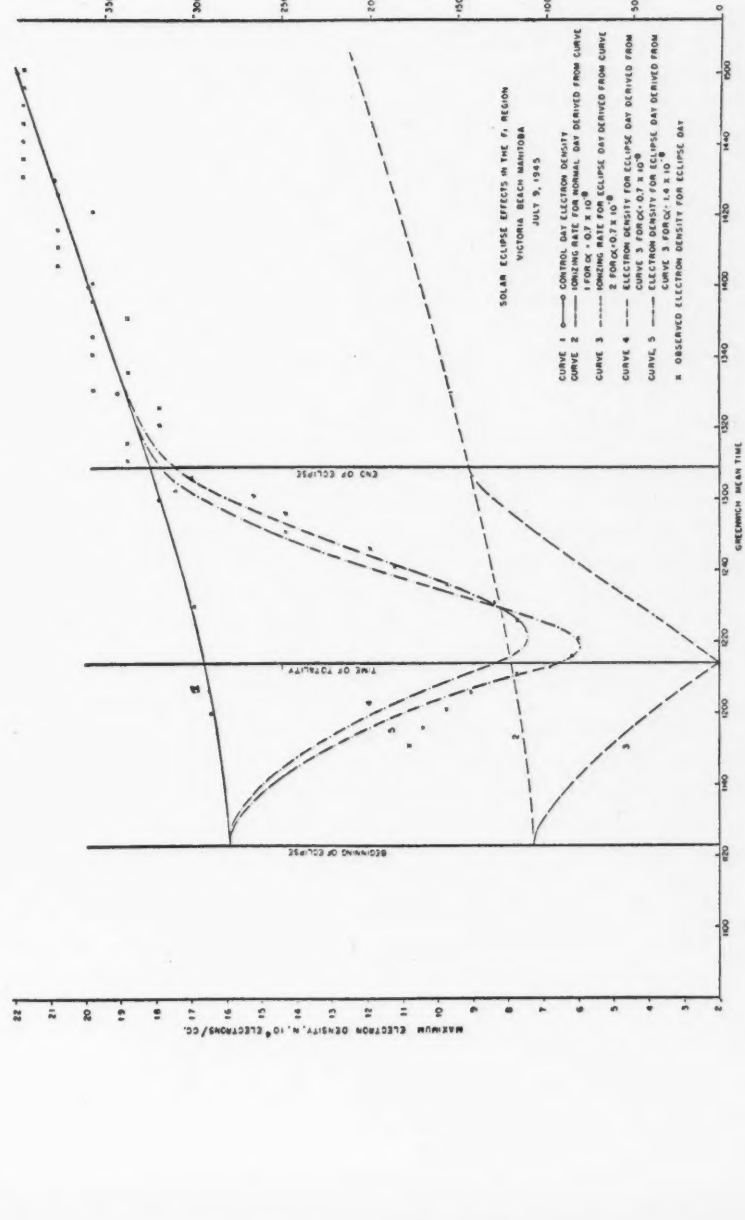
SOLAR ECLIPSE EFFECTS IN THE F1 REGION
VICTORIA BEACH MANITOBA
JULY 9, 1945
CURVE 1 ⟵ CONTROL DAY ELECTRON DENSITY
CURVE 2 —— IONIZING RATE FOR NORMAL DAY DERIVED FROM CURVE 1 FOR α = 0.7 x 10⁻⁸
CURVE 3 - - - - IONIZING RATE FOR ECLIPSE DAY DERIVED FROM CURVE 2 FOR α = 0.7 x 10⁻⁸
CURVE 4 —— ELECTRON DENSITY FOR ECLIPSE DAY DERIVED FROM CURVE 3 FOR α = 0.7 x 10⁻⁸
CURVE 5 —— ELECTRON DENSITY FOR ECLIPSE DAY DERIVED FROM CURVE 3 FOR α = 1.4 x 10⁻⁸
x OBSERVED ELECTRON DENSITY FOR ECLIPSE DAY
IONIZING RATE AT LEVEL OF MAXIMUM N (ELECTRONS/CC/MIN.)
MAXIMUM ELECTRON DENSITY, N, 10⁵ ELECTRONS/CC.
GREENWICH MEAN TIME
BEGINNING OF ECLIPSE
TIME OF TOTALITY
END OF ECLIPSE

FIG. 4.

E region results do not show the same degree of correlation as observed for F_1. Fig. 5 shows derived curves for two assumed values of α of 1.6×10^{-8} and 1.9×10^{-8}. Curve 6 is a smooth curve showing the general trend of observed points. Although Curve 6 has the same minimum N falling at about the same delay time as the curve for $\alpha = 1.6 \times 10^{-8}$, interpretation of this is limited by the accuracy of the observations to a qualitative one, but the discrepancy may be either in the assumption that the sun's radiation is proportional to exposed area only, or in the assumption that the region obeys a simple recombination law. If one assumes that the sun's corona contributes a considerable proportion of the ionizing radiation so as to cause a more rapid fall and rise of q near first and fourth contacts, then one would expect a considerable ionizing rate at totality from the annular ring of the corona which is still exposed. To allow electron density to fall as low as that observed experimentally a large value of α must then be assumed. This, however, would not result in the same order of delay time for the minimum value of N as that observed (5 ± 1 min.). This alone would seem to rule out any large coronal effect, apart from the fact that none is definitely observed in results of the other regions.

On the interpretation that the region E obeys a different recombination law from the simple one assumed, measurements of the observed curve show a large change of effective recombination coefficient from near the time of first contact to totality. The measurements fit well with the conclusions of Massey, Bates, and others (1, 4) who show that there is probably a high concentration of negative oxygen ions at E region levels. This results in an effective recombination coefficient dependent on the ratio of ion density to electron density in a neutral medium (2). The equation of equilibrium given (1) is

$$\frac{dN}{dt} = q - \left(\alpha_e + \lambda\alpha_i + \frac{1}{N_+}\frac{d\lambda}{dt}\right) N^2 \qquad (1)$$

where N is electron density, electrons per cubic centimeter,
N_+ is positive ion density, ions per cubic centimeter,
λ is ratio of negative ion to electron density,
α_e is recombination coefficient of electrons and positive ions, and
α_i is the coefficient for electron transfer from negative to positive ions.

Probable values assigned to these coefficients are $\alpha_e = 5 \times 10^{-12}$ and $\alpha_i = 2 \times 10^{-11}$, which are derived from controlled laboratory experiments. Because λ is large we may simplify Equation (1) to obtain the approximation

$$\frac{dN}{dt} = q - \lambda\alpha_i N^2 \qquad (2)$$

in which it is assumed that $\frac{d\lambda}{dt}$ is small.

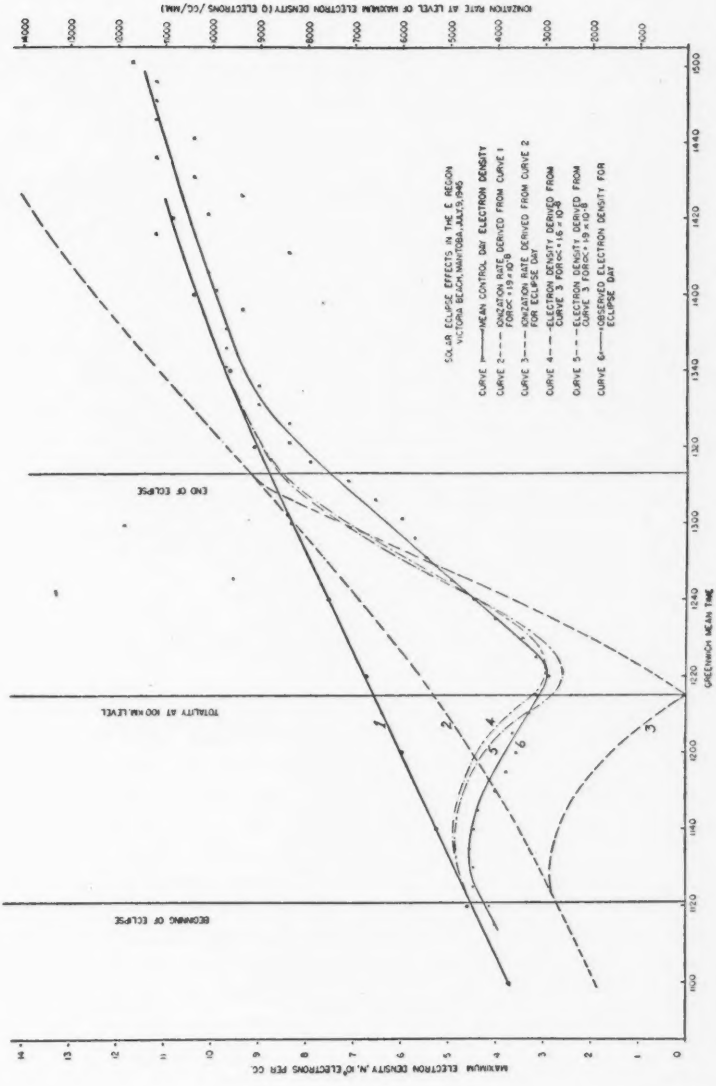
SOLAR ECLIPSE EFFECTS IN THE E REGION
VICTORIA BEACH, MANITOBA, JULY 9, 1945
CURVE 1——MEAN CONTROL DAY ELECTRON DENSITY
CURVE 2- - - IONIZATION RATE DERIVED FROM CURVE 1 FOR $I_0 = 10^8$
CURVE 3- - - IONIZATION RATE DERIVED FROM CURVE 2 FOR ECLIPSE DAY
CURVE 4- - -ELECTRON DENSITY DERIVED FROM CURVE 3 FOR $\alpha = 16 \times 10^{-8}$
CURVE 5- - -ELECTRON DENSITY DERIVED FROM CURVE 3 FOR $\alpha = 19 \times 10^{-8}$
CURVE 6——OBSERVED ELECTRON DENSITY FOR ECLIPSE DAY
BEGINNING OF ECLIPSE
TOTALITY AT 100 KM LEVEL
END OF ECLIPSE
GREENWICH MEAN TIME
MAXIMUM ELECTRON DENSITY $N_e \times 10^5$ ELECTRONS PER CC
IONIZATION RATE AT LEVEL OF MAXIMUM ELECTRON DENSITY (Q ELECTRONS /CC/MM.)

FIG. 5.

At the time 1127 1/2 G.M.T. the value of q reaches a maximum $\left(\frac{dq}{dt} = 0\right)$ so that at this point $\frac{d^2N}{dt^2} = -2N\lambda_1\alpha_i \frac{dN}{dt}$, where λ_1 is the negative ion electron ratio at this time. Measurements of Curve 6 in Fig. 5 give values at this time of $N = 4.50 \times 10^4$ electrons per cc., $\frac{dN}{dt} = 3.58$ electrons per cc. per sec., and $\frac{d^2N}{dt^2} = -0.0136$ electrons per cc. per sec.^{2}

Thus,

$$\lambda_1\alpha_i = -\frac{\frac{d^2N}{dt^2}}{2N\frac{dN}{dt}} = 4.2 \times 10^{-8} \text{ (the effective coefficient),}$$

or

$$\lambda_1 = \frac{4.2 \times 10^{-8}}{2 \times 10^{-11}} = 2100.$$

The figure λ_1 may be correct only as to order of magnitude but serves as a useful comparison with the result obtained at totality (1215 G.M.T.), when, q being zero, $\frac{dN}{dt} = \lambda_2\alpha_i N^2$, where λ_2 is that occurring at 1215 G.M.T.

From the observed curve, $N = 3.1 \times 10^4$ electrons per cc. and $\frac{dN}{dt} = -7.69$ electrons per cc. per sec. Thus

$$\lambda_2\alpha_i = 0.8 \times 10^{-8}, \text{ (effective coefficient)}$$

or

$$\lambda_2 = \frac{0.8 \times 10^{-8}}{2 \times 10^{-11}} = 400.$$

The drop in λ from 2100 to 400 indicated here shows that the term $\frac{1}{N_+}\frac{d\lambda}{dt}$ is likely to be of account in this case.

F_2 region results are shown in Fig. 6. On the eclipse day and on the control days F_2 displayed much more irregularity of critical frequency than did either of the other two regions. The experimental results are, therefore, much less significant in this case. Curve 1, the mean control day density, shows a hump at about 1230 G.M.T. Checking the records for all the days in the eclipse month showed only a slight possibility of a systematic rise of critical frequency at this time. The apparent rise in fact may be due only to the difficulties of analysis, as it appears shortly after the separation of F_2 and F_1 regions. It was, therefore, assumed that the hump was a random variation effect, not smoothed out by control day data, which could not be accepted as a characteristic of the F_2 region. Curves 2, 3, and 4 were derived from Curve 1 (neglecting the hump) for an assumed effective recombination coefficient of 0.1×10^{-8}. It can be seen that the observed points, though badly scattered, show some correlation with the curve. Electron densities were lower both before and after the eclipse than those predicted from the control days, but are well within the expected day to day spread.

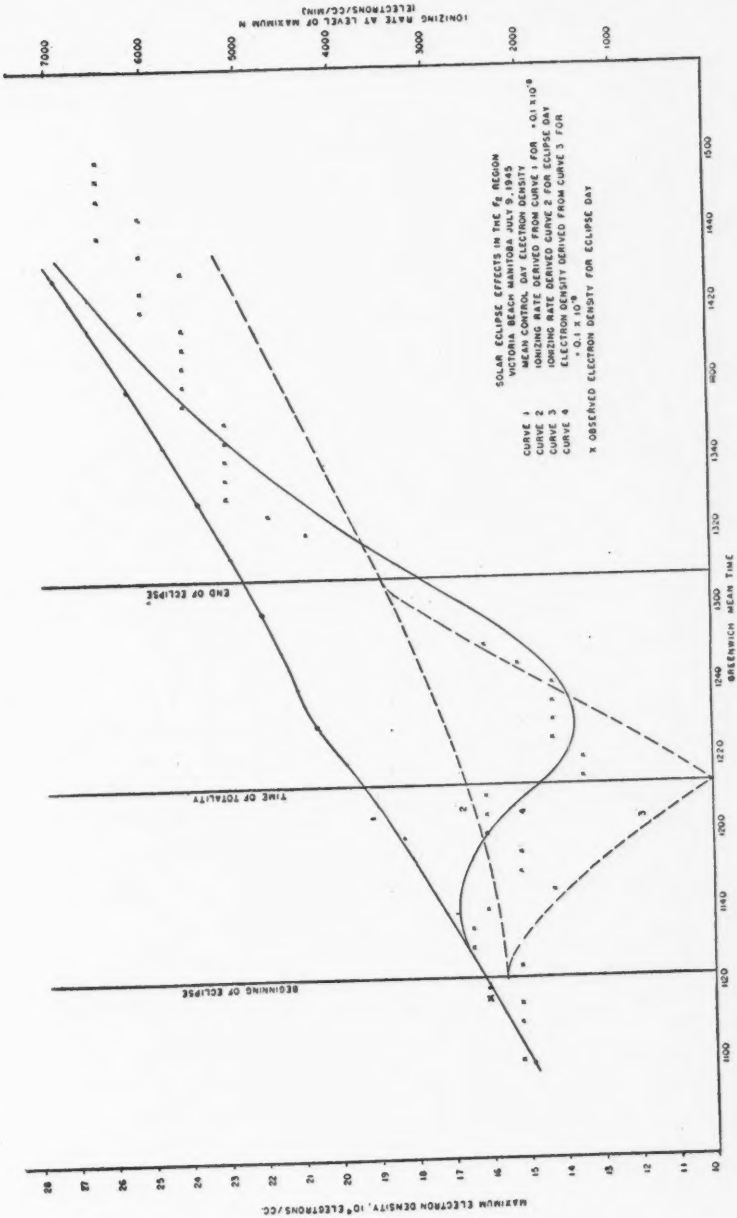
SOLAR ECLIPSE EFFECTS IN THE F_2 REGION
VICTORIA BEACH MANITOBA JULY 9, 1945
MEAN CONTROL DAY ELECTRON DENSITY
CURVE 1 IONIZING RATE DERIVED FROM CURVE 1 FOR $\cdot 01 \times 10^9$
CURVE 2 IONIZING RATE DERIVED CURVE 2 FOR ECLIPSE DAY
CURVE 3 ELECTRON DENSITY DERIVED FROM CURVE 3 FOR $\cdot 01 \times 10^9$
CURVE 4 X OBSERVED ELECTRON DENSITY FOR ECLIPSE DAY
IONIZING RATE AT LEVEL OF MAXIMUM N
ELECTRONS/CC/MIN2
MAXIMUM ELECTRON DENSITY, 10^5 ELECTRONS/CC
GREENWICH MEAN TIME
BEGINNING OF ECLIPSE
TIME OF TOTALITY
END OF ECLIPSE

FIG. 6.

An interesting point to be noted is the absence of F_2 reflections for the time between 1251 G.M.T. and 1321 G.M.T. when F_1 maximum densities recovered rapidly enough to approach the F_2 densities in this interval. Absorption in F_1 was too great to allow observation of F_2 echoes during this time.

Conclusions

From the results derived from the eclipse observations at Victoria Beach some conclusions regarding the general behavior of the three main regions of the ionosphere may be drawn.

The F_1 region behaves as though it has a constant recombination coefficient of approximately 1.4×10^{-8}. It seems unlikely that negative gas ions are formed stably at the height 200 to 250 km.

The E region apparently has a varying effective recombination coefficient, the average value during the eclipse being about 1.6×10^{-8}. By making some approximations, the value of coefficient arrived at is about 4.2×10^{-8} soon after first contact, and 0.8×10^{-8} at totality. This shows a drop in ratio of negative oxygen ions to electrons from 2100 to 400 at totality.

The F_2 region shows a distinct eclipse effect but the quantitative analysis is limited by the experimental evidence. An effective recombination coefficient of the order of 1×10^{-9} seems to hold for this region.

It may be said that there is no experimental evidence of a coronal effect in the solar eclipse, and therefore the ionization due to the corona must be small compared with that due to the main body of the sun.

Acknowledgment

The experimental work was carried out by a party from the Electrical Engineering and Radio Branch, National Research Laboratories, under the direction of H. R. Smyth. The author is indebted to the members of the party whose co-operation made the report possible.

References

1. BATES, D. R., BUCKINGHAM, R. A., MASSEY, H. S. W., and UNWIN, J. J. Proc. Roy. Soc. London, A-170: 322. 1939.
2. FERRARO, V. C. A. Terr. Magn. Atm. Elec. 50 : 223. 1945.
3. FREEMAN, R. E. and MOTT, R. I. N.R.C. Radio Dept. PRA-132. 1945.
4. MASSEY, H. S. W. Proc. Roy. Soc. London, A-163 : 542. 1937.

A HIGH TEMPERATURE CONTROL CIRCUIT[1]

BRUCE C. LUTZ AND JOHN H. WOOD[2]

Abstract

This is an electronic circuit useful in the control of electric air-bath furnaces having a long time lag. The control is accomplished by means of a relay that shunts a portion of the resistance in series with the furnace winding. The thermometric device is a thermocouple connected in series with a mirror-type galvanometer and a variable voltage supplied by a potentiometer. The setting of the potentiometer selects the temperature at which the device will control. A light beam falling on the mirror is reflected to one of two photocells. One photocell closes the shunt by means of the described circuit and increases the current in the furnace. This condition is maintained until the beam moves across the second photocell, when the shunt is again opened. The device will control temperatures over 1000° C. within a precision of ±2° C. over any desired length of time.

Introduction

The temperature control to be described here was designed for use over a wide temperature range with air-bath furnaces, electrically heated by covered resistance elements. A long time lag is an inherent property of this type of furnace. There are a number of temperature controls described in the literature (1, 3, 4) which will give a higher degree of precision but have limitations as to temperature range, power input to the furnace, or time lag.

The limitation in temperature range is usually imposed by the range of the platinum resistance thermometer. When a thermocouple is used as the thermometric device, the limit is determined by the refractory nature of the elements employed. Thus for a tungsten–molybdenum couple, temperatures in excess of 2000° C. may be controlled.

The furnace resistance wire is also a determining factor on the upper temperature limit. The furnace at present being thermostatically controlled has a nichrome element permitting operation up to 1000° C. However, a furnace is to be constructed employing tungsten windings, thus permitting temperatures in excess of 2000° C.

In the previous circuits, a thyratron was used in series with the furnace as a current regulator by controlling the relative phase of the grid voltage. The use of a thyratron has the advantage of a continuous control. However, such circuits are not applicable over a wide range of power consumption nor do they lend themselves readily to either frequent changes in the required temperature or to changes in the furnace windings. Also, the thyratron circuits depend upon the light intensity falling on a single photocell. It is felt that difficulties in maintaining a constant light source over long periods of time might arise and that, with a single photocell, there is a danger that the

[1] *Manuscript received in original form July 21, 1947, and, as revised February 6, 1948. Contribution from the Departments of Physics and Chemistry, University of Manitoba, Winnipeg, Man.*

[2] *Cominco Fellow, Department of Chemistry.*

light will move completely off the photocell if there is any appreciable time lag in the furnace. If the latter occurred all control would be lost.

The circuit to be described uses a relay to shunt a portion S (Fig. 1) of the series resistance and thus affords no practical limitation on the power delivered to the furnace. However, to gain in this respect continuous control

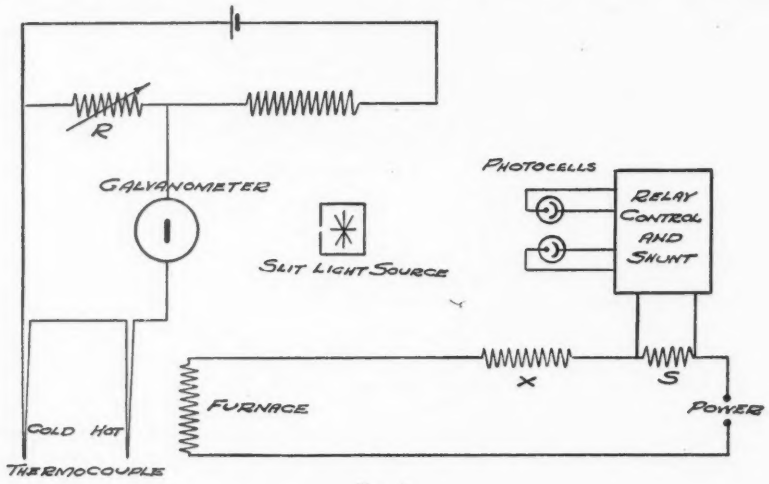

FIG. 1.

has been sacrificed; the effect of discontinuous control may be minimized by keeping the shunted portion of the series resistance as small as possible. The selection of a new controlled temperature has been simplified to two manual adjustments; the setting of the series resistance, X, for approximate temperature and the adjustment of the opposing e.m.f. for the thermocouple (Resistance R).

The chief advantage of this circuit is use of two photocells, one being employed to open and the other to close the shunt. If the light beam passes either cell, the proper action is accomplished as it does so and the light must eventually return to the opposite cell, no ill effects occurring as it repasses the first cell.

Description of the Circuit

The circuit of Fig. 2 consists of the following stages: the relay tube, 6F6, an Eccles–Jordon circuit (2) consisting of two 6C5's, and two pulse circuits functioning alternately. Each pulse circuit consists of an 884 used as a sawtooth generator, a 6F5 used as a bias amplifier, and a 927 phototube.

The relay, an Aminco 'supersensitive' mercury relay, is activated at 10 ma. and releases when the current is reduced to below 2 ma. The current is controlled by the bias on the 6F6 since this tube is in series with the relay. The

bias may be either of two values determined by the condition of the Eccles–Jordon circuit. This circuit (2) has two stable conditions, in either of which one tube is conducting while the other is cut off. When the right hand 6C5

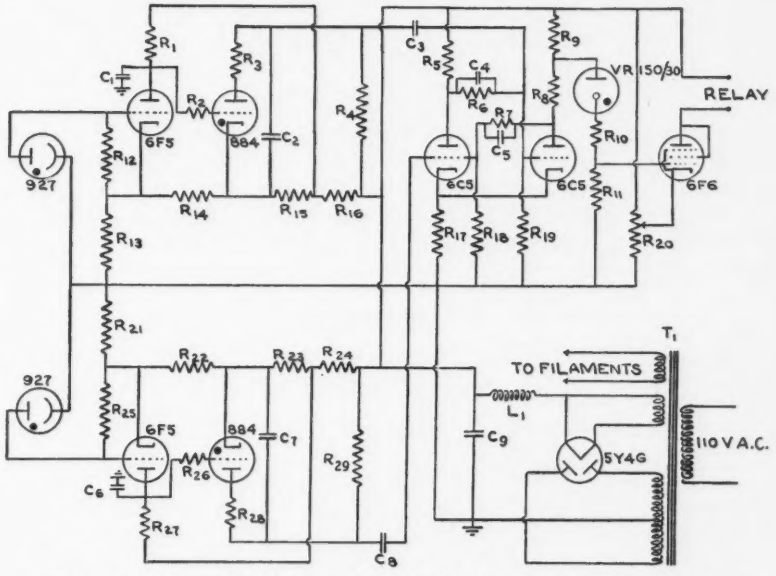

FIG. 2. $R_1 = R_{27} = 330\ K\Omega$. $R_2 = R_{26} = 10\ K\Omega$. $R_3 = R_{28} = 300\ \Omega$. $R_4 = R_{29} = 100\ K\Omega$. $R_5 = 50\ K\Omega$. $R_6 = R_7 = 400\ K\Omega$. $R_8 = 20\ K\Omega$. $R_9 = 25\ K\Omega$. $R_{10} = R_{11} = 100\ K\Omega$. $R_{12} = R_{25} = 5\ M\Omega$. $R_{13} = R_{21} = 15\ K\Omega$. $R_{14} = R_{22} = 25\ K\Omega$. $R_{15} = R_{23} = 5\ K\Omega$. $R_{16} = R_{24} = 25\ K\Omega$. $R_{17} = 20\ K\Omega$. $R_{18} = R_{19} = 100\ K\Omega$. $R_{20} = 10\ K\Omega$. $C_1 = C_6 = 0.005\ \mu fd$. $C_2 = C_7 = 0.03\ \mu fd$. $C_3 = C_8 = 0.01\ \mu fd$. $C_4 = C_5 = 0.35\ \mu fd$. $C_9 = 24\ \mu fd$. $L_1 = 30\ h$. $T_1 =$ Hammond type 275.

is cut off, the bias on the 6F6 allows the tube to conduct the necessary 10 ma. to close the relay. When this 6C5 is conducting, the relay current is reduced below 2 ma. The VR150/30 in the voltage divider permits a maximum change in grid bias at the same time reducing the d–c. drop across the grid return resistor.

The Eccles–Jordon circuit is altered from one stable condition to the other by applying negative pulses to the grid of the tube to be cut off. These pulses are formed by passing a saw-tooth wave from a standard type 884 sweep circuit through a differentiating circuit. In Fig. 2 the upper 884 thyratron supplies negative pulses through the differentiating circuit, C_3 and R_{19}, to the grid of the right 6C5, cutting it off and closing the relay. In a similar manner the lower 884 functions to open the relay.

The saw-tooth wave is produced only when the bias on the thyratron is lifted to a point where the tube can 'fire'. This bias is controlled by a bridge circuit with a 6F5 forming a variable resistance element in one arm. When

the light falls on the corresponding photocell, the negative voltage drop across the grid return resistor of the 6F5 is increased, causing an increase in the resistance of this arm of the bridge, thus permitting the 884 to function. The 6F5 is a high-gain tube and care must be taken to prevent oscillation if the leads from the photocells are long. Since this is a d-c. amplifier, it is permissible to use a large by-pass condenser from plate to ground.

Operation of the Circuit

A high degree of precision is not claimed for this circuit. It was designed for a purpose requiring a precision of only $\pm 2°$ C. at high temperatures (900° to 1500° C.), which it accomplished. If necessary this could be improved considerably by increasing the current sensitivity of the galvanometer and improving the optical system. The device has seen 1000 hr. of almost continuous operation and has given excellent performance throughout the period.

Acknowledgment

The research for which this circuit was designed was supported by a fellowship grant to John Wood from the Consolidated Mining and Smelting Company, Ltd.

References

1. BENEDICT, M. Rev. Sci. Instruments, 8 : 252. 1937.
2. ECCLES, W. H. and JORDON, F. W. Radio Rev. 1 : 143. 1919.
3. WARING, C. E. and ROBISON, G. Rev. Sci. Instruments, 14 : 143. 1943.
4. ZABEL, R. M. and HANCOX, R. R. Rev. Sci. Instruments, 5 : 28. 1934.

THE PHOTOELECTRIC TEMPERATURES OF THE P CYGNI STARS[1]

By C. S. Beals and R. D. Hatcher[2]

Abstract

The photoelectric temperatures of 52 P Cygni stars of spectral type from A4 to O5 have been determined from emission lines by Zanstra's method. For approximately half the stars, accurate spectrophotometric measures of emission line intensities were available and for the remainder the intensities were estimated on the basis of published descriptions of spectra. The computed temperatures were found to range from 10,000° to 42,000° K. and after smoothing by graphical methods a temperature scale for the O, B, and A type stars showed the following values: A0, 16,000°; B0, 35,000°; O5, 40,000° K. Comparisons are made with temperatures derived by other methods and reasons are given for attributing greater weight to the values from B0 to O5 than to those in the lower range of the sequence.

Introduction

There are three principal methods now in use to determine the temperatures of stars, (A) the application of Planck's formula to the observed distribution of energy in the continuous spectrum (6), (B) the use of ionization formulae such as those of Saha in conjunction with observations of relative line intensities of atoms in different stages of ionization (10), (C) the determination of photoelectric temperatures on the basis of the intensity of emission lines relative to the continuous spectrum (14). A fourth method makes use of the Boltzmann formula for the distribution of atoms in excited states but it is of limited application among the early type stars (13). In the present paper data on the intensities of emission lines have been used to derive photoelectric temperatures for a number of stars of P Cygni type.

Theory of Method Used

Method (C), developed by H. Zanstra (14), was originally used to determine the temperatures of planetary nebulae. It has since been adapted to include stars that have around them envelopes such as may have their origin in the ejection of atoms from the surface of the star. This has been done for the Wolf Rayet stars, for a number of stars of P Cygni type, and for several novae by C. S. Beals (1, 3), for Nova Lacertae by A. McKellar (7), and for a number of Be stars by O. Mohler (9). It is particularly advantageous to have this method available in the case of the P Cygni stars since Method (A) is invalidated by the distortion of the continuous spectrum due to space absorption, and Method (B) is made difficult of application by the combination of emission and absorption in P Cygni type spectra.

[1] *Manuscript received December 17, 1947.*

Contributions from the Dominion Observatory, Vol. 2, No. 1. Published by permission of the Director, Mines, Forests and Scientific Services Branch, Department of Mines and Resources.

[2] *At present studying theoretical physics at Yale University.*

The application of Zanstra's method involves the following assumptions,

(1) The star is assumed to be a black body radiator of temperature T, obeying Planck's radiation law.

(2) The envelope of the star is assumed to consist of atoms of one element only, and a majority of the atoms are assumed to be in the normal state.

(3) The ultraviolet starlight emitted by the star is completely absorbed beyond the ionizing frequency of the atoms present in the envelope, causing the ejection of photoelectrons.

(4) The photoelectrons recombine with the ionized atoms in the upper states of the atom and in a steady state the number of quanta of ultraviolet starlight absorbed is equal to the number of recombinations in any time interval.

The observational data required for the calculation are values of the quantity A_ν, where

$$A_\nu = \frac{L_p}{\nu \dfrac{\delta L_s}{\delta \nu}}, \tag{1}$$

where L_p represents the total energy in the emission line, of average frequency ν, and $\dfrac{\delta L_s}{\delta \nu}$ the total energy per frequency unit of the continuous spectrum for the same frequency. It has been shown by Beals (1, 3) that this quantity A_ν is equal to

$$A_\nu = \frac{1}{c} \int_{V_1}^{V_2} I \, dV, \tag{2}$$

where the V's are the velocity displacements from the center of the band to the edges, I is the intensity of the band relative to the continuous spectrum, and c is the velocity of light in kilometers per second. The quantity

$$\int_{V_1}^{V_2} I \, dV$$

is the equivalent width of the line expressed in units of velocity displacement.

On the basis of the above assumptions the theory as given by Zanstra leads to the equation

$$\int_{x_0}^{\infty} \frac{x^2}{e^x - 1} \, dx = \Sigma \frac{x^3}{e^x - 1} A_\nu, \tag{3}$$

where

$$x = \frac{h\nu}{kT} = \frac{1.432 \times 10^8}{\lambda T},$$

$$x_0 = \frac{h\nu_0}{kT} = \frac{1.432 \times 10^8}{\lambda_0 T} = \frac{11600 \, V_0}{T},$$

k is Boltzmann's constant, λ the wave length in angstroms, ν the frequency, V_0 the ionization potential in volts, ν_0 and λ_0 the ionizing frequency and wave length respectively, and the summation is carried out over all the visible emission lines for a particular atom. The equation is solved by trial in order

to determine the value of T. The temperature so determined is the 'photoelectric' temperature referred to in the title of this paper. A more detailed discussion of the theory and its application to individual observations has been given by Beals (3).

Observational Data and the Use of Estimates of Intensity

For a considerable number of the stars considered, spectrophotometric measures of equivalent width made at Victoria were available. These values of equivalent width were derived from plates calibrated with the aid of a rapidly rotating step sector (100 revolutions per second) placed in front of the slit of a calibrating spectrograph. The plates were analyzed with the aid of microphotometer tracings and the process of reducing the tracings to equivalent widths was greatly facilitated by a new intensitometer, which has been described elsewhere (2). The actual observations will be discussed in more detail in a forthcoming publication of the Dominion Astrophysical Observatory. To illustrate the general type of spectrum dealt with in this paper, portions of the spectra of two P Cygni stars have been reproduced in Plate I along with that of an ordinary absorption line star of early type for comparison.

In addition to those stars for which quantitative measurements of line intensity are available there are numerous others for which there are only general descriptions and in some cases published reproductions of spectra. Ordinarily it might be supposed that in such instances no significant calculation of temperatures could be made. However, as Zanstra has previously pointed out, this method of determining temperatures is very insensitive to observational error. This point may be illustrated by the following examples;—

(1) For the star H.D. 31293 taking the equivalent width of the line λ6563 of hydrogen to be 200 and using standard values for the ratios of H_α to H_β, H_γ and H_δ the temperature of the star was found to be 12,800° K. Then taking the value of the equivalent width to be 400, twice as much as before, and using the same ratios the value 13,500° K. was found.

(2) For higher values of the temperature the effect is more noticeable but again not very great. For the star H.D. 151804, using the measured value of the equivalent width of λ4686 He II and doubling the value, the temperatures of 40,800° and 42,800° K. were calculated, whereas, for the same star, measures on a different line from a different ion gave temperatures of 32,400° and 34,600° K. Since the method itself and the assumptions on which it is based involve uncertainties of the order of a few thousand degrees for individual stars, the errors due to the use of estimates are probably not very significant. Accordingly an estimate of line intensity has been made for every star for which a description is available and it is believed that a reasonable degree of confidence may be placed in the temperatures calculated from these estimated intensities.

In our calculations the temperature was calculated for both A_ν as measured or judged and for twice A_ν. This is the same as assuming first, that the

number of observed emission quanta is equal to the ultraviolet quanta absorbed, and second, that the observed are only half those absorbed. The first temperature may be regarded as a minimum temperature, and it will be denoted by T min. in our results.

It should be stated here that the temperatures obtained for the same star by using different atoms or ions show large differences, a result that naturally leads to doubts as to the accuracy of the method. These differences will be discussed in a later part of the paper.

Evaluation of the Integrals

For use in our calculations we require tables of the integral

$$I_1 = \int_{x_0}^{\infty} \frac{x^2}{e^x - 1}\, dx .$$

Zanstra (14) gives a table of this integral for values of x_0 between 0 and 11.0 as calculated by Debye's method. In our work the value of x_0 sometimes reaches values over 20 so that an extension is necessary. This can be seen from the formula,

$$x_0 = \frac{h\nu_0}{kT} \frac{11600 V_0}{T}$$

where V_0 is the ionization potential in volts and T the absolute temperature in degrees Kelvin. If we give V_0 a value of 25 v. or higher and T a value of 15,000° or less we reach values of x_0 near 20.

In calculating values for the integral beyond x_0 equal to 10 an approximation was made that will be shown to be justified. We require

$$\int_{x_0}^{\infty} \frac{x^2}{e^x - 1}\, dx \text{ when } x_0 > 10 .$$

If $x_0 > 10$, then $e^x > e^{x_0} \gg 1$, so that we may replace the above integral by

$$\int_{x_0}^{\infty} x^2\, e^{-x} dx .$$

Integrating by parts:

$$\int_{x_0}^{\infty} x^2 e^{-x} dx = e^{-x_0}(x_0^2 + 2x_0 + 2) .$$

On testing this approximation we obtain the values of Table I.

TABLE I

x_0	$\int_{x_0}^{\infty} x^2\, e^{-x} dx$	$\int_{x_0}^{\infty} \frac{x^2}{e^x - 1} dx$
10	0.00554	0.00554
5	0.2493	0.2500

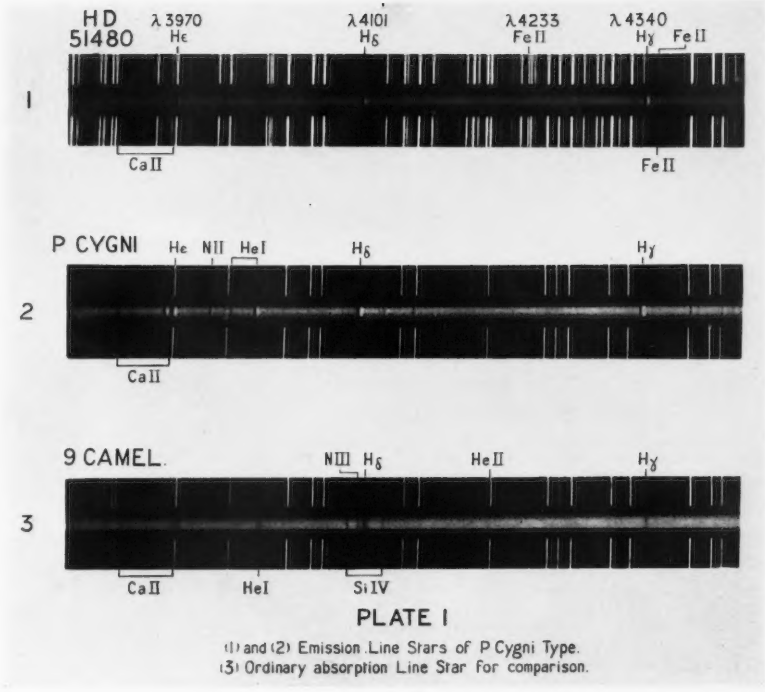

PLATE I

(1) and (2) Emission Line Stars of P Cygni Type.
(3) Ordinary absorption Line Star for comparison.

We thus see that even for values quite low in the table the approximation gives very good results.

Similarly we may calculate values of the second integral used by Zanstra. This is

$$\int_{x_0}^{\infty} \frac{x^3}{e^x - 1} dx ,$$

which becomes

$$\int_{x_0}^{\infty} x^3 e^{-x} dx ,$$

using a similar approximation.

Upon integration by parts as before this gives

$$e^{-x_0} (x_0^3 + 3x_0^2 + 6x_0 + 6) .$$

Trying $x_0 = 5$ we obtain 1.590 by this method, whereas the value by Debye's method is 1.594.

We shall however need numerical values for the first integral only and these as calculated according to the formula above are shown in Table II.

TABLE II

x_0	$\int_{x_0}^{\infty} x^2 e^{-x} dx$	x_0	$\int_{x_0}^{\infty} x^2 e^{-x} dx$
10.0	0.00554	16.0	0.0000326
11.0	0.00242	17.0	0.0000135
12 0	0.00104	18.0	0.00000551
13.0	0.000445	19.0	0.00000225
14.0	0.000188	20.0	0.000000911
15.0	0.0000786		

It may be noted that O. Mohler (9) gives a table calculated by an expansion method for values up to 15.5 in agreement with those given here.

Use of Graphs

To facilitate computation, graphs were drawn from which several of the values appearing in Equation (3) could be read off directly.

From (3)

$$x = \frac{h\nu}{kT} \frac{1.432 \times 10^8}{\lambda T} ,$$

where λ is the wave length in angstroms which for the range dealt with here varies from λ3700 to λ6700 approximately. Thus for any definite value of T a set of values of the quantity $\frac{x^3}{e^x - 1}$ may be calculated by giving values between λ3700 and λ6700. This was done initially for values of T of 10, 15,

20, 25, 30, 35, and 40 thousand degrees and this set of seven curves was used in the first few calculations, it being considered sufficient to interpolate between these to obtain the temperature to sufficient accuracy. Later, however, when it was noticed that most temperatures lay in the 10,000° to 20,000° K. group, extra curves were drawn for T equal to 12,500° and 17,500° K. and interpolations made between these values. Occasionally greater accuracy was used for special stars and interpolations between 1000 degree intervals were made. In such cases the values obtained were checked with those obtained by interpolating over wider intervals and it was noted that they agreed to a sufficient degree of accuracy. We cannot claim therefore that the values as given here are as precise as could be obtained by drawing many more intervening curves but it is felt that the accuracy is amply sufficient for the purpose.

Treatment of Hydrogen Lines

As hydrogen played an important role in the spectra of these stars a method of shortening various calculations was devised, using an assumed value for the Balmer decrement.

It will be noted that the equivalent widths for the main Balmer lines in the star P Cygni are

$$H_\alpha : H_\beta : H_\gamma : H_\delta = 3660 : 783 : 325 : 205,$$

leading to the ratios $4.7 : 1.0 : 0.40 : 0.25$. Several of the other stars showed roughly these ratios and so where only H_α or H_γ had been measured it was assumed that the ratios held, and calculations were made accordingly. In come cases when the hydrogen lines showed values different from those given above, a separate calculation was made for the temperature. This ratio is not the Balmer decrement given by some authors, but its connection with it can be seen from References (1, 3). (The values given here are in each case relative to the continuous spectrum at the appropriate wave length.)

Classification

In most cases ordinary absorption line intensity ratios are not available for the P Cygni stars because of the blending of absorption and emission lines. The spectral classes included in the second column of Table III have therefore been determined from the general level of ionization in the stellar spectra. Dr. R. M. Petrie very kindly undertook to classify all stars for which data were available during a visit to this Observatory in January, 1947, and most of the designations in Table III are his. A more detailed discussion of the problems of the classification of the P Cygni stars will appear in a forthcoming publication of the Dominion Astrophysical Observatory. In the meantime it is believed that classifications are precise enough for the present purpose of determining a general relation between spectral class and temperature for the P Cygni stars.

Table of Results

The results of the calculations are given in the following table. Column (1) shows the star, (2) its classification, (3) the atom or ion encountered in its spectrum in emission, and its ionization potential, (4) the wave length of the line, (5) the equivalent width in kilometers per second (6) T min. and (7) T. In order to distinguish between the values of equivalent width that have been directly measured and those that have been estimated, the latter values are enclosed in parentheses.

It will be noted that many more lines occur for some stars than for others. This is either because the emission spectrum is more completely developed or because more complete data are available. In some instances where a spectrum shows marked variations the temperature has been calculated for more than one epoch, as in the case of the star H. D. 108.

TABLE III

TEMPERATURES OF THE P CYGNI STARS

Star	Class	Atom I.P.	λ	E.W., km./sec.	T min., °K.	T, °K.
H.D. 108	O6–O7	H 13.54	6562.817	295	13,400	15,200
(1934–38)			4861.332	213		
			4340.468	92		
			4101.737	52		
(1944–45)			6562.817	82	10,500	11,100
			4861.332	18		
			4340.468	4		
			4101.737	3		
(1934–38)		CIII (47.67)	5696.0	32	36,300	38,300
			4647.40			
			4650.16	37		
			4651.35			
(1944–45)			5696.0	30	35,200	36,400
			4647.40			
			4650.16	8		
			4651.35			
(1934–38)		NIII 47.2	4640.64	64	37,200	39,700
			4634.16	33		
(1944–45)			4640.64	42	36,100	38,000
			4634.16	20		
(1934–38)		HeII 54.17	4685.682	47	40,500	42,300
1944–45)			4685.682	28	39,000	40,800
M.W.C.419	B9	H 13.54	4861.332	(200)	15,200	16,100
		FeII 16.16	4351.764	(75)	14,500	15,300
			4233.167	(75)		
H.D.7902	B5	H 13.54	6562.817	100	10,700	11,400

TABLE III—*Continued*

TEMPERATURES OF THE P CYGNI STARS—*Continued*

Star	Class	Atom	I.P.	λ	E.W., km./sec.	T min., °K.	T, °K.
H.D.12953	A0	H	13.54	6562.817	65	10,300	10,800
C. o Ceti	B	H	13.54	4861.332	(345)	16,000	17,400
		HeI	24.48	6678.149	(114)	24,500	25,900
				5875.618	(270)		
				650			
				5015.675	(98)		
				4471.477	(70)		
		FeII	16.16	4351.764	(75)	14,500	15,300
				4233.167	(75)		
H.D.21389	B9	H	13.54	6562.817	(100)	10,700	11,400
H.D.31293	A0	H	13.54	6562.817	(200)	12,800	13,500
H.D.31648	A2	H	13.54	6562.817	(200)	12,800	13,500
H.D.32256	B	H	13.54	6562.817	(224)	12,600	13,200
				4861.332	(13)		
P Cygni Stars in Large Magellanic Cloud	B	H	13.54	6562.817	(3660)	17,500	19,300
				4861.332	(783)		
				4340.468	(325)		
				4101.737	(205)		
				3970.074	(129)		
H.D.242257	B	H	13.54	4861.332	348	16,600	17,600
				4340.468	83		
				4101.737	77		
M.W.C.497	B	FeII	16.16	4351.764	(75)	14,500	15,300
				4233.167	(75)		
H.D.41511	AI	H	13.54	6562.817	360	13,400	14,600
H.D.45910	B6						
(1937)		H	13.54	4861.332	158	14,700	15,800
(Av. 1939–44)				6562.817	1730	16,100	17,700
(25/3/39)				6562.817	815	14,900	16,000
(1943)				4861.332	81	13,500	14,700
(Av. 1923–24)		FeII	16.16	4351.764	88.3	15,000	15,800
				4233.167	88.3		
(1926)				4351.764	30.1	13,200	14,200
				4233.167	30.1		
(1943)				4351.764	46.6	13,800	15,100
				4233.167	46.6		
H.D.51480	B7	H	13.54	6562.817	2740	16,600	18,200
				4861.332	345		
				4340.468	103		
				4101.737	47		
				3970.074	21		

TABLE III—*Continued*

TEMPERATURES OF THE P CYGNI STARS—*Continued*

Star	Class	Atom	I.P.	λ	E.W., km./sec.	T min., °K.	T, °K.
H.D.51480	B7	FeII	16.16	4583.829 4351.764 4233.167 4178.855 4173.450	31 27 68 19 22	15,000	15,700
H.D.51585		H	13.54	6562.817	(100)	10,700	11,400
H.D.53179		H	13.54	6562.817	(100)	10,700	11,400
M.W.C.560		H	13.54	6562.817 4861.332	(436) (49)	13,200	14,400
η Carinae		H	13.54	4861.332	(2349)	20,400	22,500
		FeII	16.16	4351.764 4233.167	(225) (225)	16,100	17,600
H.D.94878		H	13.54	4861.332	(783)	17,500	19,300
H.D.94910		H	13.54	4861.332	(783)	17,500	19,300
		HeI	24.48	6678.149 5875.618 650 5015.675 4471.477	(227) (540) (197) (139)	25,900	27,800
H.D.138403		H	13.54	4861.332	(783)	17,500	19,300
H.D.141969		H	13.54	4861.332	(392)	16,200	17,800
H.D.142983		H	13.54	6562.817	(360)	13,400	14,600
H.D.151804	O9	HeII	54.17	4685.682	(56)	40,800	42,800
		NIII	47.2	4640.64 4634.16	(40) (84)	38,000	40,400
		CIII	47.67	5696.0	(16)	32,400	34,600
H.D.151895		H	13.54	4861.332	(392)	16,200	17,800
H.D.152236	B1	H	13.54	6562.817 4861.332	(224) (13)	12,600	13,200
H.D.152408		HeII	54.17	4685.682	(28)	39,000	40,800
		NIII	47.2	4640.64 4634.16	(42) (20)	36,100	38,000
H.D.160529	A4	H	13.54	6562.817	(100)	10,700	11,400
H.D.161044		H	13.54	4861.332	(783)	17,500	19,300
		OII	35.00	3727.33	(500)	33,300	35,800

TABLE III—*Continued*

TEMPERATURES OF THE P CYGNI STARS—*Continued*

Star	Class	Atom	I.P.	λ	E.W., km./sec.	*T* min., °K.	*T*, °K.
H.D.161114	A0	H	13.54	4861.332	(1600)	19,000	20,900
		FeII	16.16	4351.764	(150)	15,300	16,700
				4233.167	(150)		
M.W.C.272		H	13.54	4861.332	(45)	12,500	13,400
		HeI	24.48	6678.149	(170)	25,200	26,900
				5875.618	(400)		
				650			
				5015.675	(148)		
				4471.477	(105)		
		FeII	16.16	4351.764	(68)	14,400	15,200
				4233.167	(68)		
H.D.163296	A2	H	13.54	6562.817	(360)	13,400	14,600
H.D.168607	A0	H	13.54	4861.332	(392)	16,200	17,800
H.D.169226	B3	HeI	24.48	6678.149	(170)	25,200	26,900
				5875.618	(400)		
				650			
				5015.675	(148)		
				4471.477	(105)		
H.D.169454	B2	H	13.54	6562.817	436	13,200	14,400
				4861.332	49		
		HeI	24.48	5875.618	20	18,100	18,900
				650			
H.D.169515	B0	HeI	24.48	5875.618	(400)	25,200	26,900
				650			
		NIII	47.2	4640.64	(3)	30,000	32,000
				4634.16	(3)		
H.D.174638		HeI	24.48	5875.618	(400)	25,200	26,900
				650			
H.D.183143	B7	H	13.54	6562.817	(11)	10,100	10,300
H.D.187399	B8	H	13.54	6562.817	(224)	12,600	13,200
				4861.332	(13)		
H.D.188001	O7	H	13.54	6562.817	89.7	11,800	12,700
		HeI	24.48	5875.618	16.7	17,900	18,600
				650			
		NIII	47.2	4640.64	5.8	32,800	35,100
				4634.16	10.7		
		CIII	47.67	5696.0	44.0	35,300	36,500
H.D.190073	A1	H	13.54	6562.817	1304	15,400	16,600
				4861.332	190		
				4340.468	93		
				4101.737	45		
				3970.074	20		

TABLE III—*Continued*

TEMPERATURES OF THE P CYGNI STARS—*Continued*

Star	Class	Atom	I.P.	λ	E.W., km./sec.	*T* min., °K.	*T*, °K.
H.D.190073	A1	FeII	16.16	5018.434	98	15,600	15,800
				4923.921	69		
				4583.829	24		
				4555.890	17		
				4534.166	6		
				4522.634	30		
				4515.337	16		
				4508.283	16		
				4351.764	23		
				4233.167	29		
		TiII	13.6	4571.971	22	12,700	13,300
				4549.622	29		
				4533.966	7		
				4501.270	23		
				4468.493	25		
				4443.802	23		
				4395.031	26		
				4300.052	15		
		ScII	12.8	4246.829	22	10.000	10,200
		CaII	11.82	3968.470	50	10,100	10,900
				3933.664	31		
H.D.190603	B2	H	13.54	6562.817	224	12,600	13,200
				4861.332	13		
		HeI	24.48	5875.618	14	17,600	18,200
				650			
P Cygni H.D.193237	B1	H	13.54	6562.817	3660	17,500	19,300
				4861.332	783		
				4340.468	325		
				4101.737	205		
				3970.074	129		
		HeI	24.48	6678.149	227	25,900	27,800
				5875.618	540		
				650			
				5047.736	15		
				5015.675	197		
				4921.929	62		
				4713.143	59		
				4471.477	139		
				4437.549	4		
				4387.928	25		
				4143.759	14		
				4120.812	22		
				4026.189	91		
				4009.270	5		
				3964.727	51		
				3871.819	3		
				3867.477	2		
		NII	29.49	6482.07	13.4	26,100	27,800
				5747.29	2.1		
				5710.76	8.5		

TABLE III—*Concluded*

TEMPERATURES OF THE P CYGNI STARS—*Concluded*

Star	Class	Atom	I.P.	λ	E.W., km./sec.	T min., °K.	T, °K.
P Cygni H.D.193137	B1	NII	29.49	5686.21	10.1		
				5679.56	28.0		
				5666.64	13.8		
				5007.316	19.8		
				5005.140	3.0		
				4643.086	24.5		
				4630.537	32.9		
				4621.392	15.0		
				4613.868	13.2		
				4607.153	14.4		
				4601.478	25.8		
				4447.033	6.6		
				3994.996	18.6		
				3955.851	6.7		
		CIII	47.67	5696.0	1.0	27,000	28,700
H.D.197345	A2	H	13.54	6562.817	11	10,100	10,300
H.D.198478	B2	H	13.54	6562.817	7.7	9,500	10,000
M.W.C.374	B5	FeII	16.16	4583.829	50.7	15,100	16,700
				4555.890	19.8		
				4549.467	29.3		
				4351.764	29.4		
				4233.167	27.7		
				4178.855	18.5		
				4173.450	20.9		
H.D.207757	O9	H	13.54	4861.332	(1566)	19,400	20,600
		HeI	24.48	6678.149	(340)	26,900	29,400
				5875.618	(810)		
				650			
				5015.675	(295)		
				4471.477	(219)		
H.D.218393	B8	H	13.54	6562.817	806	14,200	15,500
				4861.332	60.5		
				4340.468	7		
				4101.737	1		
		FeII	16.16	4233.167	17.9	12,500	14,700
H.D.221650 (Z Andromedae)		HeII	54.17	4685.682	123.4	43,200	45,600
		NIII	47.2	4640.64	42	36,100	38,000
				4634.16	20		
Companion of R Aquarii		HeII	54.17	4685.682	(80)	41,100	42,900
		NIII	47.2	4640.64	(46)	36,100	38,000
				4634.16	(20)		
H.D.223385	B9	H	13.54	6562.817	(100)	10,700	11,400

Discussion of Results

In discussing the validity of the results of this study it is important to bear in mind the fundamental limitation of the method, namely, that it claims only to set a minimum value for the temperature of a star. This limitation arises largely as a consequence of the two assumptions (*a*) that all the radiation to the violet of the ionizing frequency of an atom is absorbed in the process of photoelectric ionization and (*b*) that most electron captures are made in upper atomic levels.

Referring to assumption (*a*), even if it could be supposed that all, or a majority of the atoms in an envelope, were of one kind it might well happen in the case of incipient emission that the envelope would be of insufficient optical thickness for complete absorption and this would lead to too low an estimated temperature for the star. Also in a mixed atmosphere, owing to the existence of overlapping regions of absorption, assumption (*a*) could be realized only under very exceptional circumstances, and the failure of the assumption would again lead to too low a temperature.

There is thus no conflict between the different values of temperature derived for the same star by the use of lines of different atoms. Since each represents a minimum value, the highest calculated temperature (ordinarily derived from the atom of highest ionization potential) should correspond most closely to the true temperature of the star. Also, in the numerous instances where stars of the same spectral type exhibit different emission characteristics and therefore different photoelectric temperatures, the differences may be attributed mainly to the different optical thickness of their respective envelopes.

The assumption regarding electron capture in upper levels is also likely to result in too low rather than too high estimates of the stellar temperature. Here we have followed Zanstra in assuming that half the actual captures result in observable emission. In view of the work of Cillié (5) on the capture coefficients for hydrogen it would appear that most captures take place in the lower levels, the largest number being in the ground state. It is thus possible that considerably less than half the actual captures are made in atomic levels that result in emission lines in the spectral region actually observed and that all the calculated temperatures are somewhat too low.

Incomplete observation of the emission spectrum, which is inevitable in some instances, will have the same result and it would therefore appear that the results of this paper are likely to give rather conservative estimates of the temperatures attained by the O and B type stars.

On the Use of Ions other than Hydrogen

It should be noted that Zanstra's theory was developed for the case of the envelope of a star containing hydrogen only (3) because of the relative ease of the calculations for the hydrogen atom. We have not attempted further development of the theory for the more complex atoms and as a consequence the relation of the observed line intensities to the number of absorbed

ultraviolet quanta is more uncertain than for hydrogen. However, in the more important cases (HeII, NIII, CIII) we have made use of a single line or a single multiplet, and there would appear to be little likelihood that use of the observed intensities would result in an overestimate of the number of ultraviolet quanta. The original aim of the investigation to derive minimum temperatures is therefore preserved, although other considerations arise where the mechanism of fluorescence is involved.

Fluorescence Effects

Bowen's fluorescence mechanism (4) is another factor to be considered in analyzing these results. For completeness we shall give a short discussion along the lines used by McKellar (7) in treating the same phenomenon. Considering first the cycle for the hydrogen–helium case in which the line λ4686 of HeII is produced, the diagram of Fig. 1 shows quite clearly how this line may occur with anomalous intensity, to the exclusion of other lines in its series. Because of the large intensity of λ304 many of the helium ions will

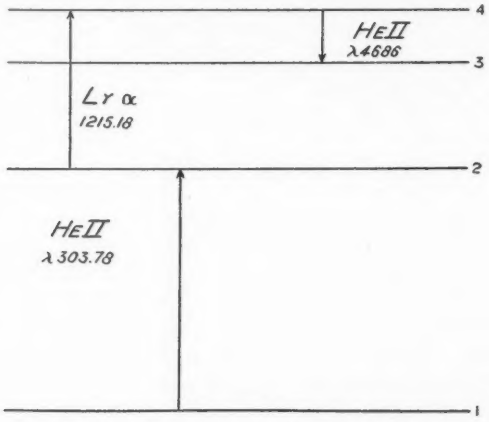

FIG. 1. *Fluorescence cycle for H and HeII.*

be in State 2 as represented on the diagram. Then because of a close coincidence with the very intense Ly_α line of hydrogen the ion may be moved up to State 4 by the absorption of a quantum of Ly_α and on falling back will produce the visible line λ4686, while other members of the series will be absent. The Ly_α line of hydrogen is λ1215.68 while that for helium is λ1215.18, so that it is seen that the coincidence is very close.

The HeII – OIII – NIII cycle is more complicated and consists of two close coincidences. Its mechanism may be seen from Fig. 2. The presence of the wave lengths λ4634–4640 of NIII unaccompanied by the strong lines λ4097–4103 is evidence for its occurrence.

In connection with the above mechanism of fluorescence McKellar makes the interesting comment that since each quantum of λ4640 due to Bowen's line absorption process follows from one of HeII 304 which resulted from the

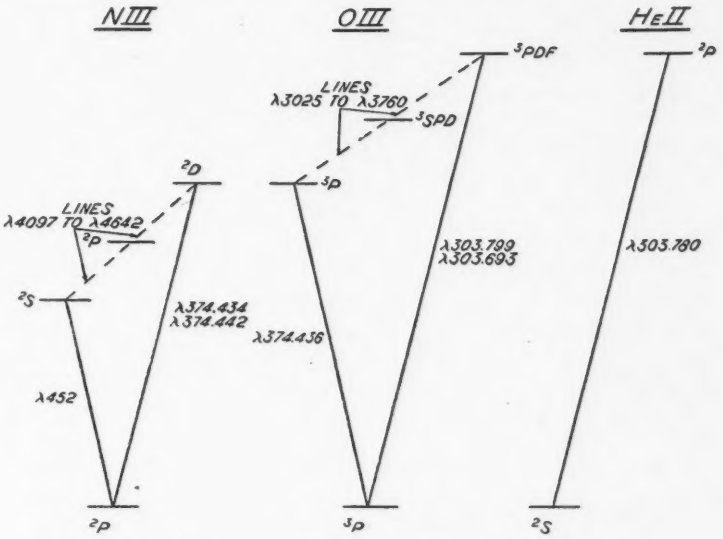

FIG. 2. *Fluorescence cycle for HeII, OIII, and NIII.*

photoelectric ionization of a HeII atom, then the λ4640 quantum should be considered as evidence of the presence of ultraviolet radiation beyond the ionizing frequency of HeII rather than of NIII. Similarly the λ4686 line should be considered as a line of hydrogen, and if so considered the calculated temperature of the star will in general be much lower. In the former case, taking λ4640 as a band of HeII and calculating the temperatures thus, the result obtained will not differ greatly from that found for NIII.

Because of the existence of the fluorescence mechanism it would appear that temperatures calculated on the basis of the lines of NIII and HeII would be somewhat unreliable although it is by no means certain that they would in all cases be too high. However since the action of the mechanism is to increase the intensity of the line it may be expected that such lines will lead to temperatures higher than those due solely to recombination. Fortunately in most instances where lines due to HeII and NIII appear there are also lines due to CIII which does not appear to be involved in the fluorescence mechanism. There is reasonable agreement between the temperatures calculated for CIII and for NIII and HeII although the latter are somewhat higher. In constructing Fig. 3 it was decided to make use of CIII only in

plotting the relation connecting temperature with spectral type, and it will be seen that the points for NIII and HeII are mostly above the curve.

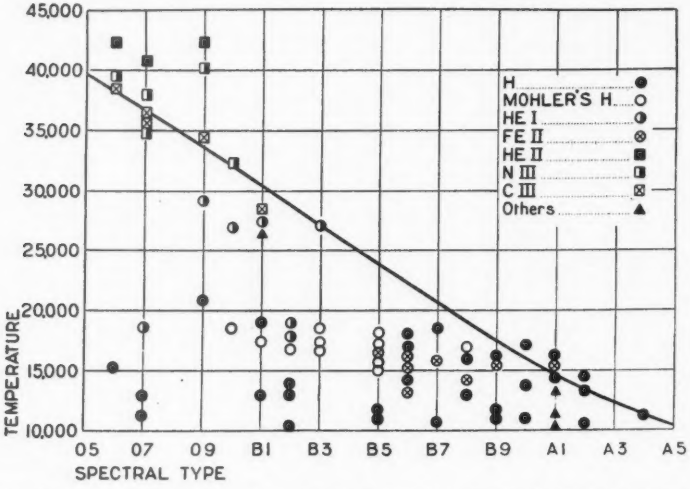

FIG. 3. *Relation between photoelectric temperature and spectra type for the P Cygni stars.*

The Stellar Temperature Scale for Early Type Stars

It will be noticed that the stars cover the range in the spectral sequence for spectral types O6 to A4. In Fig. 3 the photoelectric temperatures found have been plotted against spectral type. For the interpretation of the graph a few remarks are necessary. First, the points seen on the diagram are individual calculations for a star for a definite ion only and not an average for several ions in cases where several appeared. The curve is drawn through the highest points in each of the spectral classes, since the temperature determinations, as has been stated above, refer to minimum values, except in cases where the fluorescence effect may be acting. These latter are most noticeable at the O6 end of the sequence and as will be noticed they lie above the curve. Here the NIII and HeII determinations are generally greater than those for CIII for which no fluorescence effect or coincidences in line wave lengths have been found. The values of temperature from NIII and HeII have been disregarded in drawing the curve. Second, in addition to the values obtained by ourselves, there have also been introduced into the diagram the values of Mohler for the Be stars, principally B3 and B5 of which there were few in our group. These are indicated by open circles. Third, the sudden rise in temperature in the vicinity of B3 is due principally to the appearance in the spectra of measurable lines of ions of higher ionization potential than H, as for example HeI. If a sufficient variety of ions was available we would expect the area under the curve to be completely filled in.

It will also be noticed that temperatures derived from hydrogen do not show much variation with spectral type and the general appearance of the curve would indicate a series of steps for the different ions.

There are several discussions in scientific literature of the temperature scale of stars. One of the most recent is that of Kuiper (8), who also gives a diagram showing the log of the effective temperature against stellar sequence. R. M. Petrie (11) has also given a discussion of the temperatures of the O5–B0 stars. The values given for this part of the stellar sequence by the two writers are not in agreement, Kuiper giving 25,000° to 80,000°, whereas Petrie gives 28,000° to 36,000°. However, as Petrie has pointed out, Kuiper uses values obtained by Beals (3) for Wolf Rayet emission as being applicable to the associated O-type spectra, whereas it is now believed that a composite spectrum is really observed and that the emission line temperatures refer to the W star and not the O-type object.

It may be seen that for our curve the values obtained are, for B0, approximately 30,000°, although this is quite rough owing to lack of stars in this general region, and, for O5, an extrapolated temperature in the neighborhood of 40,000°. These figures are slightly higher than those in Petrie's corresponding classification. For the lower end of the scale our values are somewhat higher than those shown by Kuiper.

There are, as is well known, some doubts as to the validity of applying results from such unusual objects as the P Cygni stars to a determination of the general temperature scale of the stellar sequence. However the temperatures of the hotter stars are subject to so much uncertainty and the results of different investigators differ so widely among themselves that it is surely desirable to make full use of data from every possible source in attempting to arrive at a reliable conclusion. In the upper part of the scale involving the early O-type stars the presence of emission lines due to NIII, HeII, and CIII is a fairly normal feature and is shown by one of the typical stars of the group H.D. 188001. It would therefore seem quite permissible to make use of these lines to fix the temperature at this end of the scale.

Those early A-type stars that show P Cygni characteristics are on the other hand mostly quite unusual objects. A number of them have exceptional luminosities while in one or two instances it is suspected that the spectra are composite. As a consequence the present determination is probably entitled to less weight for the lower end of the range than for the O-type stars. From a number of converging lines of evidence the temperature scale has been fixed at 10,000° for class A0 and it will be noted from the diagram that our values are approximately 6000° higher. It should be pointed out however that Williams (12), on the basis of color temperatures, places the temperature of the A0 stars at 15,000° while the Greenwich observers (6) place them even higher so that it is by no means certain the present determination is in error.

For the O type stars it may be recalled that Petrie has derived temperatures of 28,000° to 36,000° while Payne (10) in an earlier work, gives 35,000° for the O stars as a class. The present determination (32,000° to 40,000°) is in

reasonably good agreement with these values and, since the discovery of the binary character of certain Wolf Rayet stars has explained the high values for the O's (65,000°) given by Kuiper, it now becomes possible to speak with some confidence of the order of magnitude of the temperatures in this part of the stellar sequence.

Acknowledgment

The writers wish to express to Dr. J. A. Pearce, Dominion Astrophysicist, their thanks for permission to make use of spectrograms and measures of intensity made at the Dominion Astrophysical Observatory, Victoria, B.C. The observational material was collected by one of the writers (Beals) while a member of the staff at Victoria, and the organization of the data and the calculations were made at Ottawa. Thanks are also due to Dr. R. M. Petrie for help in the classification of the P Cygni stars.

References

1. Beals, C. S. J. Roy. Astron. Soc. Can. 34 : 169. 1940.
2. Beals, C. S. J. Roy. Astron. Soc. Can. 38 : 65. 1944.
3. Beals, C. S. Pubs. Dominion Astrophys. Observ. Victoria, B.C. 6 : 93. 1934.
4. Bowen, I. S. Astrophys. J. 81 : 1. 1935.
5. Cillié, G. M.N. 92 : 820. 1932.
6. Dyson, Sir. F. Observations of color temperatures of stars. H.M. Stationary Office, London. 1932.
7. Harper, W. E., Pearce, J. A., Beals, C. S., Petrie, R. M., and McKellar, A. Pubs. Dominion Astrophys. Observ. 6 : 317. 1937.
8. Kuiper, G. P. Astrophys. J. 88 : 429. 1938.
9. Mohler, O. Pubs. Observ. Univ. Mich. 5 : 43. 1933.
10. Payne, C. H. Stellar atmospheres. Harvard Observ. Monograph No. 1. 1925.
11. Petrie, R. M. Pubs. Dominion Astrophys. Observ. Victoria, B.C. 7 : No. 21. (In press).
12. Williams. Pubs. Observ. Univ. Mich. 7 : 147. 1939.
13. Wright, K. O. Pubs. Dominion Astrophys. Observ. Victoria, B.C. 8 : No. 1. (In press).
14. Zanstra, H. Pubs. Dominion Astrophys. Observ. Victoria, B.C. 4 : 209. 1929.

A RADIO METHOD OF STUDYING THE YAW OF SHELLS[1]

By C. C. Gotlieb, P. E. Pashler, and M. Rubinoff[2]

Abstract

A new method of investigating the angular motion of a shell in flight is described. This is a radio method wherein the fuse of the shell is replaced by a high frequency transmitter and the radiated signal is recorded at a ground station. The theory of the method is given, the equipment described, and the procedure in the analysis of the records is discussed. Results of experiments are quoted and values of the force coefficients are deduced. In addition to those coefficients usually determined by jump card experiments, certain other coefficients, involving spin, are evaluated. The radio method of measuring yaw is compared with other methods.

I. Introduction

This paper contains an account of certain work in ballistics carried out by the authors at the Department of Physics, University of Toronto.

The subject of the work is a new method of investigating the angular motion of a shell in flight. This method was made possible by techniques originating in the radio proximity fuse development. Early in the fuse development it was found that the spin of the shell could be determined, and considerable attention was given to this both in the U.S. and Canada. Later, work was done at the University of Toronto in an effort to correlate certain features of spin recordings with secondary oscillations of the shell. The essential feature of the present method, however, was put forward by Mr. A. F. H. Thomson of the Directorate of Naval Ordnance (U.K.), who suggested a method for the measurement of the yaw angle of a shell.

In the radio method of investigating a shell's flight the fuse of the shell is replaced by a high frequency radio transmitter and the radiated signal is recorded at a suitably located ground station. The angular oscillations of the shell produce corresponding changes in signal level, and this paper describes how these fluctuations in signal strength may be used to determine the angular motion. The theory of the radio method is given, and, after certain simplifying assumptions are made, a formula suitable for application to experimental results is derived.

The angular motion of a shell in flight has been the subject of considerable study in the past. Most previous work has, of course, been devoted to problems of immediate practical concern in the design of projectiles. However, a fundamental study was made by Fowler, Gallop, Lock, and Richmond (2) who published their results just after the Great War. In their paper, a system of forces was assigned, the equations of motion were set up and solved approximately, and the theories were tested by experiment. In this paper the same force system and angular motion is assumed, and there follows a summary of those results that are employed in the radio method.

[1] *Manuscript received in original form September 9, 1947, and, as revised, February 11, 1948.*

[2] *Present address: Institute of Advanced Studies, Princeton, N.J.*

II. The Theoretical Background

1. The Force System

Let the instantaneous direction of the axis of the shell be represented in Fig. 1 by OA, and the instantaneous direction of motion of the center of mass O, by OP. By definition:

(i) The plane AOP is the plane of yaw;

(ii) The angle AOP is the angle of yaw, denoted by the letter δ;

(iii) The angle of rotation of the plane of yaw about OP is the azimuth, denoted by the letter ϕ.

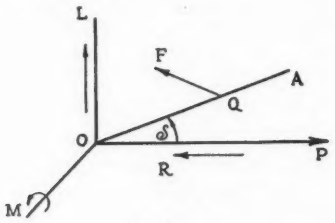

Fig. 1.

For the moment, we regard the shell as at rest and the air streaming past it with uniform velocity, v, equal and opposite to that of the shell. The aerodynamic forces can be represented through symmetry by a single force F, located in the plane of yaw, and acting through the center of pressure, Q, on the axis OA. The force F can be replaced, as shown in Fig. 1, by

(i) The drag R, which acts through O in the direction of the air stream;

(ii) The cross-wind force L, which acts through O in the plane of yaw, perpendicular to R, and is positive when it tends to move O in the direction from P to A;

(iii) The moment M about O, perpendicular to the plane of yaw, and positive when it tends to increase δ.

The following forms are assumed for R, L, and M:

$$(1) \qquad \begin{aligned} R &= \rho v^2 r^2 f_R(v/a, \delta) \\ L &= \rho v^2 r^2 f_L(v/a, \delta) \sin \delta \\ M &= \rho v^2 r^3 f_M(v/a, \delta) \sin \delta, \end{aligned}$$

where ρ is the density of the air, r the radius of the shell, and a the velocity of sound in the undisturbed medium.

These equations are of the most natural form to make the force coefficients f_R, f_L, and f_M, of no physical dimensions. Since L and M vanish with δ through symmetry, the factor $\sin \delta$ is included explicitly in order that f_L, f_M, may have non-zero limits as $\delta \to 0$. Further discussion of the dependence of the force coefficients on the constants of the medium (diameter of molecules, ratio of specific heats, etc.) is given in § 1.01 of the paper by Fowler *et* al.

In practice the direction of the axis of the shell changes relative to the direction of motion. We assume that R, L, and M are unaltered by the angular velocity of the axis, but that the effect of the angular motion of the axis of the shell can be represented by the introduction of a damping couple, H, called the "yawing moment due to yawing" and acting in such a way as directly to diminish the resultant angular velocity, ω, of the axis of the shell, as shown in Fig. 2.

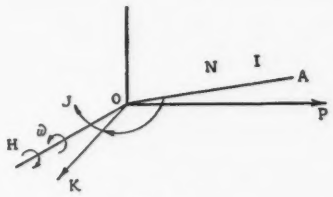

FIG. 2.

There is a possible effect due to the spin N of the shell about its axis. It is assumed that the spin does not affect any of the preceding force components but gives rise to additional components. There will be a couple I which tends to reduce N. When the shell is yawed, there will be a sideways force K', analogous to that producing swerve on a tennis ball, which need not act through O but which must act normal to the plane of yaw, if it is not to alter R or L, as assumed. The force K' can be represented by an equal force K through O and a couple J about O. The complete effects of spin can be represented, therefore, by the addition of the couples I and J and the force K, acting as shown in Fig. 2.

These forces are represented by the equations:

$$\begin{aligned} H &= \rho v \omega r^4 f_H(v/a, \ldots) \\ I &= \rho v N r^4 f_I \\ J &= \rho v N r^4 f_J \sin\delta \\ K &= \rho v N r^3 f_K \sin\delta \end{aligned} \tag{2}$$

As before, the force coefficients are of no physical dimensions. Moreover, these force coefficients may depend appreciably on other arguments, such as $\omega r/v$ and δ.

In deriving the equations of motion, Fowler *et al.* were able to simplify the algebra by defining new coefficients by the equations:

$$\begin{aligned} M &= \mu \sin\delta \\ L &= \kappa m v \sin\delta \\ H &= hB\omega \\ I &= -AN\Gamma \\ J &= AN\gamma \sin\delta, \end{aligned} \tag{3}$$

where A and B are, respectively, the moments of inertia of the shell about longitudal and transverse axes through the center of gravity, and m is the mass of the shell.

The complete force system is seen to consist of seven components; of these, by far the most important are R, L, and M; then, somewhat less important, H. Only one relation between the forces is available, that between R, L, and M. For shells of given shape moving in a given manner, the forces R and L are independent of the position, O, of the center of gravity, while the moment M varies with the position of O. If M_1 and M_2 are the values of M corresponding to positions O_1 and O_2, then

$$M_1 = M_2 + O_1O_2(L \cos \delta + R \sin \delta), \tag{4}$$

where $O_1\ O_2$ is positive when O_1 is nearer the base than O_2. For small yaw, this equation reduces to:

$$f_{M_1} = f_{M_2} + \frac{O_1O_2}{r}\,(f_L + f_R)\,. \tag{5}$$

This is the only method of finding f_L.

2. Description of the Angular Motion

We consider here only what Fowler *et al.* call "Motion of Type α". This type of motion occurs in the early part of all trajectories, and for the whole of a trajectory whose initial elevation is less than 45° and muzzle velocity greater than a few hundred feet per second. The characteristic feature of Type α motion is that the axis of the shell and the direction of motion of the C.G. deviate only by small angles from the tangent to the corresponding plane trajectory. To simplify the treatment to be employed here, the assumption is made that the directions of motion in the plane trajectory and in the actual trajectory are parallel for that region of the trajectory under investigation (up to six seconds from the instant of firing). This assumption can be justified to experimental accuracy in this case by reference to Sections 3.64 and 3.65 of Reference (2). The following system of axes is chosen; the $O1$ axis is the direction of motion of the center of gravity; the $O2$ axis is the upward normal; and the $O3$ axis is horizontal and to the right as viewed from the gun (Fig. 3).

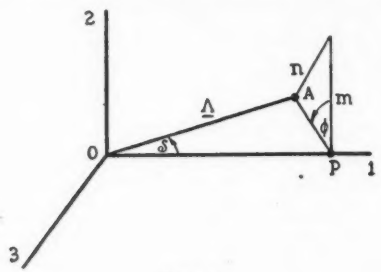

FIG. 3.

OA is the axis of the shell, which is represented by the unit vector Λ. Λ has components l, m, and n (the direction cosines of OA). The angle of yaw δ is, by definition, the angle between $O1$ and OA; and ϕ, the angle of orientation,

is specified as the angle between the plane $AO1$ and the plane $1O2$. l, m, and n are related to δ and ϕ by:

$$\begin{aligned} l &= \cos\delta \\ m &= \sin\delta\cos\phi \\ n &= \sin\delta\sin\phi. \end{aligned} \tag{6}$$

The assumptions made by Fowler, Gallop, Lock, and Richmond in treating motion of Type α are the following:

(i) The $O1$ axis makes a slowly varying angle θ with the horizontal, so $\dot{\theta}$ is small compared to the spin N,

(ii) The yaw δ is small (less than, say, 7°),

(iii) The total effect of the components h, κ, Γ, γ, is small, so that all terms other than those of the lowest order in δ can be neglected.

The stability factor for a spinning shell is defined as

$$s = \frac{A^2N^2}{4B\mu}. \tag{7}$$

It is found that the condition for stability is that s be greater than unity. This is, of course, analogous to the condition for stability of a spinning top.

When this condition is satisfied, the following solution is found for the equations of motion in the terms of the direction cosines, l, m, and n: (these equations follow directly from those of § 4.0 in the Fowler paper)

$$\begin{aligned} m &= \tfrac{1}{2}(\alpha+\beta)\cos 2\pi\int_{t_1}^{t}(n_1+n_2)dt - \tfrac{1}{2}(\alpha-\beta)\cos 2\pi\int_{t_2}^{t}(n_1-n_2)dt, \\ n &= \tfrac{1}{2}(\alpha+\beta)\sin 2\pi\int_{t_1}^{t}(n_1+n_2)dt - \tfrac{1}{2}(\alpha-\beta)\sin 2\pi\int_{t_2}^{t}(n_1-n_2)dt, \end{aligned} \tag{8}$$

where:

$$\begin{aligned} \tfrac{1}{2}(\alpha+\beta) &= \tfrac{1}{2}(\alpha_0+\beta_0)\left(\frac{\Omega_0\sigma_0}{\Omega\sigma}\right)^{\frac{1}{2}} \\ &\quad \exp.\left\{-\tfrac{1}{2}\int_0^t\left[(h+\kappa)+\frac{1}{\sigma}(h-\kappa+2\gamma-\Gamma)\right]dt\right\} \\ \tfrac{1}{2}(\alpha-\beta) &= \tfrac{1}{2}(\alpha_0-\beta_0)\left(\frac{\Omega_0\sigma_0}{\Omega\sigma}\right)^{\frac{1}{2}} \\ &\quad \exp.\left\{-\tfrac{1}{2}\int_0^t\left[(h+\kappa)-\frac{1}{\sigma}(h-\kappa+2\gamma-\Gamma)\right]dt\right\}. \end{aligned} \tag{9}$$

and α_0, β_0, t_1, and t_2 are arbitrary constants of integration, and

$$\Omega = \frac{AN}{B}, \quad \sigma = \sqrt{1-1/s}, \quad n_1 = \Omega/4\pi, \quad n_2 = \Omega\sigma/4\pi,$$

$$(n_1+n_2) = \Omega(1+\sigma)/4\pi, \qquad (n_1-n_2) = \Omega(1-\sigma)/4\pi.$$

The subscript zero is used to give a variable its value at the muzzle.

In Equation (8) it is seen that the vertical component m, and the horizontal component n, of the motion of the axis, are composed of two periodic terms. One, called the nutational term, consists of a damped oscillation of instantaneous frequency $(n_1 + n_2)$ and instantaneous amplitude $\frac{1}{2}(\alpha + \beta)$. The other, called the precessional term, is a damped oscillation of frequency $(n_1 - n_2)$ and amplitude $\frac{1}{2}(\alpha - \beta)$. The ratio of these two frequencies for the projectiles employed here was about 10 to 1. An exaggerated graph of m is shown in Fig. 4 with the contribution of each term shown separately.

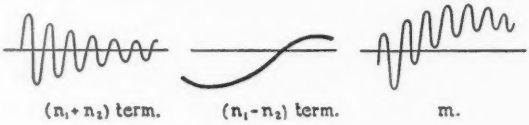

FIG. 4.

From a continuous record of the vertical component m it is possible to deduce all the force coefficients previously defined except f_R, f_I, and f_K. f_M can be derived from $(n_1 + n_2)$ and $(n_1 - n_2)$; f_L may be determined from the values of f_M found for various positions of the centers of gravity of the shells. f_H and f_J may be determined by evaluating the exponents of decay of $\frac{1}{2}(\alpha + \beta)$ and $\frac{1}{2}(\alpha - \beta)$. f_I can be determined directly from the radio trace, by a method to be described in Section IV. f_R must be determined by chronograph measurements of the retardation of the forward motion of the shells.

III. The Radio Method

1. Qualitative Description of the Method

The Thomson radio method of yaw measurement depends on the fact that for a radio fused shell, the radiation in a direction making an angle θ with the axis of the shell is very closely proportional to sin θ. This is most nearly true in the region up to 10° from the axis to the rear.

The electric axis of the shell as a radiator comes close to, but seldom coincides with, the physical axis of symmetry. A small angle between the two will be assumed in deriving the fundamental equations, but will be taken as zero in the present section.

If a receiver be located on the instantaneous axis of the shell extended, no signal will be received. For a small angular displacement of the axis, the electric field intensity at the receiver will be proportional to the sine of the angle between the axis and the line joining the shell and the receiver (line of sight). If the receiving antenna be oriented to respond, say, to the vertical component of the electric field, the signal received will be proportional to the vertical component of the angular displacement (Fig. 5). Thus the received signal will be zero when the axis is deflected horizontally, to the right or left, and will reach a maximum value when the axis is deflected vertically either

up or down. There is no method of distinguishing between these up and down deflections, and there is no means of determining the absolute value of the angular displacement from a receiver record.

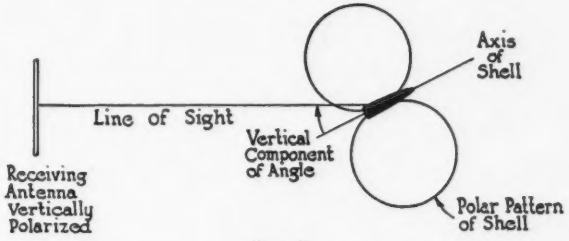

FIG. 5.

These difficulties are overcome for yaw measurement by locating the antenna so that there is always an angle between the axis and the line of sight in excess of the expected yaw angle, and by orienting the antenna to respond only to radiation polarized in the plane of this angle. To do this, the antenna is located in the plane of the trajectory, a distance ahead of the gun, and oriented to respond only to vertically polarized radiation, as in Fig. 6.

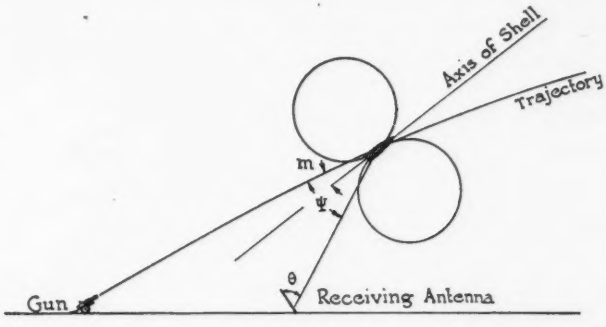

FIG. 6.

The signal will then be proportional to $\sin(\psi + m)$, where ψ is the angle between the line of sight and the tangent to the trajectory, and m is the vertical component of the angle between the axis of the shell and the tangent to the trajectory. The mean signal level is approximately proportional to $\sin \psi$. Hence the ratio $\sin(\psi + m)/\sin\psi$ is equal to the ratio between the instantaneous and mean signal levels (Fig. 7). From a knowledge of the trajectory and the geometry of the receiver and gun locations, it is possible to find the angle ψ as the shell moves through space. Then knowing the value of ψ it is possible to determine m. By proper choice of Q.E. and the distance gun to antenna, it is possible to arrange that ψ stays reasonably constant over a

desired region of the early part of the trajectory. For example, in certain of the experiments discussed later, ψ lay between $4\frac{1}{2}°$ and 3°, from one to five seconds time of flight.

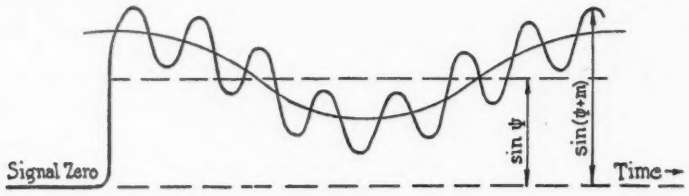

FIG. 7. *Receiver record.*

2. DERIVATION OF THE FUNDAMENTAL EQUATIONS OF THE RADIO METHOD

(*a*) *Assumptions*

The following are the assumptions in the derivation of the fundamental equations of the radio method:

(i) The polar pattern of the radiation from the shell is sinusoidal, i.e., the field strength $\boldsymbol{E}$ is proportional to the sine of the angle between the electric axis of the shell as a radiator, and the direction of propagation.

(ii) The electric axis Σ of the shell is inclined to the geometric axis, Λ, of the shell by an angle ϵ.

(iii) The radiation from the shell is plane polarized; i.e., $\boldsymbol{E}$ lies in the plane containing the electric axis Σ and the direction of propagation.

(iv) The receiving antenna responds only to the component of $\boldsymbol{E}$ lying in the plane containing the antenna, and the direction of propagation.

(*b*) *Antenna Voltage Due to a Shell in Space*

For the general case of a radiating shell, located and oriented arbitrarily in space, we define the following vectors:

(i) Λ, a unit vector coinciding with the geometric axis of the shell,

(ii) Σ, a unit vector coinciding with the electric axis of the shell,

(iii) $\boldsymbol{R}$, a unit vector in the direction of propagation, i.e., a line joining the C.G. of the shell and the reference point of the receiving antenna,

(iv) $\boldsymbol{E}$, the electric field vector at the receiving antenna, given by:

$$\boldsymbol{E} = \frac{K}{r}\{\boldsymbol{R} \times (\boldsymbol{R} \times \Sigma)\}, \tag{10}$$

where K is a scalar proportionality factor depending on power, wave length, etc., and r is the distance from the shell to the receiving antenna.

(v) $\boldsymbol{A}$, a unit vector in the direction of the antenna axis. The voltage induced by a field $\boldsymbol{E}$ in an infinitesimal dipole can be expressed as:

$$V = c\,\boldsymbol{E} \cdot \boldsymbol{A},$$

where c is a scalar quantity depending on wave length, units, etc. For a directional array, we may write:

$$V = \boldsymbol{E} \cdot \boldsymbol{A}\, F(\theta, \chi)$$

where θ is the polar angle measured from $\boldsymbol{A}$;

χ is the azimuthal angle measured from an arbitrary plane through $\boldsymbol{A}$;

and $F(\theta,\chi)$ is a scalar function, such that $F(\theta,\chi)/c$ represents the gain of the array relative to the dipole.

Then, substituting for $\boldsymbol{E}$ from Equation (10):

$$V = \frac{K}{r} F(\theta,\chi)\, \boldsymbol{A} \cdot \{\boldsymbol{R} \times (\boldsymbol{R} \times \Sigma)\}$$

(11)

$$= \frac{K}{r} F(\theta,\chi)\, \boldsymbol{A} \cdot \{\boldsymbol{R}(\Sigma \cdot \boldsymbol{R}) - \Sigma\}$$

To determine the components of these vectors we employ the system of axes, $O1$, $O2$ and $O3$, previously defined (Fig. 8). Let $\boldsymbol{O1}$, $\boldsymbol{O2}$, $\boldsymbol{O3}$ represent unit vectors on their corresponding axes.

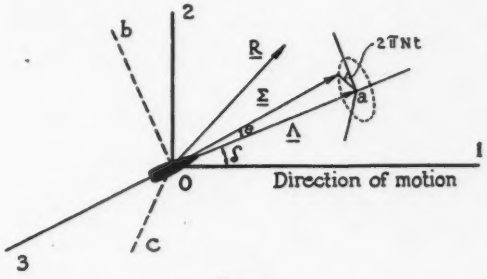

FIG. 8.

Λ makes an angle δ (the yaw angle) with $\boldsymbol{O1}$, and the plane of $\boldsymbol{O1}$ and Λ makes an angle ϕ (the angle of orientation) with the $1O2$ plane.

$$\therefore \Lambda = \cos\delta\, \boldsymbol{O1} + \sin\delta\cos\phi\, \boldsymbol{O2} + \sin\delta\sin\phi\, \boldsymbol{O3}. \tag{12}$$

At O we define another unit triad, $\boldsymbol{Oa}$, $\boldsymbol{Ob}$, $\boldsymbol{Oc}$. In it $\boldsymbol{Oa} = \Lambda$, $\boldsymbol{Ob}$ is in the plane of $\boldsymbol{O2}$ and Λ, $\boldsymbol{Oc}$ is perpendicular to $\boldsymbol{Oa}$ and $\boldsymbol{Ob}$. The electric axis Σ passes through the center of gravity, and makes an angle ϵ with Λ. Owing to the spin N, of the shell, Σ rotates with angular velocity $2\pi N$ about Λ.

Then in the $\boldsymbol{a\,b\,c}$ triad, reckoning the angle $2\pi Nt$ from the aOb plane:

$$\Sigma = \cos\epsilon\, \boldsymbol{Oa} + \sin\epsilon\cos 2\pi Nt\, \boldsymbol{Ob} + \sin\epsilon\sin 2\pi Nt\, \boldsymbol{Oc}. \tag{13}$$

To transform the Σ vector into the $\mathbf{1\,2\,3}$ triad we require the components of $\boldsymbol{Oa}$, $\boldsymbol{Ob}$, $\boldsymbol{Oc}$, referred to the $\mathbf{1\,2\,3}$ triad:

$$\boldsymbol{Oa} = \cos\delta\, \boldsymbol{O1} + \sin\delta\cos\phi\, \boldsymbol{O2} + \sin\delta\sin\phi\, \boldsymbol{O3},$$

and ***Ob***, ***Oc*** are determined as unit vectors perpendicular to ***Oa***. For δ small, so that $\sin \delta \approx \delta$, $\cos \delta \approx 1$, these reduce to:

$$\begin{aligned} \boldsymbol{Oa} &= \boldsymbol{O1} + \delta \cos \phi\, \boldsymbol{O2} + \delta \sin \phi\, \boldsymbol{O3} \\ \boldsymbol{Ob} &= -\delta \cos \phi\, \boldsymbol{O1} + \boldsymbol{O2} \\ \boldsymbol{Oc} &= -\delta \sin \phi\, \boldsymbol{O1} + \boldsymbol{O3}. \end{aligned} \tag{14}$$

Substituting the above values for ***Oa***, ***Ob***, and ***Oc***, in Equation (13), with the additional approximation that ϵ is small, so that $\sin \epsilon \approx \epsilon$, $\cos \epsilon \approx 1$, $\epsilon\delta \approx 0$ we find:

$$\Sigma = \boldsymbol{O1} + (\delta \cos \phi + \epsilon \cos 2\pi Nt)\boldsymbol{O2} + (\delta \sin \phi + \epsilon \sin 2\pi Nt)\boldsymbol{O3}. \tag{15}$$

R lies in the 1*O*2 plane, and the angle between ***R*** and ***O1*** is ψ, and therefore:

$$\boldsymbol{R} = \cos \psi \boldsymbol{O1} + \sin \psi \boldsymbol{O2}. \tag{16}$$

A lies in the 1*O*2 plane, inclined to *R* by the angle θ, so that

$$\boldsymbol{A} = \cos (\psi + \theta)\boldsymbol{O1} + \sin (\psi + \theta)\boldsymbol{O2}. \tag{17}$$

Substituting these values in Equation (11), we have:

$$V = \frac{K}{r} F(\theta, \chi) \sin \theta (\sin \psi - \cos \psi\ \delta \cos \phi - \epsilon \cos 2\pi Nt)$$

If we arrange in the experiments that ψ remains small, so that $\sin \psi \approx \psi$, $\cos \psi \approx 1$, and compressing $F(\theta,\chi) \sin \theta$ into $f(\theta)$, (since χ is nearly constant for an actual trajectory), this may be written:

$$V = \frac{K}{r} f(\theta)\ (\psi - \delta \cos \phi - \epsilon \cos 2\pi Nt). \tag{18}$$

When the spin is not of immediate interest ϵ is put equal to zero to obtain:

$$V = \frac{K}{r} f(\theta)\ (\psi - m). \tag{19}$$

3. The Equipment

The equipment required for measurement of yaw by the radio method is the following:

(i) A radio fuse that can be fitted to standard artillery shells and that radiates a signal approximately as assumed in III – 2,

(ii) A receiving antenna, responding to vertically polarized radiation,

(iii) A radio receiver, tuned to the frequency of the signal from the fuse, and whose output voltage is proportional to the input voltage from the antenna,

(iv) A cathode ray oscilloscope, permitting the output voltage to be photographed,

(v) A timing device, indicating on the film record (1) the time when the gun is fired and (2) the time at any subsequent point on the film.

The equipment developed for this work is described in this section. In Part (*a*) the fuse, or radio sonde, is discussed, in (*b*) the antenna, and in (*c*) the receiver, and its associated apparatus.

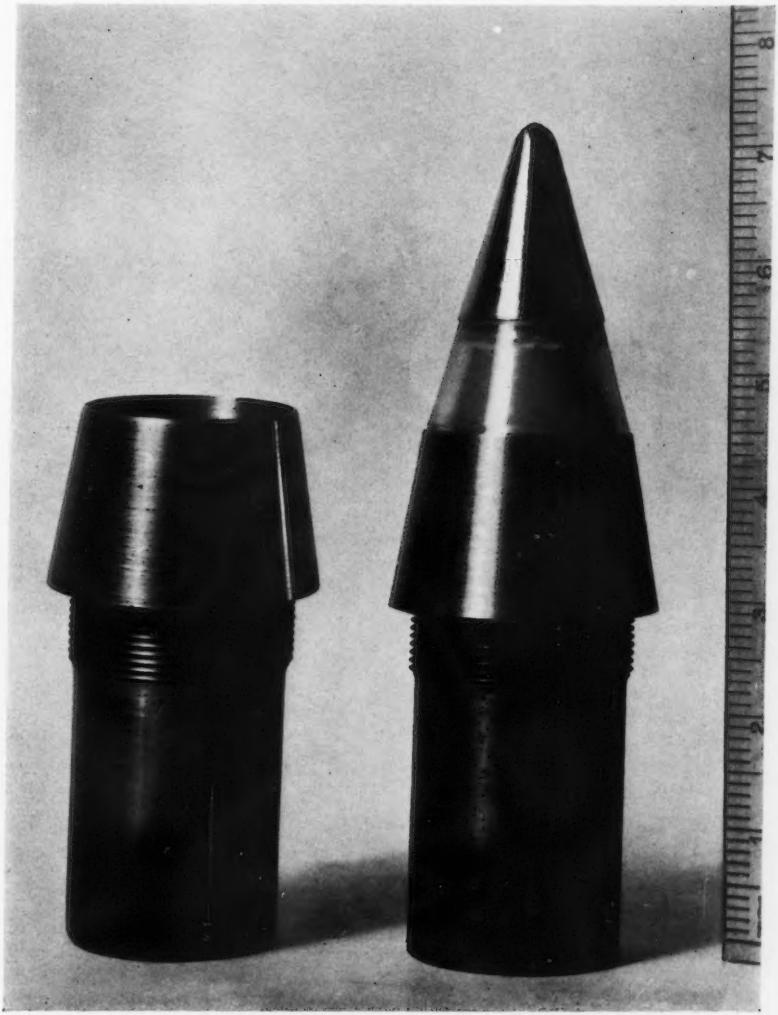

FIG. 9. *The yaw fuse.*

(*a*) *The Radio Sonde*

The requirements of the radio sonde are:

(1) The polar radiation pattern at the rear of shell must be sinusoidal, and must be a figure of revolution whose axis nearly coincides with the axis of the shell.

(2) Power radiated must be sufficient to give signals well above the noise level of the receiver, even when the shell is at the largest distance from the receiver.

(3) The frequency must be capable of adjustment in the laboratory, so that, on firing, the sonde frequency will lie as nearly as possible at the mid-band of the receiver.

(4) The frequency drift of the unit over the useful time of flight must be small.

(5) The variation in output power over the useful time of flight must be small.

A photograph of the sonde is shown in Fig. 9. The oscillator circuit is conventional, but of course employs rugged (V.T. Fuse) components. The battery is a regular V.T. Fuse battery.

Requirement (1) was attained by using the lowest possible frequency. The portion of the polar pattern actually used is that not exceeding 20° from the axis of the shell at the rear. Stationary tests were made in a large open field to check this region. The shell was supported by a polystyrene rod about 6 ft. long. The axis of the shell was horizontal and the shell was rotated about a vertical axis. Relative field strengths were then measured a few hundred feet away. These tests indicated that the polar pattern was sinusoidal in the required region, as closely as measurable. In addition, within the accuracy of these tests, the electric axis and the geometric axis of the shell appeared to coincide. As discussed in Section IV – 5(*a*), this is not strictly accurate.

Requirement (3) was met by taking special care with the oscillator coil, and by using, for final tuning, a number of nose caps of different sizes. This gave sufficient adjustment to bring all the frequencies within the desired range.

Requirement (4) of small frequency drift was checked by following a number of units in flight with a narrow-band receiver. These tests did not reveal any frequency drift.

Requirement (5) of no power drift was checked in the laboratory. Over relatively long periods (several minutes) no change in power output could be detected.

(*b*) *The Receiving Antenna*

The requirements of the receiving antenna are:

(1) A directivity pattern that discriminates in azimuth against reflections from behind and from the sides.

(2) Independence of effects due to variations in ground conditions.

(3) In the region of maximum reception a response that is independent of elevation over a range of about 10° and of azimuth over a range of at least 4°.

(4) A radiation resistance to match the 50 ohm characteristic impedance of the coaxial cable to the receiver.

(5) Maximum possible gain over a half-wave dipole.

(6) Portability and ease of assembly in the field.

(7) Provision for tilting in the vertical plane to investigate any part of the trajectory.

It was decided to use a 90° corner array, but to provide it with a ground screen in order to ensure the second requirement above. This type of antenna was first investigated by Kraus (4), whose conclusions can be summarized as follows: (1) the physical dimensions of the array are not critical, (2) a power gain of 10 is possible using a 90° corner, and (3) for dimensions smaller than two wave lengths, the performance of corner arrays equals that of parabolic reflectors and horns.

The directivity patterns of the antenna in azimuth and in elevation are shown in Figs. 10 and 11.

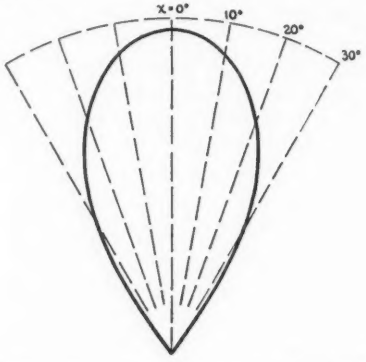

FIG. 10. *Directivity pattern of antenna in azimuth* ($\theta = 90°$).

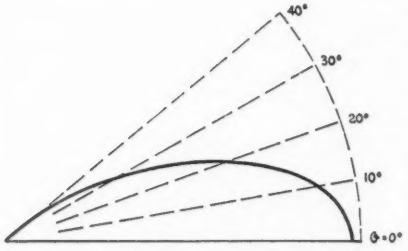

FIG. 11. *Directivity pattern of antenna in elevation* ($\chi = 0°$).

(*c*) *The Receiving System*

The requirements of the receiver are:

(1) Ability to find the signal within 0.5 sec. of firing of the shell.

(2) A sensitivity adequate for good photography for the trajectory region under investigation.

(3) A means of recording the amplitude of the radio-frequency signal.

(4) Linearity of output with input.

(5) Insensitivity to line voltage fluctuations.

(6) A method of providing an accurate time scale from the instant the gun is fired.

Fig. 12 shows the block diagram of the receiving system.

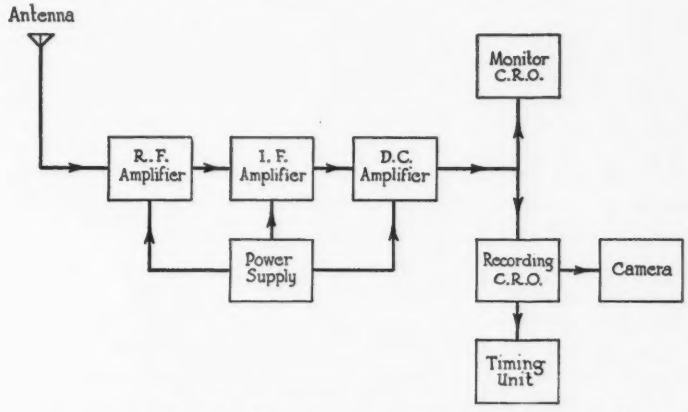

FIG. 12. *Block diagram of receiving system.*

Since the yaw is largest very early in flight, it is essential that there be as little delay as possible in obtaining a usable signal. Moreover it is necessary to hold this signal once it is found, since tuning the receiver would affect its output and make yaw measurements impossible. Therefore it was decided that manual tuning during shell flight was undesirable, and that a fixed-frequency, broad-band receiver would meet the requirements best. Because the sondes may show a certain frequency spread there was included a tuning condenser on the local oscillator. Before each round is fired the receiver is tuned to the laboratory measured frequency for that sonde. Nevertheless a bandwith of a few megacycles is desirable, because a sharply tuned receiver would respond to frequency drift as a change in signal strength which could not be distinguished from changes due to variations of orientation and distance of the shell. Automatic frequency control was considered as a means of eliminating this difficulty, but it was found unnecessary.

Preliminary calculations and experience with the proximity fuse indicated that to ensure good signals over a 25 sec. time of flight it would be necessary to employ a high sensitivity receiver. This problem of high sensitivity and wide band was exactly that which had been overcome in the construction of radar receivers, and it was decided that it would be simplest to modify such a receiver. The frequency was adjusted to cover the desired range, and a switch was introduced, thus permitting the gain to be altered in six fixed steps. For linearity of response, a diode detector was employed.

Recording the carrier level of the radio-frequency signal requires direct coupling between the detector and final indicator, the cathode ray oscillograph. A direct-coupled amplifier consisting of a single 6AC7 was employed for this purpose.

Sometimes it is an advantage to listen to the spin modulation of the sonde. For this there is an A.F. amplifier and speaker.

The d-c. amplifier is followed by two 3 in. cathode ray oscilloscopes, one with a green tube for monitoring, the other blue for photographing. The no-signal voltage on the C.R.O. plates is that of the d-c. amplifier plate, i.e., 175 v. Therefore, the high voltage must be specially insulated to make centering and focusing possible. A horizontal sweep voltage may be applied to the monitor if desired. Because of the vertical motion of the film the recording tube is rotated 90° so that horizontal deflections on it correspond to vertical deflections on the monitor.

In order to relate the instantaneous position of the shell in space to the corresponding point on the trace it is necessary to put a time scale on the records. This was provided by a series of timing marks at intervals of 1/100 sec., about 1/6 in. apart on the film. These are obtained by photographing a narrow slit illuminated by a neon bulb, pulsed from an independent timing unit.

The master timekeeper is a 1000 c.p.s. tuning fork oscillator (General Radio Type 813-A). The output of the oscillator is fed into a peak clipper and thence to a step circuit. By careful adjustment of the cathode voltage of the step tube, the step circuit is made to trigger an asymmetrical multivibrator at the beginning of the seventh step. Another four milliseconds are allowed for the step circuit to discharge; thus the full cycle is completed in 1/100 sec. The multi-vibrator delivers a 300 v. pulse of 10 μsec. duration to the neon bulb. Examination of the wave form of the voltage across the neon bulb shows that the firing time repeats itself to better than 1 μsec.

A fiducial mark for the time scale is obtained by momentarily switching a resistor in parallel with the plate load of the d-c. amplifier. This introduces a sharp rise of short duration on to the trace. The switch is operated by the pressure from the blast of the gun. The moving part is a copper disk about 3 in. in diameter. The whole switch is mounted in a box and placed to the side and slightly behind the muzzle of the gun. The time delay in switch operation was measured by a separate chronograph trial and the necessary correction was made for each round.

The zero signal position of the C.R.O. spot is extremely sensitive to voltage fluctuations, especially to the I.F. screen voltage, the d-c. amplifier heater and the high voltage of the C.R.O. The primary source of power for most of the trials was a 60 cycle, 1500 w., Homelite gasoline generator. This has quite stable operation for its type, but surges of ± 5 v. occurred frequently. Therefore it was decided to use power supplies stabilized by negative feedback. A similar type of unit is used in the 700 v. supply of the C.R.O.'s and here also the stability is more than adequate. The heater voltage of the d-c. amplifier is supplied by a 6 v. storage battery. The heater voltages on the R.F. and I.F. amplifiers are not critical. The over-all system is such that rapid generator fluctuations do not affect the spot position appreciably. A slow change causes a steady drift but this is negligible over the 20 sec. time of flight of a single round.

The Recording Camera employed is the General Radio Oscillograph recorder, Type 651-AE, with lens 651-PI. This is a continuous drive camera taking either 16 or 35 mm. film; 35 mm. film (Kodak Super XX) was used throughout on this work. For photography the lens is opened to $f/1.5$. The maximum writing speed is about 56 in. per sec.

The complete equipment is held in a shockproof steel rack and can be mounted in a three ton Dodge truck in which complete equipment for trials is carried.

IV. The Experiments and Experimental Results

1. Description of the Experiments

Experiments were performed using the radio method to measure yaw of the 25 pr. shell. The firings were performed on Nov. 15, Nov. 23, and Dec. 3, 1945. The Artillery Proof Establishment of the Inspection Board of the United Kingdom and Canada, at Hamilton, Ontario, supplied guns, propellant, and gun crews. The firings were held at the Winona Rifle Range of the Department of National Defence.

The gun employed was the 25 pr., firing H.E. MK. I. D, streamline shell. All rounds were fired with normal full charge at a quadrant elevation of 20°, from a barrel in the first quarter of wear. The gun was located about 300 yards from the shore, and pointed over Lake Ontario. The antenna was located 227.4 ft. in front of, and 6.1 ft. below, the muzzle of the gun, in the vertical plane containing the trajectory. A mound of earth, 20 ft. high by 30 ft. thick was located between the antenna and recording station, and the gun.

The velocities and retardations of all rounds fired were measured by officers of the Canadian Armament Research and Development Establishment, Valcartier, Quebec, using the counter chronographs and photoelectric screens normally used in these measurements. At the trial, measurements were made of temperature, relative humidity, and wind velocity at ground level. The mass, the transverse and longitudinal moments of inertia through the center of gravity (A and B), and the position of the center of gravity, were

determined for all rounds fired. In order to determine f_L by Equation (5) shells of three different mass distributions were fired. In one group sulphur filling was employed, in another, lead, and in the third, a steel plug was placed at the nose beneath the fuse. This produced a range of positions of the centers of gravity of about $\frac{3}{4}$ in.

2. Description of the Trace

A typical trace is reproduced in Fig. 13. The following are salient points:

(i) In the region one to three seconds, three frequency components are evident:

(*a*) A high frequency, of about 250 c.p.s., with fairly small amplitude. This is the spin N.

(*b*) A medium frequency, of about 20 c.p.s., with amplitude of the order of one-quarter film width. This is the $(n_1 + n_2)$ term of the vertical component, m, of the shell's angular motion (see Section II – 2).

(*c*) A low frequency, of about 2 c.p.s., with amplitude of the same order as (*b*) above. This is the $(n_1 - n_2)$ term.

(ii) The $(n_1 + n_2)$ component is gradually decreasing in amplitude, until three seconds, when it has almost wholly disappeared. There is, meanwhile, no marked change in the $(n_1 - n_2)$ component, or in the spin.

(iii) In the region one to two seconds, the level of the entire trace is shifting downwards. Later, it remains almost constant, when the decrease due to $f(\theta)/r$ nearly balances the increase due to increasing ψ.

Certain other points should be noted. Through the middle of the film there is a series of small rectangles. These are the timing light marks, 1/100th sec. apart. They are numbered every 1/10th sec. Before the point marked zero, the trace is at the lower edge of the film, in a steady straight line. At zero time, and following it for 0.15 sec. there are several jogs in the film. These are caused by the pressure switch, actuated by the gun blast. At about 0.2 sec. the first signal is received, but it is so great as to send the trace off scale. By about 0.8 sec. the signal has decreased and is on scale after that. The sudden jump in the height of the trace at 2.2 sec. is caused by a scale change. When the receiver operator saw the signal becoming too low on the monitor oscilloscope, he switched the receiver to a higher gain position, causing this discontinuity.

3. Procedure and Theory of Analysis

The voltage at the receiving antenna, due to the shell in space, is:

$$V = \frac{K}{r} f(\theta)\,(\psi - \delta \cos \phi - \epsilon \cos 2\pi N t). \tag{18}$$

The trajectory of the shells, of course, must be known to permit analyses of the records. The trajectory data specifically required are: the distance along the line of sight from the antenna to the shell; r, the angle between the

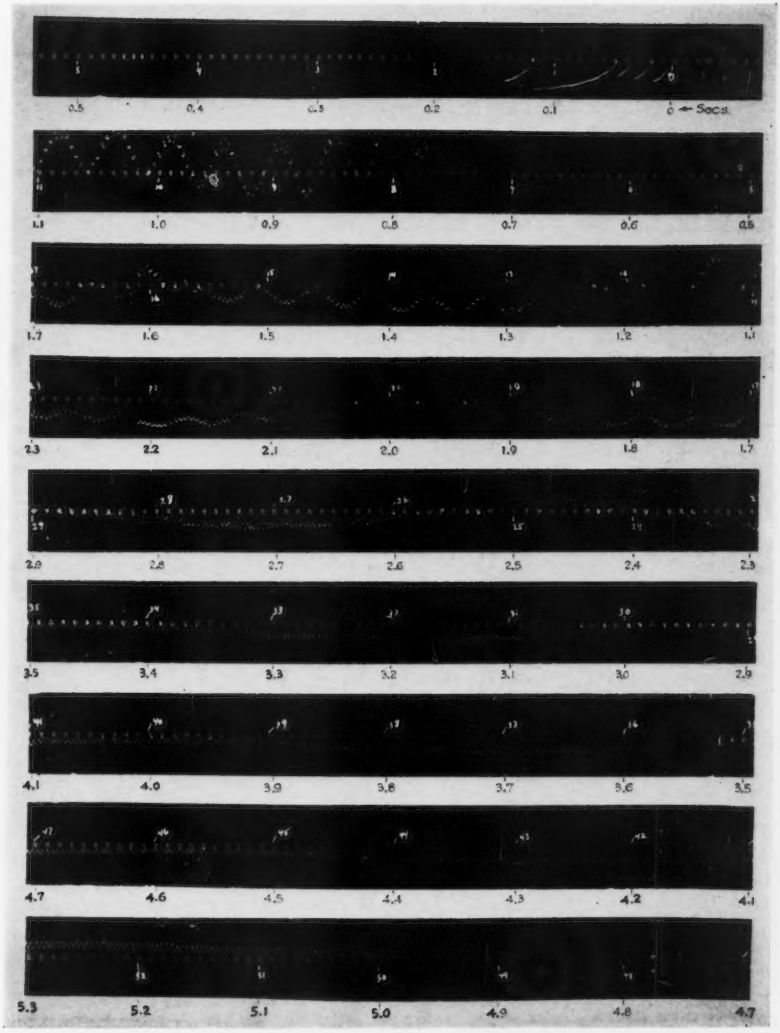

FIG. 13. *Photographic trace of Round 67. 0 to 5.3 sec.*

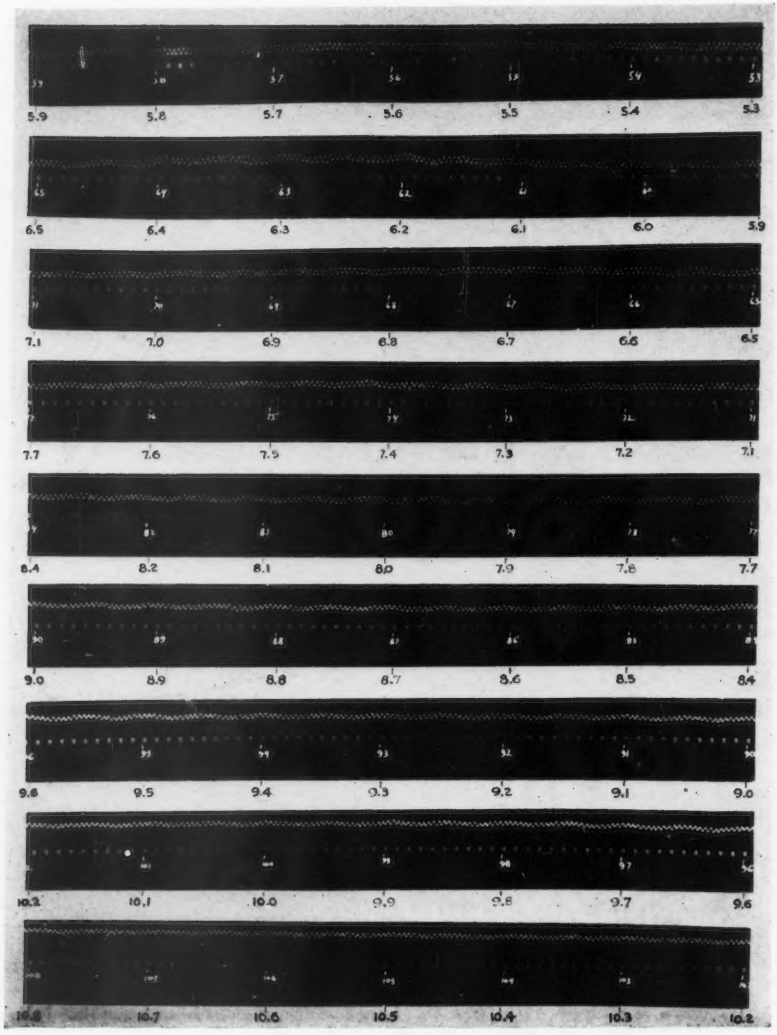

FIG. 13, *continued, 5.3 to 10.8 sec.*

line of sight and the tangent to the trajectory, ψ; and the angle between the line of sight and the reference axis of the antenna, θ (Fig. 6). These can be determined from the trajectory and from the position of the antenna relative to the gun. From these data, and from the calculated response pattern of the antenna, values of $\frac{f(\theta)}{f(\theta_1)} \frac{r_1}{r}$ and ψ were tabulated and plotted against time. r_1 and θ_1 are the values of r and θ at one second. It was necessary to calculate the trajectory of these shells, since the shape of the yaw fuse is different from the fuses regularly employed. A short-arcs method was used for this purpose, the ballistic coefficient being determined by a separate retardation trial.

(*a*) *Preliminary Steps*

To facilitate measurements, enlarged copies of the trace were made by projecting its image on to continuous graph paper, and tracing it in pencil. The complete motions of the oscilloscope spot and the timing dots were carefully reproduced. A magnification of about seven was employed, and, since the distance between sprocket holes on the film is 1 in., the working traces were 7 in. wide.

The first operation on the graph paper was to smooth out the spin modulation, either by estimating the mid-point directly or by drawing the envelopes of the peaks and taking the curve midway between.

(*b*) *The Analysis*

H, the height of the curve above the zero signal level, is a linear* function of the input voltage V; i.e.,

$$H = gV.$$

By Equation (19)

$$V = K\frac{f(\theta)}{r}(\psi - m), \text{ spin being smoothed out.}$$

Hence

$$H = gK\frac{f(\theta)}{r}(\psi - m). \tag{20}$$

It is useful to define two new quantities, as follows:

(i) The variable E, where

$$E = \frac{r}{r_1}\frac{f(\theta_1)}{f(\theta)} H = g\frac{f(\theta_1)}{r_1} K(\psi - m). \tag{21}$$

The factor $g\frac{f(\theta_1)}{r_1}$, which is constant, will be included in K hereafter, so that the dimensions of K become inches displacement on the graph, per degree angular displacement of the shell's axis. That is, we write

$$E = K(\psi - m).$$

** There is a slight 'foot' on the input vs. output of the receiver, but since this can be eliminated by addition of a small constant to H, or use of the input–output curve itself, the above discussion is not in error.*

E was calculated from H for several hundred points on each trace, using Equation (21), and the curve of $\frac{r}{r_1}\frac{f(\theta_1)}{f(\theta)}$.

(ii) The variable G, where

$$(22)\quad G = E - K'\psi = -Km + (K - K')\psi,$$

where K' is a constant, the first approximation to K.

The purpose of the remaining preparatory work was to replace the curve of H by a curve of G. The latter is proportional to m, to a good approximation, since the contribution of $(K - K')\psi$ is very much smaller than the contribution of Km. Thus G is a more suitable graph for analysis of the shell's motion.

It was not difficult, by inspecting the curve of H, to locate approximately the times of the maxima and minima of the low frequency modulation. It was assumed, for this approximation, that at the time t_m, midway between a maximum and a minimum, this low frequency gives no contribution to the trace amplitude. By inspection, or by drawing the envelope of the peaks of the medium frequency $(n_1 + n_2)$, it was possible to estimate the contribution of this frequency component at the time t_m. Thus a good estimate could be made of the trace amplitude for zero vertical component of yaw, i.e., $m = 0$. But then $E = K\psi$, and since ψ is known at all times, this permitted an estimate of K, known as K', to be made. In general K' lay within 5% of the K finally determined.

From the values of K' obtained at a series of points on the trace, from the tabulated values of ψ, and from the values of E, G was calculated by Equation (22). A graph of G versus time was then superimposed on the original tracing of H. Two curves, G_1 and G_2, the envelopes of the maxima and minima, respectively, of the $(n_1 + n_2)$ term, were drawn. A graph typifying the curves G and the envelopes G_1 and G_2 is shown in Fig. 14.

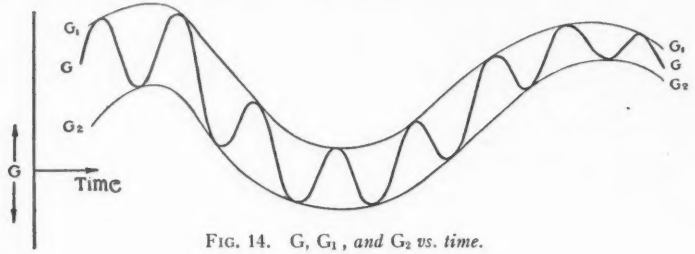

FIG. 14. G, G_1, *and* G_2 *vs. time.*

The equations of these curves are:

$$(23)\quad G = -K\left[\tfrac{1}{2}(\alpha + \beta)\cos 2\pi\int_{t_1}^{t}(n_1 + n_2)\,dt - (\alpha - \beta)\cos 2\pi\int_{t_2}^{t}(n_1 - n_2)dt\right] + (K - K')\psi.$$

$$(24)\quad G_1 = -K\left[-\tfrac{1}{2}(\alpha+\beta)-\tfrac{1}{2}(\alpha-\beta)\cos 2\pi\int_{t_2}^{t}(n_1-n_2)dt\right] + (K-K')\psi.$$

$$(25)\quad G_2 = -K\left[\tfrac{1}{2}(\alpha+\beta)-\tfrac{1}{2}(\alpha-\beta)\cos 2\pi\int_{t_2}^{t}(n_1-n_2)dt\right] + (K-K')\psi.$$

By adding Equations (24) and (25) we get:

$$(26)\quad S = G_1 + G_2 = K(\alpha+\beta)\cos 2\pi\int_{t_2}^{t}(n_1-n_2)dt + 2(K-K')\psi.$$

(c) The Low Frequency

$(K-K')\psi$ is small compared to $K(\alpha-\beta)$, and changes slowly with time. Hence, at a maximum of S,

$$(27)\quad 2\pi\int_{t_2}^{t_{max}}(n_1-n_2)\,dt = 2n\pi, \quad \text{and at the next minimum}$$

$$(28)\quad 2\pi\int_{t_2}^{t_{min}}(n_1-n_2)dt = (2n+1)\pi.$$

Combining Equations (27) and (28),

$$2\pi\int_{t_{max}}^{t_{min}}(n_1-n_2)dt = \pi,$$

where t_{max} is the time of a maximum of S, and t_{min} is the time of the adjacent minimum. Assuming (n_1-n_2) is constant over this interval, we may write:

$$(29)\quad n_1 - n_2 = \frac{1}{2(t_{min}-t_{max})}.$$

This can, of course, be applied equally well from a minimum to a maximum of S.

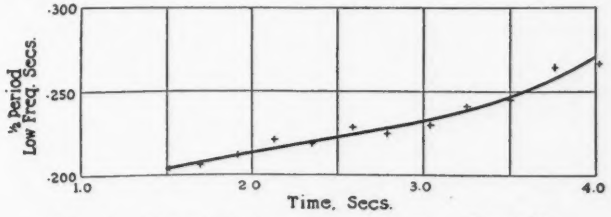

FIG. 15. *Half-period of low frequency vs. time. Round 89.*

The values of (n_1-n_2) for a typical round (No. 89) are plotted against time in Fig. 15, and a smooth curve drawn through them. The value of (n_1-n_2) employed to determine force coefficients were taken from such

curves for each round. These values, and their corresponding times, are shown in Table I, for each round.

TABLE I

Round No.	$(n_1 + n_2)$, c.p.s.	$(n_1 - n_2)$, c.p.s.	Time of evaluating $(n_1 - n_2)$, sec.
2	22.01	2.31	1.60
3	22.01	2.46	1.18
11	22.42	2.19	1.60
13	22.35	2.24	1.60
80	20.41	2.89	0.98
82	20.37	2.50	1.35
83	20.75	2.50	1.22
89	20.55	2.42	1.60
60	20.73	2.25	1.60
67	21.19	2.19	1.60

(*d*) *The High Frequency*

It was observed, for all rounds analyzed, that $(n_1 + n_2)$ was constant over the region in which it could be observed on the trace. Thus, it was readily determined by noting the times of its minima and maxima, and thereby calculating the mean period from the time taken for 10 or 12 complete cycles. The range generally used was that from one point in a low frequency cycle to the corresponding point on the next cycle.

In Table I, the values of $(n_1 + n_2)$ are shown for each round.

(*e*) *Determination of K*

From a knowledge of

$$2\pi \int_{t_2}^{t} (n_1 - n_2)dt$$

we can determine the times t_0 at which

$$\cos 2\pi \int_{t_2}^{t_0} (n_1 - n_2)dt = 0 .$$

Then from Equation (26) at such times:

$$S_0 = 2(K - K')\psi$$

$$\text{or } K = K' + \frac{S_0}{2\psi} . \tag{30}$$

This determines K. If K differs from K' by more than 5%, the variation of ψ with time may have affected S sufficiently to impair the accuracy of the determination of $(n_1 - n_2)$, and hence the t_0. In this case, K as determined by Equation (30) must be regarded as a second approximation to the true K.

The process must then be repeated. In almost every case, repetition was found unnecessary. The values of K prior to the first scale change are shown in Table II, and with them, the corresponding K'.

TABLE II

Round No.	K, inches per degree	K', inches per degree
2	1.72	1.75
3	0.92	0.90
11	1.23	1.22
13	2.18	2.24
80	0.96	0.91
82	0.86	0.85
83	0.72	0.70
89	1.51	1.47
60	2.27	2.27
67	1.04	

(f) Determination of the Amplitudes

Adding and subtracting Equations (24) and (25) we have:

$$\tfrac{1}{2}(\alpha - \beta) = \frac{G_1 + G_2 - 2(K - K')\psi}{2K \cos 2\pi \int_{t_2}^{t} (n_1 - n_2)dt} \tag{31}$$

$$\tfrac{1}{2}(\alpha + \beta) = \frac{G_1 - G_2}{2K}. \tag{32}$$

Equations (31) and (32) were used to determine the yaw amplitudes.

A typical set of determinations of $\frac{1}{2}(\alpha + \beta)$, for Round 67, is plotted on semilogarithmic scales in Fig. 17. The corresponding least squares straight line is also plotted. Values of $\frac{1}{2}(\alpha - \beta) \cos 2\pi \int_{t_2}^{t} (n_1 - n_2)dt$ for the same round are plotted in Fig. 16.

4. The Derived Quantities

The quantities determined by direct measurement from the trace are the following:

Frequencies: Spin, $(n_1 + n_2)$, $(n_1 - n_2)$
Amplitudes: $\frac{1}{2}(\alpha + \beta)$, $\frac{1}{2}(\alpha - \beta)$.

In addition, the following quantities were determined, either by laboratory measurement, or by independent measurement at the trial:

The moments of inertia, A and B of the shell,
The position of the center of gravity,
The velocity and mean ballistic coefficient of the shell,
Meteorological data at the time of the trial.

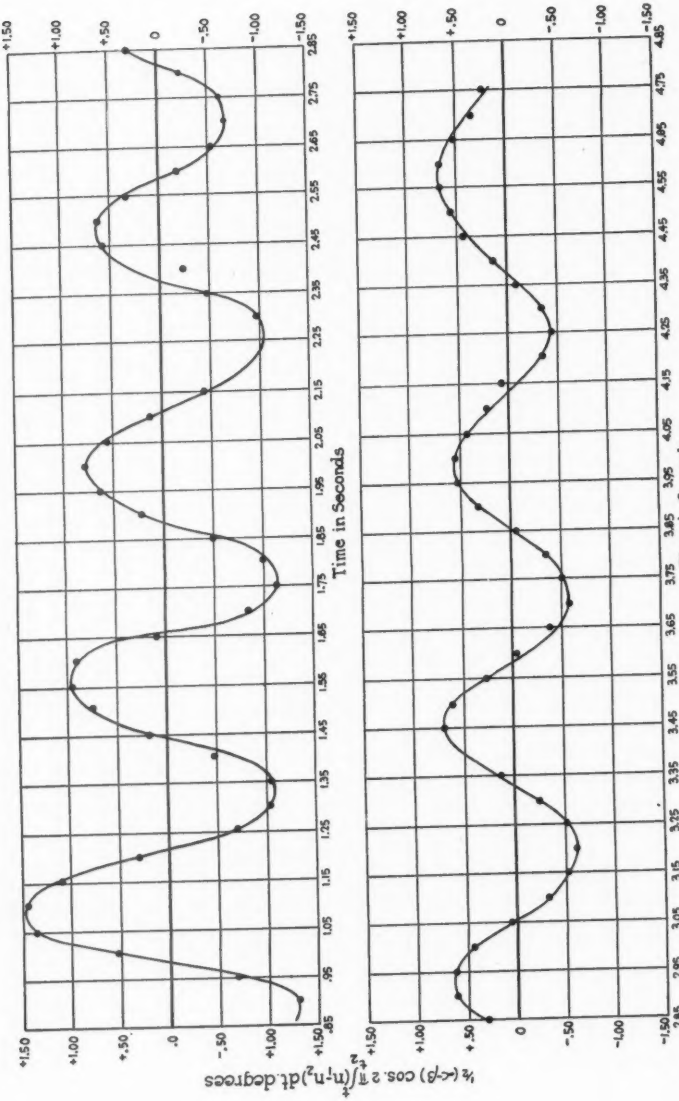

FIG. 16. $\frac{1}{2}(\alpha - \beta)\ cos\ 2\pi \int_{t_2} (n_1 - n_2)dt$. *Round 67*

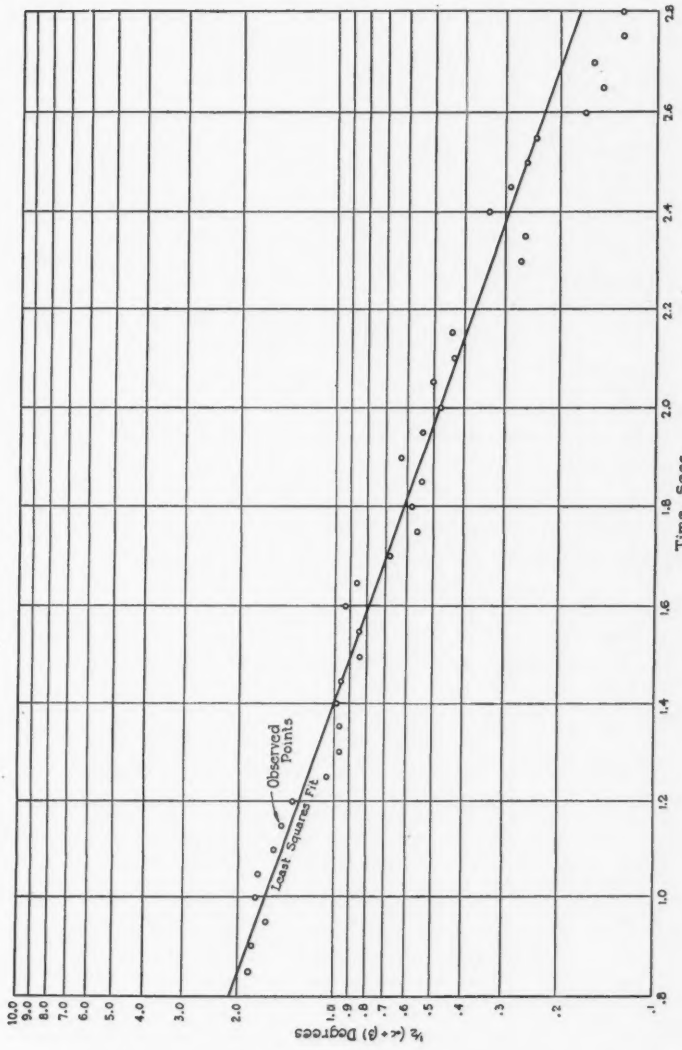

FIG. 17. $\frac{1}{2}(\alpha + \beta)$ *vs. time. Round 67.*

Certain of these measured values are shown in Table III.

TABLE III

Round No.	Position of center of mass		Mass, lb.	Axial moment of inertia, A lb-in.^{2}	Transverse moment of inertia, B lb-in.^{2}	Muzzle velocity, V $\frac{\text{ft.}}{\text{sec.}}$
	Type	Distance to base, in.				
2	Normal	6.64	24.97	40.42	418.9	1487
3		6.64	24.98	40.19	418.7	1486
11		6.62	24.95	39.93	413.0	1499
13		6.62	24.94	40.32	415.6	1491
80	Back	6.31	25.00	40.10	441.7	1495
82		6.33	24.97	40.21	445.2	1486
83		6.25	24.94	39.96	437.9	1498
89		6.27	24.98	39.94	439.1	1488
60	Forward	7.03	25.08	39.99	440.1	1490
67		7.03	25.11	39.94	433.6	1490

The velocities of the shells, as tabulated functions of time, were calculated by the standard methods of external ballistics. The force factors were then determined from the above data, as described in Sections IV – 4(*a*) and IV – 4(*b*), which follow.

(*a*) *The Overturning Moment Coefficient*

From Equation (9)

$$n_1 = \frac{\Omega}{4\pi},\ n_2 = \frac{\Omega\sigma}{4\pi},\ \sigma = \sqrt{1 - 1/s}.$$

Hence, adding $(n_1 + n_2)$ and $(n_1 - n_2)$ we obtain $\frac{\Omega}{2\pi}$.

Subtracting, we obtain $\frac{\Omega\sigma}{2\pi}$, and dividing n_2 by n_1 we obtain σ.

Then $\sigma^2 = 1 - 1/s$, whence $s = \frac{1}{1 - \sigma^2}$,

and since

$$s = \frac{A^2N^2}{4B\rho v^2 r^3 f_M}$$

$$f_M(v/a) = \frac{A^2N^2}{4Bs\rho v^2 r^3}. = \frac{\Omega^2 B}{4s\rho v^2 r^3}. \tag{33}$$

$\Omega/2\pi$ may be obtained independently by the relation $\Omega = \frac{AN}{B}$, using the measured values of A, B, and the spin N. Using Ω determined in this way, and the measured values of $(n_1 + n_2)$, σ may be evaluated, since

$$(n_1 + n_2) = \frac{\Omega}{4\pi}(1 + \sigma).$$

This determination of σ is independent of $(n_1 - n_2)$,and permits another evaluation of s and f_M. The values of $\Omega/2\pi$ and f_M found by both methods are given in Table IV.

TABLE IV

Round No.	Time of determination of $(n_1 - n_2)$, sec.	$\Omega/2\pi$, c.p.s.		$f_M(v = 1350 f/s)$		Distance of C.G. from base, in.
		From $(n_1 + n_2)$ and $(n_1 - n_2)$	From N	From $(n_1 + n_2)$ and $(n_1 - n_2)$	From N and $(n_1 + n_2)$	
2	1.60	24.32	24.12	13.61	12.41	6.64
3	1.18	24.47	24.31	13.85	12.93	6.64
11	1.60	24.61	24.61	12.90	12.94	6.62
13	1.60	24.59	24.60	13.36	13.41	6.62
82	1.35	22.87	22.96	14.55	14.55	6.33
83	1.22	23.25	23.33	13.93	14.33	6.25
89	1.60	22.97	22.87	14.01	13.40	6.27
60	1.60	22.98	22.95	13.20	13.00	7.03
67	1.60	23.38	23.28	12.94	12.33	7.03

(b) The Cross-wind Force Coefficient

By comparing the values of f_M for shells of three different positions of the centers of gravity, the values of f_L may be deduced from Equation (5). Using the data of Table IV, f_M was plotted against position of center of gravity and a straight line fitted by least squares (Fig. 18). From the slope of this straight line it was found that $f_L = 2.0$, whence κ (as defined in equation (3)) $= 0.18$.

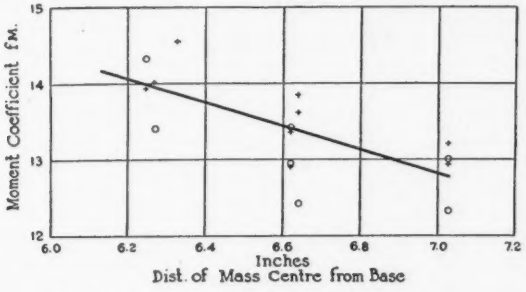

FIG. 18. f_M *vs. distance of mass center from base.*

(c) The Damping Factors

The quantities κ, h, γ, Γ, are called the 'damping factors', and are related to their corresponding force factors by Equation (3).

The determination of κ has been described above. Γ is determined from spin data as described in Section IV – 5.

TABLE V

Round No.	$\frac{1}{2}(\alpha_0+\beta_0)$, degrees	Exponent, sec.$^{-1}$	$\frac{1}{2}(\alpha_0-\beta_0)$, degrees	Exponent, sec.$^{-1}$	$h+\kappa$, sec.$^{-1}$	$\frac{1}{\sigma}(h-\kappa+2\gamma-\Gamma)$, sec.$^{-1}$	σ	$h-\kappa+2\gamma-\Gamma$, sec.$^{-1}$	κ, sec.$^{-1}$	h, sec.$^{-1}$	Γ, sec.$^{-1}$	γ, sec.$^{-1}$
2	4.23	1.32	0.81	0.09	1.41	1.23	0.82	1.01	0.18	1.23	0.01	−0.02
11	2.30	1.53	1.04	0.06	1.59	0.98	0.82	0.80	0.18	1.41	0.01	−0.21
13	2.96	1.02	2.24	0.25	1.27	0.97	0.82	0.63	0.18	1.09	0.01	−0.14
89	3.04	0.93	2.83	0.35	1.28	0.58	0.80	0.46	0.18	1.10	0.01	−0.23
60	2.20	0.87	1.36	0.34	1.20	0.53	0.80	0.42	0.18	1.02	0.01	−0.21
67	5.65	1.24	1.90	0.34	1.58	0.90	0.82	0.74	0.18	1.40	0.01	−0.24

The factors h and γ may be determined from the observed values of $\frac{1}{2}(\alpha + \beta)$ and $\frac{1}{2}(\alpha - \beta)$, using Equations (9). The best exponential curves of the form $y = Ae^{-bt}$ were fitted to the observed values by least squares. This involves neglecting the effect of variations of $\left(\frac{\Omega_0\sigma_0}{\Omega\sigma}\right)^{\frac{1}{2}}$ and assuming that the exponents are linear functions of time. Consideration of the rate of change of $\Omega\sigma$ shows that $\left(\frac{\Omega_0\sigma_0}{\Omega\sigma}\right)^{\frac{1}{2}}$ changes by only a fraction of a per cent per second. The assumption regarding the exponents can be justified by regarding the values obtained as averages. The semilogarithmic graph of $\frac{1}{2}(\alpha + \beta)$ against time in Fig. (17) shows that this procedure is reasonable.

By adding and subtracting the exponents of $\frac{1}{2}(\alpha + \beta)$ and $\frac{1}{2}(\alpha - \beta)$, $(h + \kappa)$ and $(h - \kappa + 2\gamma - \Gamma)$ can be determined. It is then possible to determine h and γ.

In Table V the values of $\frac{1}{2}(\alpha_0 + \beta_0)$, $\frac{1}{2}(\alpha_0 - \beta_0)$ and their corresponding exponents, are tabulated. The values of h, κ, Γ, and γ are also shown.

It will be noted that γ is negative. The significance of this is that the force K' acts behind the center of gravity, O, rather than in front.

5. Spin

(a) *Modulation Amplitude*

Equation (18) contains a term $\epsilon \cos 2\pi Nt$ which is a component varying at the spin frequency. For those times when $\delta \cos \phi = 0$ it follows that:

$$\epsilon = \frac{h_s\psi}{\overline{H}}, \tag{34}$$

where h_s is the height of the spin modulation on the trace and $\overline{H}$ = height of trace when averaged over a spin cycle. Measurements on the traces show that, to within experimental accuracy, ϵ remains constant throughout flight, so that the spin term in the signal is adequately explained by postulating the existence of an angle ϵ between the electric axis and the spin axis of the shell. For Round 67, ϵ was found to be 0.27°, and for Round 89 it was 0.19°.

(b) *Measurement of Spin and Spin Decay*

The small amplitude of spin modulation and the relatively low film speed make a statistical method of measurement necessary. Every tenth spin cycle on the trace was numbered, and ΔT_i, the observed time for 50 cycles, was obtained. N was thus calculated, and Fig. 19 shows a typical graph of spin against time. For each round a curve of the form $N = N_0e^{-\Gamma t}$ was fitted by determining the least squares straight line:

$$\log N = \log N_0 - \Gamma t. \tag{35}$$

The values of N_0 and Γ so found are listed in Table VI. For most rounds this equation was applied over a five or six second interval.

TABLE VI

Round	N_0, rev./sec.	Γ, sec.$^{-1}$	Round	N_0, rev./sec.	Γ, sec.$^{-1}$
2	253.7	0.0092	60	257.0	0.0109
3	256.2	0.0095	67	257.2	0.0109
11	259.0	0.0107	82	257.2	0.0123
12	254.8	0.0108	83	259.3	0.0115
13	257.8	0.0103	89	254.9	0.0087

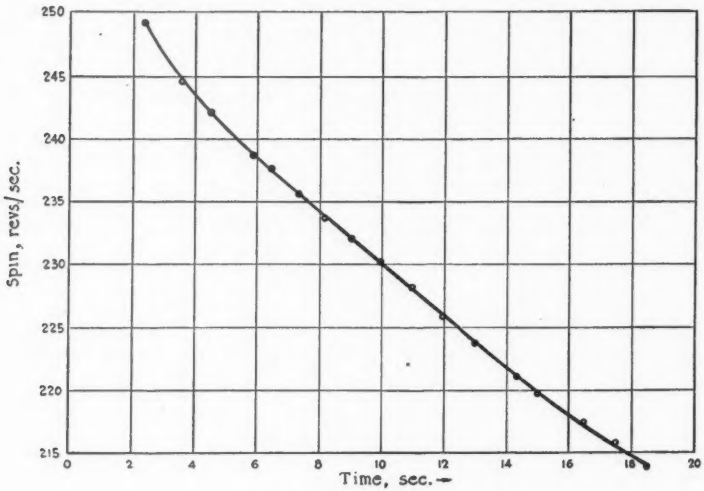

FIG. 19. *Spin. Round 12.*

Application of Equation (35) over shorter time intervals showed that there was a significant trend in Γ. This trend was investigated by determining Γ for two-second intervals, on five rounds. About 30 points were obtained, all but a few in the range 0 to 10 sec., and a smooth curve drawn through them. The mean distance of the points from the curve was about 3%. Using the relation connecting f_I, Γ, and the spin reducing couple, I,

$$\text{viz.:} \quad I = \rho v N r^4 f_I = -AN\Gamma \qquad \text{(Equations (2) and (3))}$$

the curve of f_I versus time in Fig. 20 was obtained.

(*c*) *Skin Friction*

Spin decay results from friction due to the viscosity of the air and it is possible to estimate f_I from the theory of skin friction. The usual hydrodynamic treatment is in terms of the boundary layer theory (3) according to which the shell is surrounded by a thin layer of air of which the inner surface is at rest relative to the shell, and the outer surface moves with the velocity

TABLE VII

CALCULATION OF f_I

Time, sec.	$M^* = V/a$	f_I from Γ	f_I from drag	Time, sec.	$M^* = V/a$	f_I from Γ	f_I from drag
0	1.368		0.0766	10	0.898	0.0715	0.0837
1	1.285	0.0808	0.0779	11	0.882	0.0719	0.0839
2	1.208	0.0772	0.0787	12	0.866	0.0733	0.0842
3	1.140	0.0735	0.0797	13	0.852	0.0754	0.0842
4	1.079	0.0720	0.0809	14	0.841	0.0772	0.0844
5	1.025	0.0706	0.0814	15	0.829	0.0801	0.0847
6	.987	0.0695	0.0819	16	0.820	0.0837	0.0850
7	.959	0.0692	0.0824	17	0.810	0.0872	0.0850
8	.935	0.0702	0.0832	18	0.802	0.0914	0.0850
9	.917	0.0709	0.0834				

* *Mach number* = V/a, *where* a = *velocity of sound in the undisturbed medium and* V = *velocity of air stream.*

(36) $$V^2 = v^2 + \left(\frac{Nr}{2\pi}\right)^2 .$$

of the air stream. Although the viscosity is small, the normal velocity gradient may be large, and the integrated effect of the shear stresses can give rise to an appreciable force. The drag is written in the form:

(37) $$D = \tfrac{1}{2}\rho V^2 C_f A ,$$

where C_f is a dimensionless coefficient,
and A = area of surface = $2\pi rL$ for a shell,
(L = effective length of shell = length + fuse correction).

From this it follows that the spin reducing couple

$$I = \rho V \pi r^3 L N C_f ,$$

and comparing this with Equation (2):

(38) $$f_I = \frac{\pi L}{r}\frac{V}{v} C_f .$$

For turbulent flow Falkner has modified a theory of Karman's to show that (1):

(39) $$C_f = \frac{0.036}{(N_{RL})^{\frac{1}{5}}} ,$$

where N_{RL} = the Reynold's number, $\dfrac{\rho VL}{\mu}$.

The values of f_I calculated from Equation (38) and those from the measured values of Γ are shown in Table VII and Fig. 20. It is seen that the magnitudes are in reasonable agreement but the shapes of the curves are different. It should be noted that the above theory for the drag does not take into account any possible changes in the nature of the equations of flow that occur in the

trans-sonic region. The minimum at 6.5 sec. corresponds to a Mach number of about one.

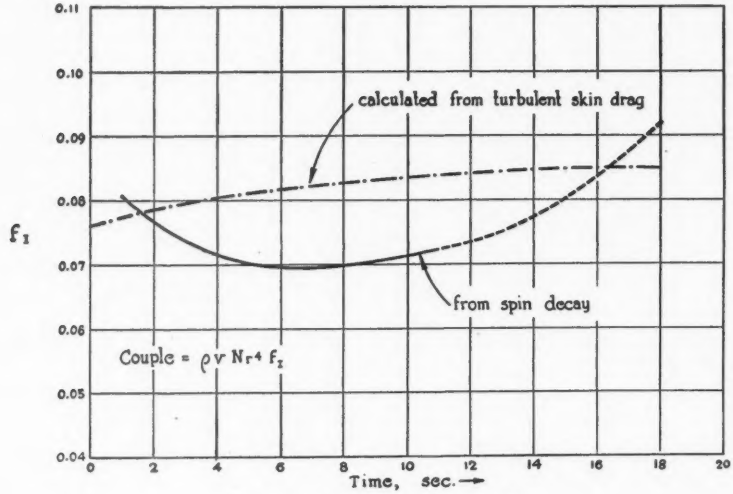

FIG. 20. *Coefficient of spin couple.*

It is of interest to see how much the drag due to skin resistance contributes to the total drag of a shell. The total force is due mainly to wave drag and is given by the empirical equation:

$$D = \frac{m}{10^4 C} \frac{\rho}{\rho_0} v^2 P(u) , \tag{40}$$

where

C = ballistic coefficient,

and

$P(u)$ is a tabulated function of $\left(\frac{va_0}{a}\right)$

(a_0 = velocity of sound under standard conditions).

From Equation (2) it follows that;

$$\frac{\text{Skin drag}}{\text{Total drag}} = \frac{r^2 C 10^4 \rho_0}{m} \frac{f_I}{P(u)} \tag{41}$$

It is found that the skin drag contributes from 10 to 25% of the total drag, the fraction being least at $M = 1$.

V. Summary and Conclusions

1. Summary of Preceding Results

The system of forces acting on a shell in flight is described, after the analysis of Fowler, Gallop, Lock, and Richmond. The solutions of the equations of motion found by those authors are quoted, indicating the manner in which the

forces affect the angular motion. A radio method of measuring this motion over a wide range of distances from the gun is described, the theory of the method is derived, and the equipment developed for the measurements is described. An account of certain experiments using this method is given, and the photographic record is described. The theory and examples of the analysis are given. Results for some 10 rounds are quoted. From these results, the force factors and damping coefficient have been deduced. The overturning moment coefficient f_M has been determined at a velocity of 1350 ft. per sec.; and from values of f_M for shells of various mass distributions, the cross-wind force coefficient f_L, has been found. Average values of the damping factors, h, and γ have been deduced by evaluating the exponents of the decay of the yaw angle. By accurate measurements of spin, the spin decay exponent Γ has been determined, and the spin decay coefficient, f_I, has been evaluated at different times. f_I has also been calculated from hydrodynamic theory, and a comparison is made with the values determined by spin decay.

2. Comparison of the Radio and Other Methods

Prior to this development, two other methods of yaw measurements have been employed. These are the jump card method and the photographic method. The jump card method consists of firing a shell through a series of cardboards, spaced down a range. By measurements of the shape and orientation of the resulting holes in the cards, it is possible to determine δ and ϕ. The photographic method consists of firing a shell down a range, between pairs of cameras which photograph the shell in perpendicular planes, at a number of points down the range. From these photographs, δ and ϕ may be determined.

It is possible at this point to compare the radio method with the jump card and photographic methods of yaw study.

The relative advantages of the radio method are:

(*a*) It permits measurement over the whole trajectory;

(*b*) It provides a continuous record;

(*c*) No mechanical contact with the shell is required;

(*d*) It permits measurement of the spin and spin decay;

(*e*) The accuracy of all measurements is comparable with either card or photographic method, and for a number of quantities, e.g., nutation and precession frequencies, damping factors, it is better;

(*f*) Measurements are not confined to a flat trajectory.

The relative disadvantages of the radio method are:

(*a*) It requires special fuses and equipment;

(*b*) The labor and time required for analysis is considerably greater;

(*c*) Analysis requires independent determination of trajectory data.

Acknowledgments

The authors wish to acknowledge the considerable assistance of Professors E. F. Burton, C. Barnes, and V. G. Smith of this University, and Dr. D. C. Rose, of C.A.R.D.E. Valcartier. Proximity fuse components were made available by the co-operation of Dr. M. A. Tuve, O.S.R.D., Washington. Velocity measurements at the trials were made by Mr. P. T. Demos and Lt. J. Orr, R.C.A. The project was financed by the National Research Council of Canada.

References

1. FALKNER, V. M. Aircraft Eng. 15 : 65. 1943.
2. FOWLER, R. H., GALLOP, E. G., LOCK, C. N. H., and RICHMOND, H. W. Trans. Roy. Soc. London, A, 221 : 295. 1921.
3. HEMKE, P. E. Elementary applied aerodynamics. Prentice-Hall Inc., New York. 1946.
4. KRAUS, J. D. Proc. Inst. Radio Engrs. 28 : 513. 1940.
5. STRATTON, J. A. Electromagnetic theory. McGraw-Hill Book Company, Inc., New York and London. 1941.
6. TERMAN, F. E. Radio Engineers' handbook. McGraw-Hill Book Company, Inc. New York and London. 1943.

GRAVITY ANOMALIES IN NORTHWESTERN CANADA[1]

By M. J. S. Innes

Abstract

Free air, Bouguer, and isostatic anomalies are listed in a table of principal facts for 23 stations established by the Dominion Observatory in the area between latitudes 55 and 70 degrees, bounded on the east by Hudson Bay and on the west by Athabaska, Slave, and Mackenzie rivers. There is some evidence that the predominantly negative anomalies at stations in the Pre-Cambrian may be due to lack of isostatic adjustment following removal of glacial loads.

Introduction

The first gravity observations in northern Canada were made by the Dominion Observatory in 1921 when a series of pendulum stations were established along the water routes between Edmonton and the Mackenzie River delta (7). Observations were made at seven stations in the Arctic as far north as Cambridge Bay on Victoria Island on a combined gravity and magnetic airborne expedition in 1945. Three determinations were made at points along the Hudson Bay railroad in 1946. Altogether 23 stations have been established in the area between latitudes 55 and 70 degrees, bounded on the east by Hudson Bay and on the west by Athabaska, Slave, and Mackenzie rivers. The results of all observations are listed in Table I and are shown in Fig. 1.

To interpret the results of gravity observations the value of gravity is compared with theoretical values computed for the latitude and elevation of the station. Several methods of reduction may be employed. The observed value minus the computed value is the gravity anomaly. A positive anomaly represents an excess of gravity and a negative anomaly a deficiency. In this report three methods of reduction have been used, the free air, Bouguer, and the Hayford and Bowie isostatic reduction for a depth of compensation of 113.7 km. (7). The theoretical value of gravity at sea level for each station is computed from the International Gravity Formula* and is shown in the sixth column of Table I. The corrections that are applied to this value to obtain the computed value of gravity at the elevation of the station are shown in the next five columns of the table. The free air computed value is obtained by simply applying a negative correction for the elevation of the station above sea level to account for the diminution in gravity due to the

[1] *Manuscript received December 12, 1947.*

Contribution from the Dominion Observatory, Ottawa, Canada. Vol. 1, No. 2. Contributions from the Dominion Observatory. Published by permission of the Director, Mines, Forests, and Scientific Services Branch, Department of Mines and Resources.

* *Theoretical gravity (γ_0, in centimeters per second per second) at sea level for each station is obtained by substitution of the latitude φ of the station in the formula $\gamma_0 = 978.049 (1 + 0.0052884 \sin^2 \varphi - 0.0000059 \sin^2 2\varphi)$, adopted by the International Union of Geodesy and Geophysics. In this formula 978.049 is the most probable value of gravity at the equator, as deduced from numerous gravity observations at many places over the earth. The coefficients of $\sin^2 \varphi$ and $\sin^2 2\varphi$ are deduced from theoretical expressions for gravity on the adopted spheroid.*

TABLE I

PRINCIPAL FACTS FOR GRAVITY STATIONS

Station		Longitude	Latitude	Elevation H, ft.	Theoretical gravity, γ_0, gals	Corrections in milligals to theoretical gravity for					Computed gravity (free air), gals	Observed gravity, gals	Gravity anomalies in milligals		
						Elevation	Topography A–O	Hayford-Bowie 113.7 km.							
No.	Name	° ′	° ′					Comp. A–O	$t+c$ 18–1	$t+c$ A–1			Free air	Bouguer	Hayford-Bowie 113.7 km.
175	Churchill	94 09.3	58 46.0	17	981.826	− 2	+ 1	− 2	− 2	− 3	981.824	981.770	−54	−55	−51
174	Gillam	94 42.0	56 21.0	447	981.628	−42	+15	−11	− 3	+ 1	981.586	981.576	−10	−25	−11
173	Wabowden	98 37.9	54 54.5	759	981.507	−71	+26	−18	− 7	+ 1	981.436	981.416	−20	−46	−21
172	Brochet	101 39.5	57 53.0	1117	981.775	−105	+39	−28	− 7	+ 3	981.670	981.651	−19	−58	−22
170	Cambridge Bay	105 04.1	69 07.4	6	982.562	0	0	− 5	0	− 5	982.562	982.515	−47	−47	−42
167	Stoney Rapids	105 49.5	59 15.5	727	981.865	−68	+25	−25	− 8	− 8	981.797	981.785	−12	−37	− 4
171	Ile à la Crosse	107 54.0	55 26.9	1385	981.553	−130	+48	−36	−13	− 1	981.423	981.409	−14	−62	−13
51	Chipewyan	111 08.8	58 42.7	750	981.822	−71	+24	−22	−14	−12	981.751	981.727	−24	−50	−12
62	Waterways	111 15.3	56 40.5	820	981.655	−77	+26	−36	−14	−24	981.578	981.555	−23	−51	+ 1
61	Lac la Biche	111 58.3	54 46.5	1801	981.495	−169	+60	−46	−18	− 4	981.326	981.322	− 4	−65	0
47	Resolution	113 40.5	61 10.1	500	982.014	−47	+17	−15	−11	− 9	981.967	981.946	−21	−38	−12
169	Coppermine	115 09.5	67 48.8	18	982.481	− 2	+ 1	− 8	− 3	−10	982.479	982.468	−11	−12	− 1
60	Kinuso	115 25.9	55 19.9	1922	981.543	−181	+65	−55	−20	−10	981.362	981.353	− 9	−75	+ 1
166	Fort Rae	116 05.7	62 49.3	515	982.138	−48	+18	−17	− 7	− 6	982.090	982.070	−20	−38	−14
43	Peace River	117 17.3	56 14.1	1063	981.619	−100	+34	−47	−25	−38	981.519	981.486	−33	−69	+ 5
44	Providence	117 39.3	61 21.2	512	982.028	−48	+17	−22	−13	−18	981.980	981.959	−21	−38	− 3
168	Cameron Bay	117 54.4	66 03.7	128	982.367	−39	+14	−17	− 4	− 7	982.328	982.306	−22	−36	−15
59	Grand Prairie	118 47.5	55 10.3	2154	981.529	−203	+73	−59	−27	−13	981.326	981.321	− 5	−79	+ 8
45	Simpson	121 20.8	61 51.7	433	982.067	−41	+15	−20	−18	−23	982.026	982.008	−18	−33	+ 5
48	Liard River	123 47.5	59 58.5	525	981.922	−49	+16	−49	−26	−59	981.873	981.794	−79	−97	−20
46	Norman	125 34.4	65 54.0	285	982.287	−27	+ 9	−29	−16	−36	982.260	982.218	−42	−52	− 6
49	Good Hope	128 38.3	66 15.3	195	982.380	−18	+ 6	−20	−15	−29	982.362	982.344	−18	−25	+11
50	Arctic Red River	133 44.3	67 26.6	135	982.457	−13	+ 4	−18	−12	−26	982.444	982.438	− 6	−11	+20
											Mean anomaly with regard to sign		−24	−48	− 9
											Mean anomaly without regard to sign		24	48	13

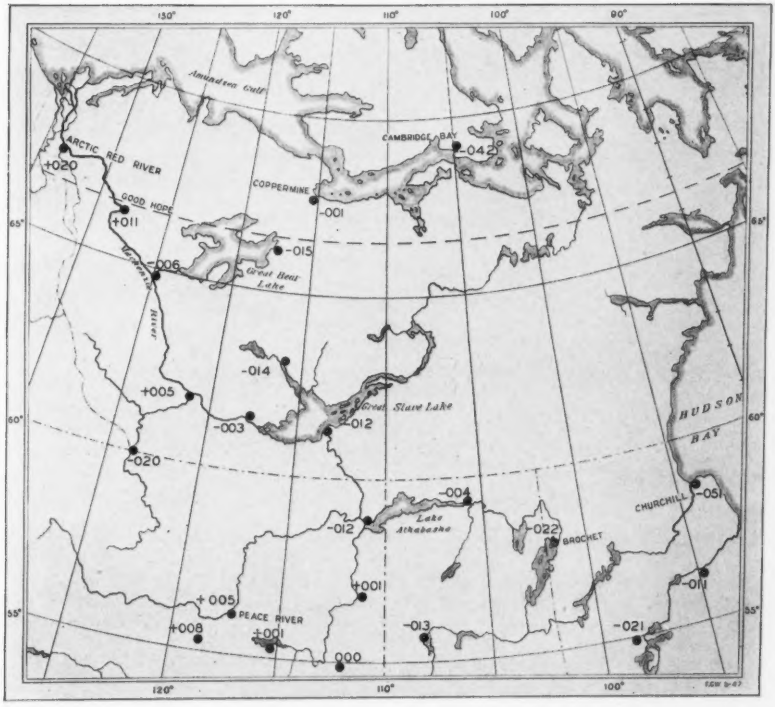

FIG. 1. *Isostatic anomalies for a depth of compensation of 113.7 km. at gravity stations in northwestern Canada.*

increased distance from the center of the earth. For the Bouguer (modified) reduction a further positive correction is made for the attraction of the topography out to a distance of 103.5 miles (Hayford Zone O) from the station. For the Hayford and Bowie (6) reduction the theoretical value at sea level is first corrected for the elevation of the station and then for the topography of the whole earth and finally for the compensation corresponding to the topography. E. C. Bullard's (1) method for computing the effects corresponding to the lettered zones was used and maps of Canada based on Heiskanen's charts for Zones 10 to 1 were employed to obtain the corrections for these more distant zones.

Discussion of Results

If perfect isostatic equilibrium prevailed and if in the vicinity of the station there were no large masses differing in density from 2.67 (the value adopted as the mean density of the solid part of the earth) the isostatic anomalies would tend to be negligible. Isostatic anomalies for the 23 stations, grouped according to the geological formations (on which they are situated), are shown in Table II. There are seven Palaeozoic stations, five with negative anomalies

TABLE II

TABLE SHOWING ANOMALIES FOR THE VARIOUS STATIONS GROUPED ACCORDING TO THEIR GEOLOGICAL FORMATIONS

Pre-Cambrian		Palaeozoic		Mesozoic	
Station number	Anomaly in cm./sec.^{2}	Station number	Anomaly in cm./sec.^{2}	Station number	Anomaly in cm./sec.^{2}
175	−.051	170	−.042	62	+.001
174	−.011	171	−.013	61	.000
173	−.021	47	−.012	60	+.001
172	−.022	44	−.003	43	+.005
167	−.004	45	+.005	59	+.008
51	−.012	46	−.006	48	−.020
169	−.001	49	+.011	50	+.020
166	−.014	—	—	—	—
168	−.015	—	—	—	—
Mean anomaly with regard to sign	−.017	Mean anomaly with regard to sign	−.009	Mean anomaly with regard to sign	+.002
Mean anomaly without regard to sign	.017	Mean anomaly without regard to sign	.013	Mean anomaly without regard to sign	.008

Note.—1 milligal = 1 × 10^{-3} cm. per sec.^{2}

and two positive. The mean anomaly with regard to sign is −0.009 cm. per sec.^{2} Five out of seven Mesozoic stations have positive anomalies. Only one Mesozoic station has a negative anomaly. The mean anomaly with

regard to sign for the Mesozoic stations is + 0.002 cm. per sec.^{2} All the nine Pre-Cambrian stations have negative anomalies and the mean anomaly is −0.017 cm. per sec.^{2}

Similar results have previously been observed in Canada over all these formations, including the Pre-Cambrian. As Pre-Cambrian rocks are on the average most likely considerably heavier than normal, persistent negative anomalies over such an extensive Pre-Cambrian area point to a departure from isostatic equilibrium or overcompensation.

The center of the Pre-Cambrian area in question may have been near the center of the great Keewatin ice sheet during the Pleistocene period in North America. Coleman (2) describes the Keewatin as having at different times three main centers, the first to the west of Chesterfield Inlet, the second near Dubawnt Lake, and the third near the mouth of the Nelson River, the ice centers reaching an estimated depth of 12,000 ft. It has been well established by geological studies that, owing to the tremendous loads, glaciated areas were depressed far below present levels and that the land surface still stands lower than in preglacial times (4). Although the few statistics of rate of regional uplift that are available have been the subject of debate (3) it is generally agreed that equilibrium will be reached only after the termination of thousands of years.

Lack of isostatic equilibrium should then prevail in regions of postglacial upwarpings of the crust, gravity anomalies would be negative, and increasingly negative toward the area where the load was the greatest (5). The gravity measurements made over this large area exhibit to some extent this expected deficiency of gravity. Churchill and Cambridge Bay, both stations near the former center of the ice sheets, have negative anomalies of −0.051 cm. per sec.^{2} and −0.042 cm. per sec.^{2}, respectively. On the other hand Arctic Red River and Good Hope near the Mackenzie River delta have positive anomalies, which is in agreement with geological evidence that this region was on the outer limits of the ice cap and was not disturbed by glaciation (2). There is also some evidence of algebraic decrease of the anomalies in passing from west to east. The area covered by the Prairie Provinces to the south and extending through the central United States is also for the most part one of positive anomaly.

Conclusion

The question whether the negative anomalies so predominant in this Pre-Cambrian area are due to lack of isostatic adjustment following removal of glacial loads cannot yet be definitely answered. Although the existing measurements of gravity suggest an affirmative answer, a greater density of gravity stations, especially in regions to the northeast, may present a different picture. It is hoped in the near future to make use of a gravimeter to extend the system of gravity measurements throughout this area in such a way as to answer some of the questions raised in this paper.

Acknowledgments

The writer wishes to acknowledge his indebtedness to Mr. A. H. Miller of the Dominion Observatory, Ottawa, for very helpful suggestions in the planning of the work and the preparation of the paper; and to the Royal Canadian Air Force who supplied air transportation in 1945.

References

1. Bullard, E. C. Trans. Roy. Soc. London, A, 235 : 445. 1936.
2. Coleman, A. P. The last million years. University of Toronto Press, Toronto. 1941.
3. Cooke, H. C. Am. J. Sci. 240 : 144. 1942.
4. Cooke, H. C. Trans. Roy. Soc. Can. 24 (IV) : 51. 1930.
5. Daly, R. A. Strength and structure of the earth. Prentice-Hall, Inc., New York. 1940.
6. Hayford, J. F. and Bowie, W. U.S.C.G.S. Spec. Pub. No. 10. 1912.
7. Miller, A. H. Pubs. Dominion Observ. 8 : No. 6. 1923.

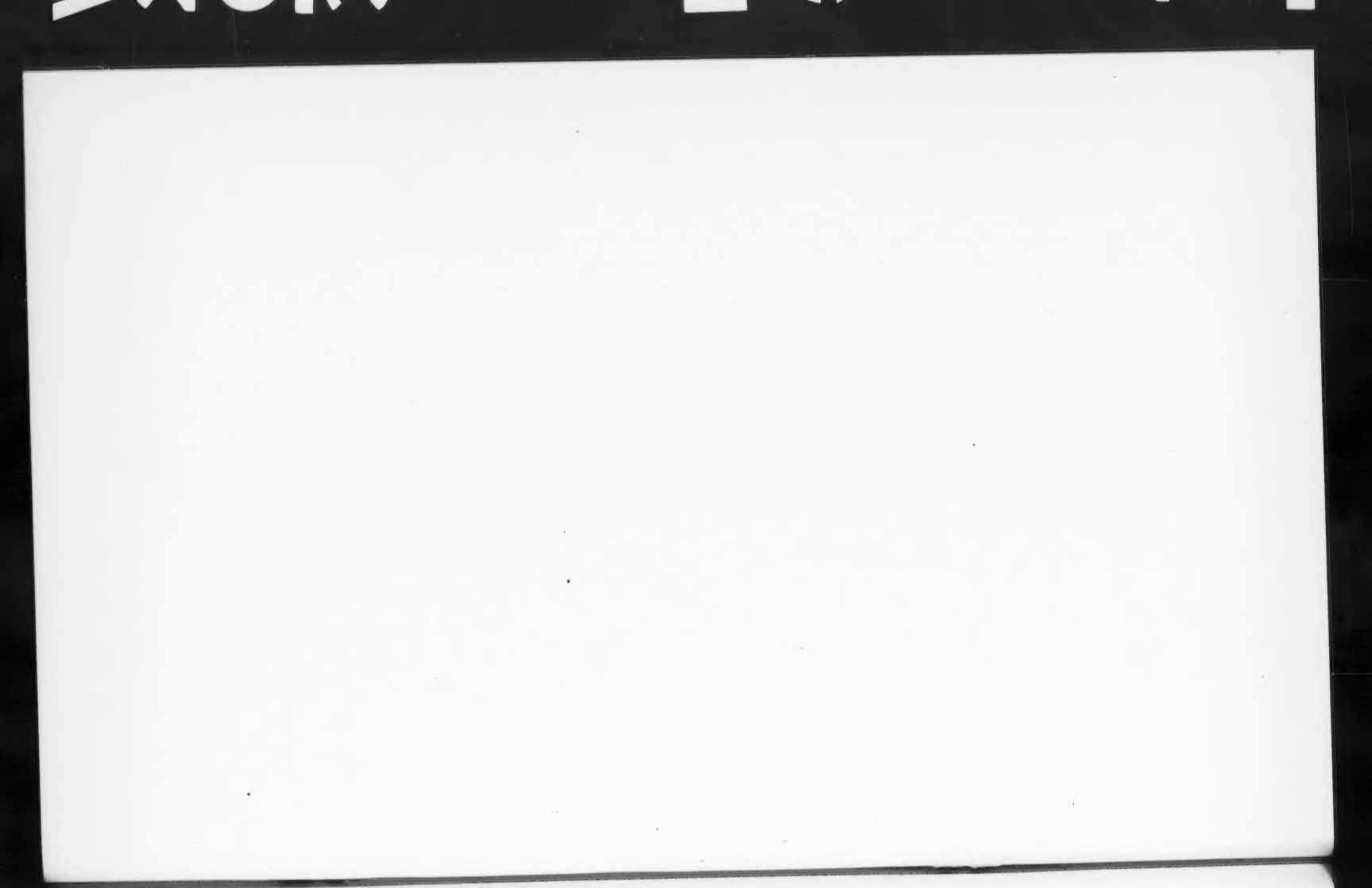

CANADIAN JOURNAL OF RESEARCH

Notes on the Preparation of Copy

GENERAL:—Manuscripts should be typewritten, double spaced, and the **original and one extra copy** submitted. Style, arrangement, spelling, and abbreviations should conform to the usage of this Journal. Names of all simple compounds, rather than their formulae, should be used in the text. Greek letters or unusual signs should be written plainly or explained by marginal notes. Superscripts and subscripts must be legible and carefully placed. Manuscripts should be carefully checked before being submitted, to reduce the need for changes after the type has been set. If authors require changes to be made after the type is set, they will be charged for changes that are considered to be excessive. **All pages, whether text, figures, or tables, should be numbered.**

ABSTRACT:—**An abstract of not more than about 200 words, indicating the scope of the work and the principal findings, is required.**

ILLUSTRATIONS:

(i) *Line Drawings:*—All lines should be of sufficient thickness to reproduce well. Drawings should be carefully made with India ink on white drawing paper, blue tracing linen, or co-ordinate paper **ruled in blue only**; any co-ordinate lines that are to appear in the reproduction should be ruled in black ink. Paper ruled in **green, yellow, or red should not be used** unless it is desired to have all the co-ordinate lines show. Lettering and numerals should be neatly done in India ink preferably with a stencil (**do not use typewriting**) and be of such size that they will be legible and not less than one millimeter in height when reproduced in a cut three inches wide. All experimental points should be carefully drawn with instruments. Illustrations need not be more than two or three times the size of the desired reproduction, but the ratio of height to width should conform with that of the type page. **The original drawings and one set of small but clear photographic copies are to be submitted.**

(ii) *Photographs:*—Prints should be made on glossy paper, with strong contrasts; they should be trimmed to remove all extraneous material so that essential features only are shown. Photographs should be submitted **in duplicate**; if they are to be reproduced in groups, one set should be so arranged and mounted on cardboard with rubber cement; the duplicate set should be unmounted.

(iii) *General:*—**The author's name, title of paper, and figure number should be written in the lower left-hand corner (outside the illustration proper) of the sheets on which the illustrations appear.** Captions should not be written on the illustrations, but typed on a separate page of the manuscript. All figures (including each figure of the plates) should be numbered consecutively from 1 up (arabic numerals). **Each figure should be referred to in the text.** If authors desire to alter a cut, they will be charged for the new cut.

TABLES:—Titles should be given for all tables, which should be numbered in Roman numerals. Column heads should be brief and textual matter in tables confined to a minimum. **Each table should be referred to in the text.**

REFERENCES:—**These should be listed alphabetically by authors' names, numbered in that order, and placed at the end of the paper.** The form of literature citation should be that used in the respective sections of this Journal. **Titles of papers should not be given in references listed in Sections A, B, E, and F, but must be given in references listed in Sections C and D.** The first page only of the references cited in papers appearing in Sections A, B, and E should be given. **All citations should be checked with the original articles.** Each citation should be referred to in the text by means of the key number; in Sections C and D the author's name and the date of publication may be included with the key number if desired.

The *Canadian Journal of Research* conforms in general with the practice outlined of the *Canadian Government Editorial Style Manual*, published by the Department in Public Printing and Stationery, Ottawa.

Reprints
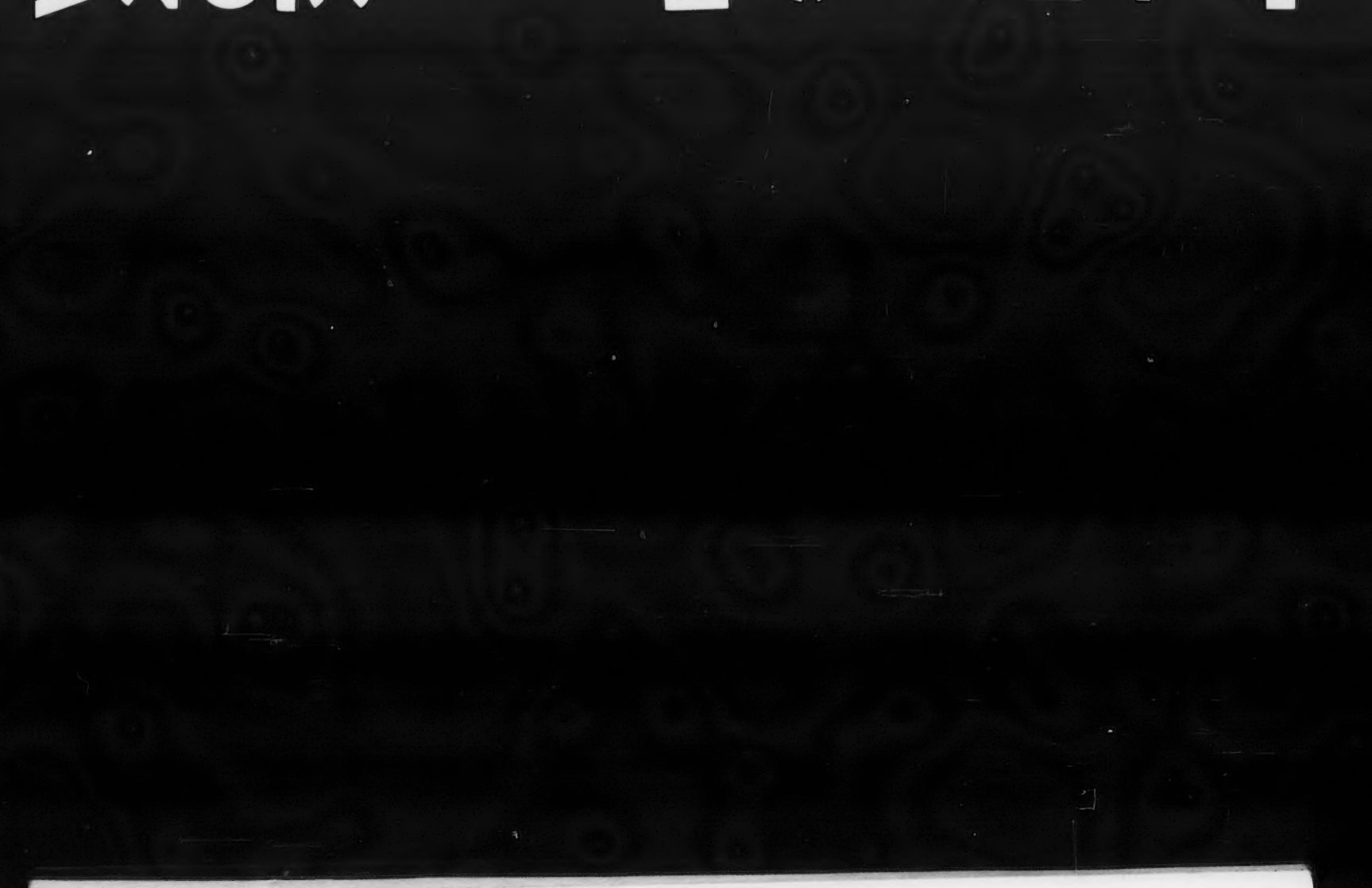
Fifty reprints of each paper without covers are supplied free. Additional reprints, if required, will be supplied according to a prescribed schedule of charges. On request, covers can be furnished at cost.